EVALUATION OF THE PARTITION INTERWELL TRACER TEST AND EXTENSION TO DETERMINE DNAPL ARCHITECTURE IN HETEROGENEOUS MEDIA

by

Elena Moreno-Barbero

ProQuest Number: 10797077

ProQuest 10797077

A thesis submitted to the Faculty and Board of Trustees of the Colorado School of Mines in partial fulfillment of the requirements for the degree of Doctor of Philosophy (Environmental Science and Engineering).

Golden, Colorado

Date 01 / 24 / 05

Signed:_____
Elena Moreno-Barbero

Approved:_____
Dr. Tissa Illangasekare
Thesis Advisor

Golden, Colorado

Date 01 / 24 / 05

_____ (for RLS)
Dr. Robert L. Siegrist
Professor and Division Director
Division of Environmental Science and Engineering

ABSTRACT

The Partition Interwell Tracer Technique (PITT), initially developed in the petroleum industry, is promoted in the environmental field as a non-intrusive method to determine DNAPL mass in source zones. A suite of chemical tracers, some of which partition into the DNAPL phase, is injected into the source zone to estimate the entrapped saturation of contaminant. Current application of the techniq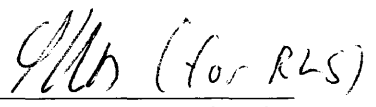ue can determine DNAPL at residual saturation, but does not provide reliable mass estimates of DNAPL in high saturation areas (e.g. pools) that may occur in some source zones.

The objective of this research was to analyze fundamental processes of partitioning tracer behavior and use the findings to improve current application of the technique. The experimental data, in conjunction with model analysis were used to determine the limitations and the extent of PITT technique for characterization of DNAPL under complex entrapment architecture.

Results confirmed that traditional application of the technique could lead to major estimation errors (up to 80% in some cases) when high saturation zones are present. The estimation errors are the result of tracers bypassing and the assumption of local equilibrium in data interpretation. Inverse modeling analysis demonstrated that more accurate volume estimates could be obtained using effective partition coefficients and evaluating tracer signatures using multilevel samplers.

A numerical modeling study following a simplified Monte Carlo approach established relationships between estimation errors and different parameters: vertical distribution of DNAPL, location of the well, degree of heterogeneity and injection-extraction patterns.

The findings of this investigation clarified the limitations of the technique under conditions of heterogeneity that result in complex DNAPL entrapment architecture. They also provided a set of guidelines in the form of design considerations to improve performance of PITT under those conditions.

TABLE OF CONTENTS

LIST OF FIGURES

LIST OF TABLES

ACKNOWLEDGMENTS

To my parents, Miguel and Carmen

Chapter 1

INTRODUCTION

1.1 Motivation

Organic chemicals are introduced into the subsurface from a variety of sources; accidental spills, improper disposal or leaking from underground tanks. Once in the subsurface, these chemicals can be found in vapor, dissolved form or as a non-aqueous phase liquid (NAPL). Chlorinated solvents in the form of dense non-aqueous phase liquids (DNAPL) exist in a large number of hazardous-waste sites; they are considered the most common health-threatening chemicals in groundwater and the most difficult to remediate (Mackay and Cherry, 1989). Once the DNAPL enters the subsurface, its distribution is controlled by fingering (Held and Illangasekare, 1995), preferential channeling and heterogeneity of the subsurface formation (Kueper and Frind, 1991a). All these factors increase the complexity of NAPL movement and subsequent entrapment (Schwille, 1988; Kueper et al., 1989; Illangasekare et al. 1995; Oostrom et al., 1999).

Due to this complexity of source zone architecture, the tasks of delineating and characterizing source zones could be a challenge. If the morphology and distribution of the NAPL source are unknown, the implementation of an effective remediation technique becomes difficult. Traditional soil coring methods have proven to be ineffective as a result of remobilization during sampling (Rao et al. 2000); in addition they have shown difficulties in resolving the spatial distribution of NAPL from discrete samples (Dai, et al. 2001). Considering the heterogeneity of the subsurface, it is very likely that the

interpolation of data in this manner will not reproduce successfully the distribution of contaminants.

The importance and prevalence of the NAPL problem creates the need for investigation of new techniques of characterization. Except for the tracer tests and concentration/flux matching techniques (Saenton, 2003), all the current methods are based on discontinuous, discrete measurements of the system. An evaluation of the potential of partitioning tracer techniques to provide information about the continuous system in heterogeneous sites is conducted in this research.

The Partition Interwell Tracer technique (PITT) was developed for detecting and characterizing the distribution of NAPL contaminants in subsurface environments (Jin et al., 1995). This technique adapts and extends several existing methods from the fields of groundwater hydrology and petroleum reservoir engineering (Allison et al., 1991). Inter-well tracer tests have been used in petroleum engineering for accurate reservoir description in enhanced oil recovery (Allison, 1988). The same principles of the technique applied in petroleum engineering are used in DNAPL characterization. In both applications, tracers undergo retardation when they reversibly partition between the oil and aqueous phase.

In implementing PITT, a tracer solution consisting of at least one conservative tracer and a mixture of chemicals with different partition coefficients is injected into the aquifer. Partitioning tracers are affected by the presence of DNAPL; their different solubility in the aqueous and oil phase will cause the partitioning tracers to lag behind the conservative tracers. The amount of DNAPL in the source zone swept by the tracer mixture can be estimated by analyzing tracer breakthrough curves observed down-gradient.

The use of PITT for DNAPL characterization has increased in recent years. In most cases, this technique has been used to assess remediation performance (Rao et al., 1997; Annable et al., 1998; Jawitz et al., 1998; Meinardus et al., 2002). Although this technique and its extensions have been applied with some success in a number of sites, its

limitations under complex DNAPL entrapment morphologies have not been completely evaluated. Dai et al. (2001) demonstrated the sole influence of NAPL distribution in tracer performance in one-dimensional column experiments. Tracer tests are expected to result in underestimation in certain conditions where the hydrodynamic accessibility is constrained or non-equilibrium mass transfer occurs (Rao et al., 2000). Traditional application of this technique assumes local equilibrium exists between phases. This may be true for low saturations, but may not be applicable in situations where DNAPLs are entrapped under high saturations such as in pools (Wilson et al., 2000; Jalbert et al., 2003).

The focus of this research study is to carefully evaluate the characterization of sites with unidentified NAPL sources by the PITT to improve application design, data interpretation and analysis. Laboratory studies are necessary to quantitatively assess the performance of current tracer methods. These controlled experiments allow for a precise characterization of the heterogeneous system that would not be possible in the field. In this way, fundamental processes, hypotheses and data analysis of partitioning tracer methods can be investigated. The objectives are to identify the sources of estimation error, to refine tracer methods, and to obtain more information about the architecture of the NAPL source zone. The knowledge gained from these investigations can be used to improve design protocols for field characterization of NAPL entrapment morphologies encountered at geologically complex field sites.

1.2 Thesis Outline

In the next chapter, a detailed background and literature review are presented, as well as the hypotheses and objectives of this work. Chapter 3 contains detailed information about all the materials and experimental apparatus used in the laboratory

throughout this research; it also contains a detailed description of the design and set up of the column and intermediate scale experiments. Chapter 4 describes the numerical models used to attain the computational needs of the investigation. Chapters 5, 6 and 7 represent the major contributions of this study. Chapter 5 describes the influence of the pool morphology on the performance of tracer tests. The experimental investigation as well as the modeling analysis to evaluate this issue is described along with results and conclusions. A method to improve mass estimation of NAPLs by PITT is presented in this chapter. In Chapter 6, an investigation of the performance of the PITT in more complicated systems is presented. The description of the set up and procedures of the intermediate scale experiment is followed by the methods used for analysis and the validation of the method developed in the previous chapter. Chapter 7 generalizes findings for different heterogeneous systems through a set of Monte Carlo simulations. Finally, Chapter 8 includes conclusions and suggestions for future research.

Chapter 2

LITERATURE REVIEW AND BACKGROUND

2.1 Non-aqueous Phase Liquids

The widespread production of chlorinated solvents and petroleum products has been followed by accidental release or improper disposal of these compounds into the subsurface.

2.1.1 Contamination by NAPLs

The aqueous solubility of these organic liquids contaminants is low enough for them to exist in the subsurface as non-aqueous phase liquids (NAPLs) but great enough to exceed safe drinking water standards.

Petroleum products are frequently present as light, nonaqueous phase liquids (LNAPLs) and chlorinated solvents such as trichloroethylene (TCE), tetrachloroethylene (PCE) and carbon tetrachloride are normally in the form of dense, non-aqueous phase liquids (DNAPLs). When NAPLs are introduced to the subsurface, gravity will cause the NAPL to migrate downward through the vadose zone as a separate liquid. LNAPLs will spread laterally along the capillary fringe since they are lighter than water. On the other hand, NAPLs with a density greater than water (DNAPLs) will keep migrating until an

impermeable layer is encountered. This vertical migration is also accompanied to some extent by lateral spreading due to the effect of capillary forces.

DNAPL migration in the subsurface is affected by (1) volume of NAPL released, (2) area of infiltration, (3) time duration of the release, (4) properties of the NAPL, (5) properties of the porous media, and (6) subsurface flow conditions (Mercer et al., 1990).

A variety of remediation techniques has been studied by researchers and evaluated in the field. Most of these remediation techniques are site specific; the entrapment configuration, properties of the chemical and the geological features of the site are determinant as a decision-making criteria to remediation selection. No matter what technique is used for NAPL source removal (excavation, extraction, destruction stabilization, containment, etc.), the volume of "soil" containing the NAPLs must be accurately delineated (Rao et al., 2000). The characterization of NAPL contamination in aquifers should involve the location of NAPL zones, the compositional characterization of NAPL, and the estimation of the amount of NAPLs within zones.

2.1.2 DNAPL Entrapment

When DNAPLs are released into the subsurface, the liquid phase contaminant leaves behind a trail of immobile residual when it migrates through the vadose zone and the saturated media. The contaminant present in the vadose zone will exist in the form of vapor and liquid phases. In the saturated zone, DNAPLs can be trapped in the pores by capillary forces that resist natural groundwater gradient and produce a long term source of contamination. Figure 2.1 represents a typical scenario of DNAPL contamination.

Figure 2.1. Example of a DNAPL spillage.
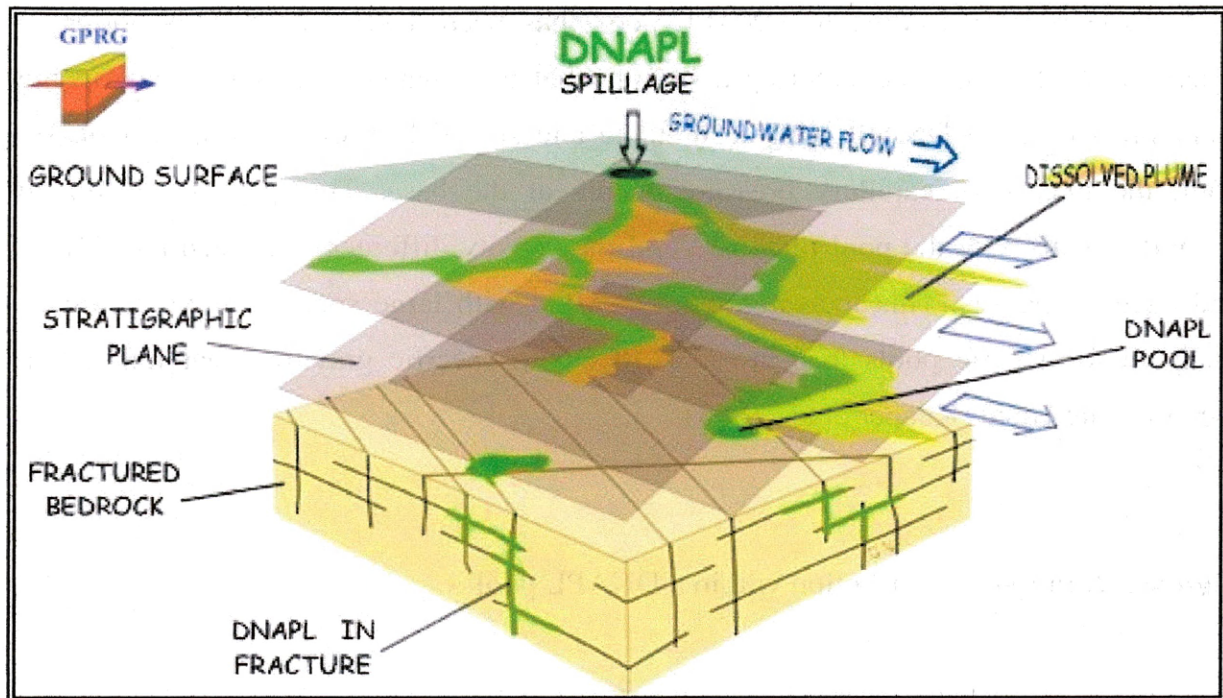
If spilled in sufficient quantities, DNAPLs will penetrate the water table, sinking until the supply is exhausted or reaches less permeable layers (Schwille, 1998). DNAPLs can migrate relatively easily in the saturated zone under gravity forces, penetrating deeply into aquifers, and in some cases travel significant horizontal distances from the original location where they were spilled.

The final entrapment is commonly conceptualized as one of two idealized geometries: residual ganglia and blobs (regions of low saturation) and pools (regions of high saturation). Pooling may occur in different entrapment scenarios like accumulation on a low permeability layer (Kueper et al., 1989) or entrapment within coarse lenses

(Saba and Illangasekare, 2000). Pools will provide an additional contaminant source with a longevity far in excess of that of residual liquid (Kueper and Frind, 1991a).

The process leading to DNAPL pools has been described by McWhorter and Kueper (1996). Upon encountering a stratum that it is unable to penetrate due to high entry pressures, the DNAPL will accumulate and spread laterally to form a pool. In a pool, the maximum capillary pressure occurs at the base. This pressure is directly proportional to both the pool thickness and the density difference between the DNAPL and aqueous phases. This indicates that DNAPLs with large specific gravities are less likely to form large pools than are DNAPLs with specific gravities near unity, other factors being equal (Kueper et al., 1993).

Figure 2.2. Pressure distribution within a DNAPL pool
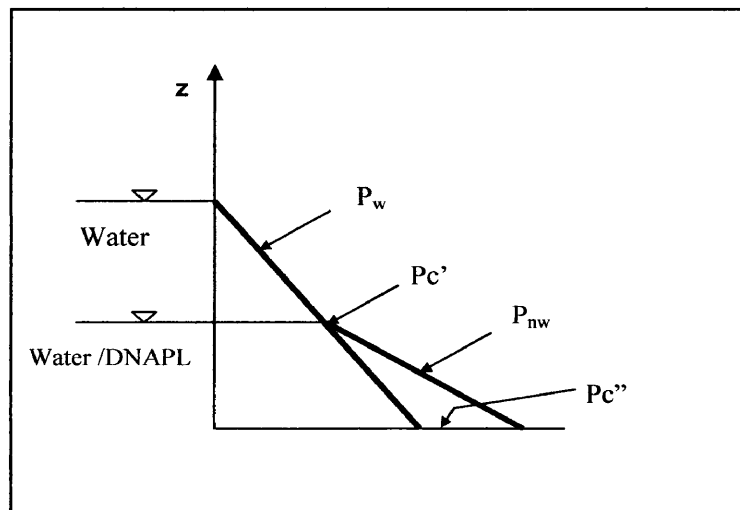
The thickness of a pool can be represented using the following equation:

$$H = \frac{Pc''-Pc'}{\Delta\rho g} \tag{2.1}$$

where Pc" is the capillary pressure at the bottom of the pool, Pc' is the capillary pressure at the top, $\Delta\rho$ the density difference between DNAPL and water and g is gravity (see Figure 2.2).

If investigations eventually establish the thickness and area of a given DNAPL pool, it will be possible to estimate the volume of DNAPL. This is accomplished by evaluating:

$$V_{NW} = \phi \int_{0}^{T} (1 - S_W)dZ \tag{2.2}$$

where V_{NW} is the volume of DNAPL per unit area, S_w is the water saturation, and Φ is the porosity of the medium.

The DNAPL entrapment affects the permeability distribution in a heterogeneous porous media. This dissertation focuses on the impact of DNAPL entrapment in tracer characterization. To evaluate the impact of tracer behavior in this issue, it is necessary to have an understanding of how DNAPLs are distributed in porous media. The final architecture depends on all the entrapment mechanisms.

In a recent report, DNAPL source zone architecture was defined as the sizes, shapes, volumes and connections of the DNAPL sub-zones and their hydrodynamic interactions with the more permeable regions within the aquifer. That is, "architecture" defines both the morphological features of the NAPL sub-zones (such as spatial distribution patterns, DNAPL saturation, etc) and their functions in terms of

hydrodynamic accessibility (i.e. dissolution rate, mass transfer coefficient, etc) (Kavanaugh et al., 2003).

The distribution of DNAPLs has been evaluated in theoretical terms, laboratory experiments and field experiments. Since laboratory experiments are performed in one-dimensional columns and two dimensional cells, the spreading is constrained due to the dimensionality. Field experiments offer the opportunity to evaluate the DNAPL migration into a naturally occurring aquifer. Kueper et al. (1993) examined the distribution of residual and pooled PCE after the release of the contaminant below the water table. It was observed during the excavation process that the PCE was distinctly present in the form of pools ranging in thickness from a few millimeters to several centimeters. A small number of experiments in the literature have evaluated the NAPL distribution in field settings (Michalski et al.,1995; Oolman et al., 1995). Even though the number of field studies is limited, they all suggest that high saturation zones are present when DNAPL is spilled in natural heterogeneous systems.

2.2 Characterization of DNAPL Sites

Due to the physical and chemical properties of DNAPLs and the natural heterogeneity of the subsurface, detection and delineation of contaminant source zones has become one of the most significant challenges limiting effective cleanup (Rao et al., 2000).

As pointed out by Kram et al. (2001), different approaches in site management include a particular method as a part of the overall characterization effort. Therefore in the field, a combination of these methods is applied to successfully achieve effective remedial design.

The different methods will be classified in three groups:

- Baseline and sampling methods (groundwater sampling, soil sampling)
- Geophysical techniques
- Tracer methods

Baseline characterization methods typically consist of sampling during drilling operations. Samples are collected using conventional drilling equipment and are analyzed using EPA-approved methods for identifying VOCs. This can lead to underestimation of actual concentration due to mass losses during handling and transport (Kram et al. 2001).

One of the methods found in the literature to help identify DNAPL source zones is to analyze concentrations in monitoring wells. Johnson and Pankow (1992) and Anderson et al. (1992) described the use of downgradient solute concentration to locate DNAPL source zones through the application of analytical models. One of the main disadvantages of this technique is the difficulty to determine DNAPL volume.

The main disadvantage of traditional techniques for characterization is the inability to resolve the spatial variability of most of the DNAPL sites; however, they are useful as prior information in the application of other techniques.

The application of geophysical methods to assess soil contamination has become possible as data handling has become more and more accurate (Weil et al. 1994). Circumstances in which hydrocarbon and organic contamination can be detected by noninvasive geophysical methods at hazardous waste sites are described by Olhoeft (1992a). The lack of background data prior to the spill limits the capability of geophysical methods to detect DNAPLs. However, they can be successfully applied to assess plume migration.

Different geophysical methods could be applied for characterization; seismic reflection methods have only recently been developed into a practical tool for evaluating shallow environmental sites at depths from 2 to 100 meters (Phillips and Fitterman, 1995). Steeples and Miller (1993) reviewed the principles behind shallow seismic

reflection profiling. Miller (1992) discussed the importance of using appropriate signal processing for shallow seismic reflection data.

The use of Ground Penetrating Radar for observing DNAPL migration has been carried out since the late 1980's. An investigation by Brewster et al. (1995) was made in a saturated sandy aquifer. Tetrachloroethylene (TCE) was spilled into the aquifer and the migration of the plume was successfully monitored with GPR and other geophysical methods. Pooling and lateral spreading of TCE on low permeability layers were observed.

Other geophysical methods that are being investigated, improved or satisfactorily applied for contaminant plume characterization are: electromagnetic methods, where the use of higher frequencies is being investigated since they can provide greater resolution and increased sensitivity to variations in dielectric properties of the ground (Stewart et al., 1994); complex resistivity (Olhoeft, 1992a); borehole geophysical logging (Paillet, 1993); tomography and cone penetrometer.

The performance of geophysical methods is constrained by the available computational resources, the type and density of data collected and the type of information desired from inversion. Also, some techniques have limited penetration in the subsurface, their resolution is constrained when encountering low permeability layers and they are susceptible to interference.

One of the advantages of tracer versus geophysical methods for NAPL characterization is that tracers can provide information about the system without the need of high performance computational resources. However, this may not be true as the need for detail in the site increases and more data have to be processed.

There are many classifications of tracers in the literature. Rao et al. (2000) classified tracers into four categories: (1) non reactive tracers used for hydrodynamic characterization (2) partitioning tracers that selectively partition into the NAPL (3) interfacial tracers that only accumulate at the NAPL-water interfaces, but do partition into the NAPL and (4) bio-geochemical tracers that are used to quantify abiotic and biotic

reactivity. All of the tracer techniques are based on the injection of tracers into the aquifer through one or more injection wells and subsequent measurement of tracer concentration downstream at production wells.

Non reactive or conservative tracers used for aquifer characterization provide information about critical parameters like hydraulic conductivity, porosity and dispersivity (Barth et al. 1999). Characterization of aquifer parameters using this type of tracer is well established in environmental hydrology (Sudicky, 1986; Garabedian et al., 1991; Thorbjarnason et al., 1994; Farrel, 1994; Mackay et al., 1994).

Partitioning and interfacial tracers follow the same experimental approach; a pulse of non-reactive and reactive tracers is forced through the contaminated zone. In practice, identification of a DNAPL zone is necessary prior to setting up the tracer test using other types of characterization (e.g. groundwater sampling, core sampling). While partitioning tracers provide values of saturation (S_n), interfacial tracers provide values for the NAPL-water contact area (a_{nw}).

Interfacial tracers utilize a water-soluble surfactant as a tracer that is adsorbed at the NAPL-water or air-water interface, but does not partition into the bulk NAPL or air phase from the flowing phase (Kim et al., 1999). Annable et al. (1998b), Rao et al. (1998) and Dai et al. (2002) discussed the tandem use of partitioning and interfacial tracers for characterizing the NAPL amount as well as the spatial distribution and morphology of the entrapped NAPL regions.

Bio-chemical tracers are used to estimate the kinetics of microbial or abiotic reactions (Rao et al., 2000). Reactive tracers here serve as electron acceptors or electron donors for a particular microbially mediated redox reaction (Istok et al., 1997).

14

2.3 The Partition Interwell Tracer Technique

Partitioning tracer tests, whether in the saturated or unsaturated zone, may be used to (1) detect and locate NAPL contamination; (2) estimate the NAPL volume present; (3) assess remediation performance.

Different chemicals have been used as partitioning tracers; Hunkeler et al. (1997) investigated the use of ^{222}Rn, a naturally occurring radioactive isotope as a partitioning tracer. The advantage of using ^{222}Rn versus artificial tracers is that ^{222}Rn avoids the use of a groundwater injection scheme that artificial tracers require. However, when using ^{222}Rn as a partitioning tracer, the saturation close to the monitoring well is weighted more strongly than the NAPL saturation further away since ^{222}Rn activities re-equilibrate in response to changes in NAPL saturation. Therefore, the location of the wells with respect to the source zone is a factor that has to be carefully considered in the application of this technique (Hunkeler et al. 1997).

Other chemicals used as partitioning tracers for hydrocarbon detection and quantification are sulfur hexafluoride (Wilson et al., 1993) and chlorofluorinated hydrocarbons (Tang et al., 1991). The perfluorocarbon family has also been found suitable for use as air/LNAPL partitioning tracers for vadose zone characterization, demonstrating a spectrum of partition coefficient values adequate for detection of a wide range of LNAPL saturations (Mariner et al., 1999; Deeds et al., 2000).

Dissolved helium and neon gases have been recently evaluated as partitioning tracers for the saturated zone; they were used previously used as conservative tracers to determine hydrogeological parameters (Wilson and Mackay, 1996; Vulava et al., 2002). The low analytical detection limits possible with dissolved helium and neon (4 to 5 orders of magnitude below aqueous solubility) may permit improve characterization of the tail region of the breakthrough curves compare to commonly used alcohol partitioning tracers (Divine et al., 2003). However, application of these tracers may be complicated if trapped air is present in the aquifer.

Another variation of the PITT is the "Push-Pull" partitioning tracer test that is based on single-well injection-extraction. In this type of test, retardation factors for injected partitioning tracers are estimated from the increase in apparent dispersion observed in extraction-phase breakthrough curves in the presence of DNAPL (Davis et al., 2002). Preliminary studies show that this technique is able to detect the presence of DNAPL, however, additional research is needed to verify the ability of the test to quantify NAPL saturations.

The objective of this dissertation is the improvement of partitioning tracer test in the field, so alcohols were the chemicals selected as tracers for this study. Alcohols have been object of many investigations and so far, they have demonstrated more applicability in the field than other chemicals.

2.3.1 Description of the PITT

In implementing PITT, a tracer solution consisting of at least one conservative tracer and mixture of chemicals with different partition coefficients is introduced in the NAPL source zone. Partitioning tracers undergo retardation while the conservative tracer will not be affected by the presence of DNAPL (see Figure 2.3). The chromatographic separation of the non-partitioning and partitioning tracer pulses depends of fraction the time that the tracer spends in the NAPL phase compared to that in water.

Figure 2.3. Schematic of the partitioning and conservative tracer pathways when they encounter the DNAPL phase.
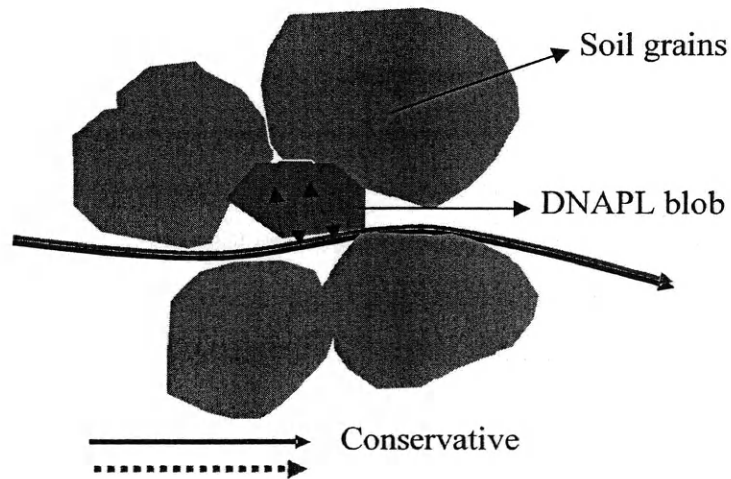
The retardation of the tracers will depend on the partition coefficient and NAPL saturation. The theoretical basis of the use of partitioning tracers has been described in detail by Jin et al. (1995). The assumptions made in the development of the technique are:

1. The only mechanism responsible for retardation is the presence of NAPL.
2. Small changes in NAPL composition don't affect the water-NAPL partition coefficient. These coefficients have to be robust.

2.3.2 Data Analysis: Method of Moments and Inverse Modeling

Several data analysis methods are available to estimated subsurface properties from field data. In particular, these methods are: method of moments, automatic history matching and trial and error calibration (Jin et al. 1995).

Since analytical solutions for tracer transport are not always available, a method originally described by Aris (1958) can be applied. The method derives expressions for the time moments of the concentration curves that would result from an instantaneous input of mass (Valocchi, 1985). This technique called "moment analysis" is a standard chemical engineering method that has been successfully employed for the estimation of rate parameters in packed-bed reactors (Fahim et al., 1982).

The nth temporal moment m_n at a particular location is defined as:

$$m_n = \int_0^\infty t^n C(t) dt \qquad (2.3)$$

where t is time and C(t) is the value of concentration at that given time.

The nth normalized temporal moment μ'_n is given by:

$$\mu'_n = \frac{\int_0^\infty t^n C(t) dt}{\int_0^\infty C(t) dt} \qquad (2.4)$$

The zeroth moment at a particular location is the area under the breakthrough curve recorded at that location. The product of the zeroth moment and the groundwater flux provides a measure of the mass to pass the location (Harvey and Gorelick, 1995).

If the tracer input deviates from the instantaneous tracer pulse (Dirac function), then the corrected mean residence time is given by

$$t_i = \mu_i^{'} - \frac{t_D}{2} \qquad (2.5)$$

where t_i is the travel time of a tracer i, μ_1 is the normalized first moment and t_D is the time of a constant tracer injection.

The retardation of a partitioning tracer can be calculated estimating travel times (with Equation 2.5) for both conservative and partitioning tracers.

Knowing the retardation and the DNAPL-water partition coefficient, the average saturation can be estimated using (Jin et al., 1995)

$$R = 1 + \frac{Kp \cdot S_N}{(1 - S_N)} = \frac{t_p}{t_n} \qquad (2.6)$$

where t_p and t_n are the travel times of the partitioning and conservative tracer respectively, Kp is the partition coefficient of the partitioning tracer and S_N is the NAPL saturation.

Knowing both saturation and t_n, the tracer-swept pore volume (Vp) can be estimated for a particular extraction well by;

$$V_p = \frac{m}{M} \frac{Q \cdot t_n}{1 - S_N} \qquad (2.7)$$

where M is the total mass of tracer injected, m is the tracer mass produced from the extraction well under consideration, and Q is the total fluid injection rate at the injection well. The DNAPL volume in the tracer-swept pore volume is then calculated by $V_D = S_N$ $*V_p$ (Young et al., 1999).

Even though Jin et al. (1995) used these equations for partitioning tracers assuming that local equilibrium between phases exists, it has been shown that Equation

2.6 is still valid under non equilibrium conditions. As stated by Harvey and Gorelick (1995), the zeroth and first moment are independent of rate coefficients, regardless of non-equilibrium conditions or spatial heterogeneities in either the velocity or the rate coefficients.

This method has some disadvantages that could introduce some error in the analysis of partitioning tracer data and consequently affect the estimation of DNAPL mass. One of the shortcomings that method of moments presents is that the weighting factor t_n (Equation 2.3) puts a large weight on the tail portion of the signal. Errors in tail portion of the concentration curves are magnified in evaluating central moments. This issue is investigated in detail by Fahim et al. (1982). Another disadvantage is that it produces a lumped value of saturation and does not provide any information about location of the NAPL within the tracer swept volume.

Other methods available for parameter estimation of saturation using field tracer data are trial-and-error calibration and inverse modeling (automated calibration). Both of them are based on the same principle: adjusting parameters and simulated values to match field observations (Poeter and Hill, 1997).

In this dissertation, method of moments and inverse modeling were used for parameter estimation. The code is based on the nonlinear least-square regression method. Some of the advantages of using automated calibration versus trial-and-error are based on the additional results that the former provides, like the quantification of (1) quality of calibration, (2) data shortcoming and needs, and (3) confidence intervals (Poeter and Hill, 1997).

Using this method, we hope to overcome some of the problems that the method of moments presents. Also, using inverse modeling procedures, it is possible to obtain more than one lumped value of saturation. If the number of observations is enough, parameterization of the saturation can provide different values for different zones of the aquifer. However, most data only support the estimation of relatively few parameters (Poeter et al., 1998). The approach suggested by the authors of this code is to begin with

simple models and incorporate complexity, in this case begin with one or a few parameters and increase this number based on the ability of the model to match observed values.

Evaluation of estimation performance of DNAPL mass by both methods (moments and inverse modeling) is conducted in this work.

2.3.3 Limitations of the PITT

The use of PITT for DNAPL characterization has increased in recent years, primarily to assess remediation performance (Rao, 1997; Jawitz et al,, 1998; Meinardus et al., 2002; Brooks et al., 2002). Comparisons between traditional methods and this new technique were performed in order to validate the reliability of the estimated parameters.

Some of the factors that have been identified to decrease the accuracy of NAPL characterization by partitioning tracers are: nonlinear partitioning behavior (Wise et al., 1999), non-equilibrium partitioning (Dwarakanath et al., 1999; Willson et al., 2000), background tracer retardation (Jin et al., 1997), poor sweep efficiency (Jin et al., 1997; Nelson et al., 1999), variable NAPL composition (Dwarakanath et al., 1999), co-tracer effects (Imhoff et al., 2003), tracer degradation (Annable et al., 1998), and heterogeneous NAPL distributions (Nelson et al., 1999; Rao et al., 2000). Most of these limitations have been reduced over the years with experimentation that led to improvement of tracer protocols, however, issues related to NAPL distribution have not been resolved yet.

The technique shows still major limitations in conditions of heterogeneity; tracer tests are expected to result in an underestimation under certain conditions where the hydrodynamic accessibility is constrained or non-equilibrium mass transfer occurs. Traditional application of this technique assumes local equilibrium exists between

phases. This may not be applicable in situations where DNAPLs are entrapped under high saturations such in pool. Jin et al. (1997) used UTCHEM model simulations to estimate the relative error associated with NAPL detection in pools. Data obtained at DNAPL sites suggest that the estimation errors are larger than the estimated based on numerical modeling analysis (Rao et al., 2000).

Others researchers looked at this problem in the laboratory; Nelson et al. (1999), observed the influence of heterogeneity on tracer performance, using a 2D tank with two different types of TCE entrapment. Dai et al.(2001) extended this work with the tandem use of interfacial and partitioning tracers in high LNAPL saturation zones created in 1D column experiments. Results of that study showed that improvement of design protocol and testing methodology had to be implemented, suggesting the use of kinetic (as opposed to equilibrium) data assessment models. The validity of the equilibrium assumption (Valocchi, 1985) applied to tracers has been explored by different authors. This assumption considers that the tracer residence time is enough to achieve equilibrium concentrations in both water and NAPL phases. The value of the equilibrium concentration depends on the tracer partition coefficient:

$$Kp = \frac{C_{i,N}}{C_{i,w}} \qquad (2.8)$$

where $C_{i,N}$ represents the concentration of tracer i in the NAPL phase, and $C_{i,w}$ is the concentration of that same tracer in water.

The resistance to equilibrium due to non uniform distribution or high local velocities is called "mass transfer limitations". To explore this issue, researchers have analyzed tracer breakthrough data using single and dual domain models. Willson et al. (2000) evaluated mass transfer limitation effects comparing local equilibrium and rate models in combination with laboratory experiments and concluded that a greater understanding of the tracer limitations in the field scale is necessary. Jalbert et al. (2003)

developed a dual domain model where a fraction F of the NAPL consists of instantaneous sites and a fraction (1-F) consisted of rate-limited sites. Imhoff and Pirestani (2004) also compared single and dual domain models to interpret the data obtained from a set of one dimensional experiment. Both modeling approaches were capable of matching experimental data. However, the input parameters necessary to use these models are normally unknown in the field as well as the importance of mass transfer limitations before conducting a tracer test.

Evaluation of the up-scaling methodologies, where parameters measured at the pore scale are up-scaled to analyze tracer breakthrough curves at much larger scales have not been explored yet and it is within the scope of this study.

2.4 Stochastic Theory

The geological properties of natural aquifers are intrinsically deterministic. However, the limitations and cost of direct or indirect sampling reduces the number of observations and we usually have an incomplete knowledge of their values. Observations are made in a few locations and the degree of variability between observed points is uncertain. Despite the improvement in characterization techniques, the uncertainty, as a result of heterogeneity and number of observations, cannot be eliminated.

The theory of stochastic processes provides a method for evaluating uncertainty. In the stochastic formalism, uncertainty is represented by probability or by statistical moments (Zhang, 2002).

Parameters like porosity or hydraulic conductivity are not purely random, so they are treated as random space functions whose variabilities exhibit some spatial correlation structures. When the hydraulic conductivity field is treated as a random space function

(or a spatial stochastic process), the dependent variables head and flux also become random space functions. The governing equations (in this case Darcy's law and continuity) become stochastic differential equations whose solutions are no longer deterministic numbers but probability distributions of the dependent variables. When the distribution is normal, it can be statistically described with the mean μ_k, the variance of the mean $\sigma^2_{\ln k}$, and the correlation length λ.

$$\mu_K = E[K] = \int\limits_{-\infty}^{+\infty} k f_K(k)\,dk \tag{2.9}$$

$$\sigma_K^2 = E\left[(K - \mu_K)^2\right] = \int (k - \mu_k)^2 f_K(k)\,dk \tag{2.10}$$

The mean and the variance provide overall statistics that are independent of the spatial organization. The correlation length is also used to describe the hydraulic conductivity field. It can be described as the distance in which there is correlation to that property. In other words, beyond that distance, the correlation starts to become insignificant (Gelhar and Axness, 1983).

Stochastic analysis requires that the random field is stationary and that it satisfies the ergodic assumption. Stationarity requires that the mean is constant and the covariance is only a function of separation. The ergodic assumption requires that all states of the ensemble of a stochastic process are available in each realization of the process.

Two different approaches are used to solve stochastic equations: the moment equation methods, where governing equations are first derived from the stochastic differential equations and are then solved numerically or analytically, and the Monte Carlo simulation method. This last one is an alternative method to the moment equation approach and perhaps the most straightforward technique for solving stochastic equations

(Zhang, 2002). The Monte Carlo approach involves three steps; the first one is the generation of multiple realizations with known statistical properties. Some of the techniques available for random field generation are the turning bands method (Matheron, 1973), spectral methods (Gutjahr, 1989) and matrix decomposition (Clifton and Neuman, 1982; Robin et al. 1993). The second step involves solving, for each realization, the governing equations by numerical methods. The last step is to average over the solutions of all the realizations generated in the first step.

The stochastic theory in this investigation is used in an attempt to generalize findings using the Monte Carlo approach. In Chapter 7, a mean and a variance representative of a heterogeneous field site is applied to create a collection of realizations with those statistical properties. One of these realizations is selected and physically created in a two dimensional tank; the rest of the realizations are analyzed using numerical simulations. The average of the results is used as a tool to evaluate the influence of certain input parameters on tracer performance for heterogeneous aquifers.

2.5 Preliminary Experiments

A set of 2D cell experiments was performed to evaluate tracer behavior for simple isolated NAPL entrapment configurations. The objective of these experiments was to investigate possible causes for underestimation of saturation by PITT in simple DNAPL formations. An understanding of the processes and mechanisms of tracers in the laboratory is a prerequisite to develop improved methods for conducting and interpreting partitioning tracer tests.

The experiments were conducted in a 53 cm long by 40 cm tall by 5 cm wide flow cell (see Figure 2.4). The tank was constructed using a 0.5 cm thick polycarbonate sheet to allow frontal visualization attached to an aluminum frame.

An injection well was used to release the tracers in the cell with an Acuflow Series II HPLC pump to provide constant flow rate for the injected tracer solution.

In all experiments, white silica sand with the trade name Unimin Silica was used as the porous medium. Two different sand sizes, classified as course (No.8) and fine (No.70) were selected (see Table 2.1). A layer of bentonite clay was packed at the top of the cell, to create confined conditions and avoid evaporation of the alcohols.

Table 2.1. Table of properties of test sands (Illangasekare et al., 1995)

Sand	D_{50}	Uniformity	$P_d(m)$	S_r	K(m/s)
8	1.50	1.39	0.037	0.11	0.01200
70	0.19	1.86	0.250	0.30	0.00024

Two distinctive zones were created in the cell (see Figure 2.4). Zone A contained the fine number 70 sand homogenously packed and zone B contained a coarser sand block where DNAPL was injected. These conditions represent a system where DNAPL moving downward has been entrapped in a coarser media and arrested by an aquitard. Upon encountering a stratum that it is unable to penetrate, the DNAPL will accumulate and spread laterally to form a pool (McWhorter and Kueper, 1996). The dimensions of the coarser zone block were 10 cm x 5 cm x 3 cm.

HFE-7100 was used as the representative DNAPL (see Chapter 3 for characteristics) and it was injected in the source zone block using a syringe. HFE was fully contained due to capillary barrier effects. Through an injection/sampling port located at the bottom of the number 8 sand- block, a volume of 25 ml was injected until

the HFE reached the top area of the coarser sand block. The creation of the source zone in this way allowed the saturation to be longitudinally homogenous.

Initially, within the block, a high saturation HFE pool was created and then, a volume of HFE was drained out of the cell consecutively creating four different pools defined by the DNAPL volume entrapped (see Figure 2.4). Tracer tests were performed for each of these pool configurations to evaluate tracer response to different volumes of DNAPL.

When packing and emplacement of DNAPL were finished, steady state conditions were achieved. The flow rate across the cell was set at 5 ml/min, which is low enough to allow equilibrium partitioning and large enough to not be affected by the sampling volume.

Sodium bromide served as the conservative tracer and 2,4-dimethyl-3-pentanol, n-hexanol, and 6-methyl-2 heptanol were selected as the partitioning tracers. The partition coefficients for all the alcohols was previously determined in batch experiments (6.55, 1.46 and 13.38, respectively)

Figure 2.4. Schematic of the flow cell and pictures of the contaminated block for the four experiments.
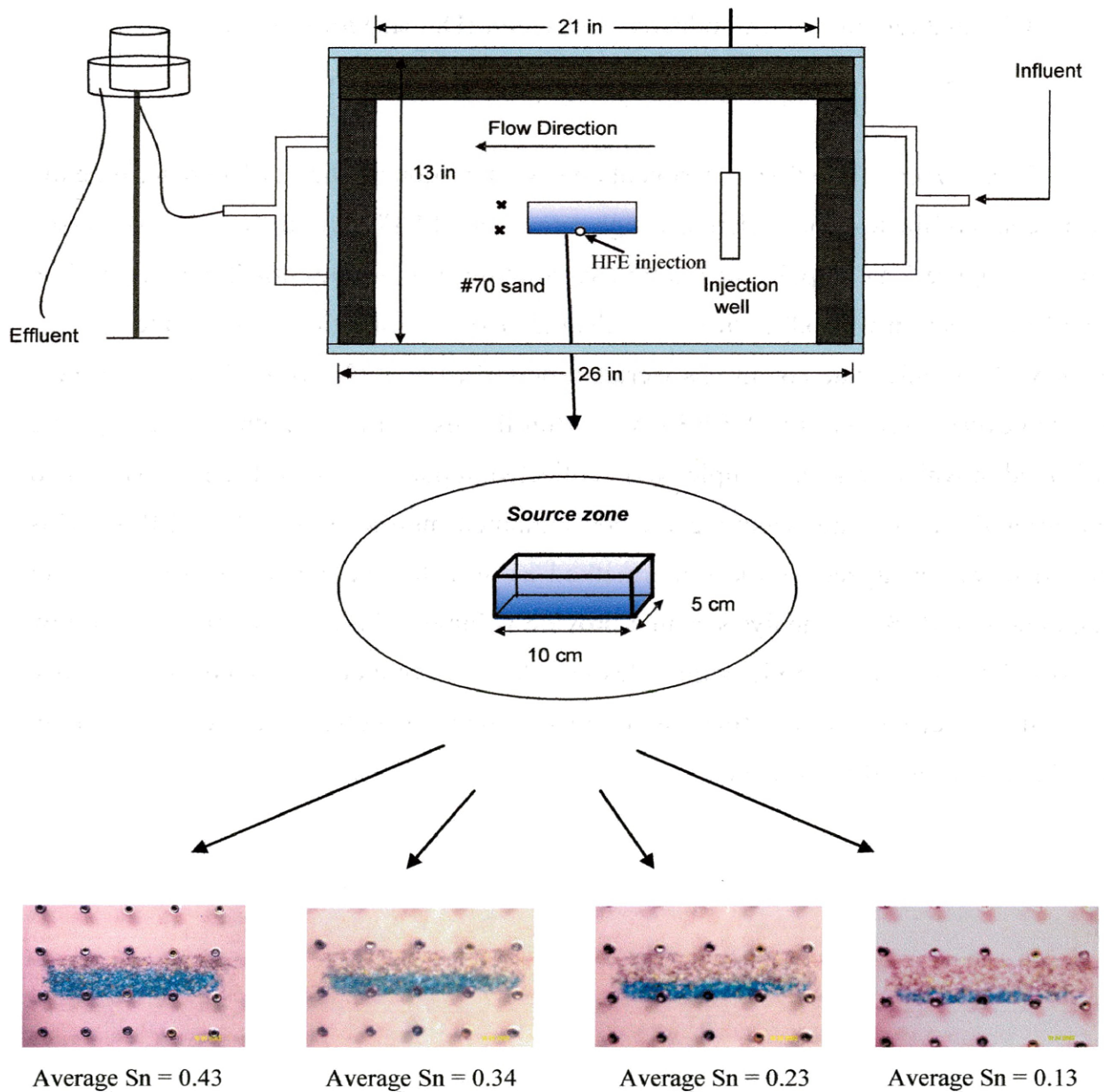
A pulse of tracer solution containing 400 ppm of DMP, 600 ppm of hexanol, 500 ppm of 6M2H, and 500 ppm of sodium bromide was pumped into the injection well. The samples collected during the experiments were analyzed using HP6890 Gas Chromatography with Flame Ionization Detector (Hewlett Packard) for alcohol tracers and Ion Chromatography with Conductivity Detector (Dionex) for bromide.

Experiment 1. The first experiment consisted in running the PITT to determine the effectiveness of the test for a relatively high saturation of HFE over the coarser block (see Exp. 1 in Figure 2.4). A pulse of multitracer solution was injected for 2 hours, the flow rate of the injection was 0.8 ml/min, less than 20% of the total flow through the tank. In this way, the steady state conditions were not perturbed. Samples from the effluent were collected every 30 minutes in 1.5 ml vials. After this experiment, another tracer test was performed in which aqueous samples were collected in ports A and B (Figure 2.4) located right after the pool. This sampling method emulated multilevel samplers (MLS). This tracer data was analyzed by the same method as used for the extraction well or outlet data, although MLS data analysis cannot provide volume estimates since there is no flow rate associated with the sample points. Hexanol data are not included in the analysis since the partition coefficient of this tracer is so low (1.46) that a negligible value of retardation was obtained from HFE presence.

Table 2.2. Results of tracer experiments for the first HFE entrapment volume.

POOL WITH 25 ML OF HFE. S=0.41			DMP	6M2H
Outlet	Retardation (R)		1.023	--
	Saturation		0.002	--
	Swept volume (ml)		458.85	--
	% Estimated		**3.55%**	--
Sampling ports	R	Port A	1.12	1.08
		Port B	1.14	1.08

Experiment 2. For the second experiment, a fraction of HFE was extracted from the source zone. This was executed using a syringe connected to a two way valve. The syringe was placed at the bottom of the source zone and the valve was opened, extracting 4.41 ml of DNAPL. The average saturation over the source zone was reduced to 0.34 (see Exp. 2 in Figure 2.4). After the HFE drainage, a partitioning tracer test with the same exact conditions as in Exp. 1 was performed (see Table 2.3)

Table 2.3. Results of tracer experiments for the second HFE entrapment volume.

POOL WITH 14.79 ML OF HFE. S = 0.34			DMP	6M2H
Outlet	Retardation (R)		1.115	1.059
	Saturation		0.017	0.0045
	Swept volume (ml)		413.80	408.61
	% Estimated		**34.95%**	**8.85%**
Sampling ports.	R	Port A	1.06	1.08
		Port B	1.08	1.08

Experiment 3. The same procedure from Exp. 2 was repeated, leaving a remaining volume of HFE in the coarser block of 14.03 ml. Sampling port experiments were not performed for this configuration.

Table 2.4. Results of tracer experiments for the third HFE entrapment volume.

POOL WITH 8.23 ML OF HFE. S = 0.23		DMP	6M2H
	Retardation (R)	1.13	1.136
Outlet	Saturation	0.02	0.010
	Swept volume (ml)	463.58	444.49
	% Estimated	**66.40%**	**32.12%**

Experiment 4. The extraction of 3.93 ml left a remaining volume of 10.1 ml. All the rest of the parameters were maintain for all the experiments; flow rate, injection and extraction patterns, etc. The purpose is to evaluate the efficacy of the PITT as a function of saturation.

Table 2.5. Results of tracer experiments for the forth HFE entrapment volume.

POOL WITH 1.73 ML OF HFE. S = 0.16		DMP	6M2H
	Retardation (R)	1.14	1.25
Outlet	Saturation	0.021	0.018
	% Estimated	**69.00%**	**59.95%**

Results and discussion. A dye tracer test was performed before the tracer experiments. A red food dye was pumped through the injection well as the same rate as the multitracer solution was injected in the experiments. Pictures were taken during the experiment. The objective was to observe the area captured by the tracer front and the uniformity of the packing. The packing of the matrix seemed fairly uniform, the dye also showed an appropriate location of the injection well to create a front that captured the whole contaminated area. The dye traveled faster through the upper region of the coarser block than through the finer sand and it bypassed the area of lower relative permeability at the bottom of the contaminated zone where the DNAPL was pooled.

As the volume of the source zone was reduced, the saturation estimates obtained from the PITT became closer to real values. The retardation was very low in every case (less than 1.2). As studied by Jin at al. (1995) and Dwarakanath et al. (1999), this implies that all the saturation estimates may have error, since there is not enough separation between tracer breakthrough curves.

Results from the four experiments show that as the volume of HFE was reduced in the coarser block, better estimation of the total volume was obtained. Our hypothesis is that as the volume in the pool decreases, DNAPL stays at lower saturations at the top part of the pool and the high saturation zone at the bottom of the pool becomes thinner. This implies that as DNAPL volume is reduced, more DNAPL is exposed to the tracer due to the saturation distribution. This new distribution results in less mass transfer limitations.

Figure 2.5 shows the percentage estimated as the volume of HFE decreases. The estimation percentage reaches a plateau at 65 %. This is probably happening because of the physical properties of HFE; its viscosity is so low that even at low volumes it creates a sharp pool. Also the media used in this experiment is fairly coarse, so capillary forces are expected to be really small, contributing to this sharpness.

Concentrations of all the tracers from the outlet were extremely dilute, introducing error in the method of moment calculations. In subsequent experiments, the injection well was not used. Tracers were injected as water flow through the whole

experimental domain, and water flush followed the tracer pulse. In this way, stronger signals were expected, enhancing the precise determination of chromatographic separation between tracers.

This set of experiments provided a good qualitative study of how tracers behave in a single isolated DNAPL pool.

Figure 2.5. Plot representing the efficacy of the PITT as a function of DNAPL volume in the coarser block.
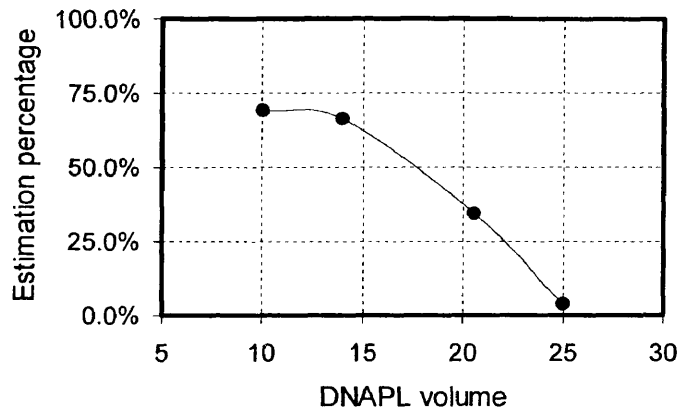
2.6 Hypotheses

With information obtained from preliminary experiments and extensive literature review, the following hypotheses were developed:

a) The influence of natural heterogeneity on the distribution and saturation of NAPL creates entrapment configurations (pools) where the tracer behavior is not necessarily controlled by local equilibrium. This results in underestimation of contaminant mass (as

shown in preliminary experiments). However, tracers may have identifiable tracer signatures that could be used to conduct estimation error analysis.

b) The morphology of the DNAPL entrapment has a great influence on the performance of PITT. The pool is conceptualized in this investigation as a <u>zone of high saturation that doesn't have a defined upper boundary; it has a transition zone that ranges from residual to high saturation</u> (see Figure 2.6). The greater the transition zone is with respect to the total contaminated area the less underestimation of the total DNAPL volume will be obtained using the PITT test. Consequently, the ratio depth of transition zone/high saturation zone could be a key factor on performance of the test. This ratio will depend of the factors that influence the formation of source zone; type of DNAPL, porous media, volume of the spill, etc.

Figure 2.6. Conceptual pool model.

34
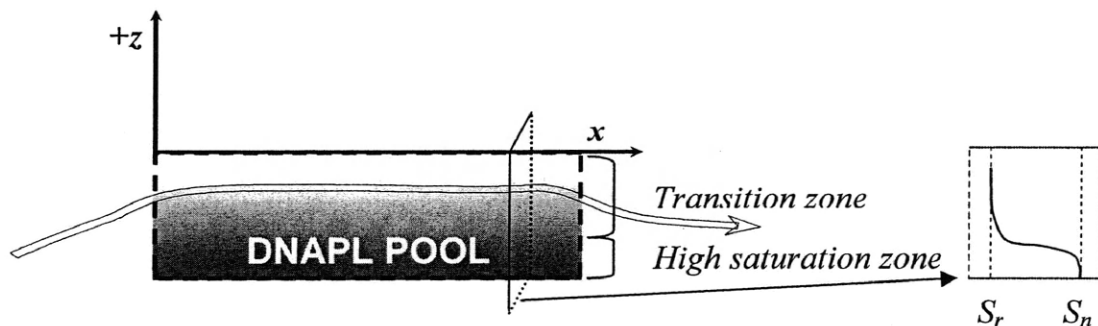
c)   Underestimation of DNAPL volume is attributed to hydrodynamic inaccessibility in combination with non equilibrium behavior. Evaluation of the sensitivity of parameters that affect this underestimation could provide information about correction actions that could be taken in the PITT.

d)   Using an intermediate scale tank and numerical modeling analysis, the technique could be validated for sufficiently complex conditions. Results from this experiment could provide some indication of the method's potential in the field.

2.7 Objectives and Tasks

The primary objective of this research is to evaluate the extensions and limitations of tracer tests to improve NAPL characterization. The detailed investigation in the laboratory scale will provide the opportunity to obtain an understanding of the limiting processes, allowing modification of current tracer protocols.

To achieve the stated objectives, the following research tasks were performed:

1)   Conduct a series of batch experiments in the laboratory to create a data set of partition coefficients and the influence of equilibration time. Properties of the selected partitioning tracers and representative DNAPLs were studied as well.

2)   Conduct a set of 2D cell experiments using X-ray characterization in combination with PITT to evaluate the influence of pool morphology on tracer performance.

3)   Evaluate capability of existing numerical models to simulate flow, tracer transport and partitioning behavior. Selection of the codes that will suit better these purposes.

Comparison of the data analysis performance of the selected numerical model with respect to method of moments.

4) Calibrate preliminary experiments with the selected numerical models and perform sensitivity analysis to investigate parameters that affect the PITT effectiveness. Establish methods to improve mass estimation errors.

5) Conduct a set of 2D intermediate scale tank experiments emulating real spills. A stochastic heterogeneous random field was generated to represent the effect of field heterogeneity to study tracer behavior in more complex entrapment morphologies. Validation of the methods developed in previous task to improve mass estimation by tracers.

6) Generalize findings for different entrapment architectures using Monte Carlo analysis of all the realizations generated for the intermediate scale tank experiment.

7) Establish a set of guidelines to determine the error or uncertainty that the PITT presents in heterogeneous settings.

Chapter 3

EXPERIMENTAL METHODS AND PROCEDURES

The experimental methods and experiments conducted during this investigation are described in this chapter.

The objective was to create a large data set in controlled settings that allowed for evaluation of the parameters that affect tracer performance. To evaluate the tracer behavior, the study started with simplistic scenarios in the batch scale and complexity was introduced once that fundamental processes were understood. Investigation of the process at different scales is necessary to address issues related to up-scaling processes from the laboratory to the field. The experimental investigation started in the batch scale (1.5 ml vials) and evolved to the intermediate scale (5 m x 1.5 m x 0.05 m artificial aquifers).

All the experiments involved the emplacement or spill of the DNAPL phase. In the 2D cell experiments the DNAPL was emplaced in a coarse layer to create one high saturation zone. In the 2D tank experiments, the DNAPL was spilled into the heterogeneous media and allowed to distribute freely to create a more realistic entrapment configuration. With the use of X-ray or gamma-ray scanning, the DNAPL source zone was accurately characterized. This information was crucial when evaluating the important of DNAPL architecture on the response of tracers in PITT.

Tracer tests were carried out in controlled conditions where flow and head in the domain were monitored and concentration samples were collected and analyzed using ion and gas chromatography.

In this section, all the materials and procedures necessary to generate the experimental data set are described in detail.

3.1 Materials

The materials used for this research are described in this section.

3.1.1 Sands

All the sands used in the experiments were obtained from Unimin Corporation. Clay was also used in some of the experiments to create confined conditions or to protect the bottom of the cells to the DNAPL. The properties of all the sands are described in Table 3.1. Most of the properties have been determined by previous researchers.

Table 3.1. Physical properties of sands used (Saba, 1999) and (Barth, 1999).

Properties	#8	#16	#30	#50	#70	#110
Hydraulic conductivity K, $(10^{-3}$ m/s)	12.0	8.03	1.98	0.406	0.243	0.053
Mean grain size d_{50}, mm	1.50	1.08	0.50	0.32	0.20	0.12
Residual water saturation[b]	0.11	0.07	0.26	0.29	0.30	0.26

3.1.2 DNAPL

The use of DNAPL surrogates was evaluated; the generation of high volumes of toxic NAPL waste (such as PCE and TCE) as well as other issues relating exposure and toxicity during intermediate or large scale tracer test was a major concern. A DNAPL surrogate was chosen based on lack of toxicity, aqueous solubility (high enough to observe dissolution downstream and low enough to allow long-term exposure of the tank), and alcohol tracer partition coefficients similar to common contaminant DNAPLs.

Two single component NAPLs were selected in this study, a surrogate DNAPL Hydrofluoroether (HFE-7100) and a common DNAPL encountered in contaminated sites; tetrachloroethylene (PCE). HFE is a proprietary mixture of methyl ether (nonaflourobutyl) and methyl ether (nonaflouraisobutyl) produced by 3M Novec. This is a clear, colorless and low-odor fluid intended to replace ozone-depleting materials in many applications. HFE-7100 has been accepted for commercial use by regulatory agencies in the USA, and it has been approved under the Significant New Alternatives Policy (SNAP) of the U.S EPA. In addition, HFE-7100 has been excluded by the EPA from the definition of VOC, on the basis that this compound has a negligible contribution to tropospheric ozone formation. Physical properties of this compound are listed in Table 3.2. HFE was used in the preliminary experiments described in section 2.4.

Tetrachloroethylene (PCE) was used as the representative "real" DNAPL for these experiments (Aldrich Chemical). Both DNAPLs (HFE and PCE) were evaluated and properties of interest were measured.

40

Table 3.2. Properties of HFE and PCE

Property	HFE-7100	PCE
CAS number	163702-07-6	127-18-4
Density (g/ml)	1.52	1.623
Viscosity (cp)	0.494	0.89
Interfacial tension (dynes/cm)	13.6	47.5
Solubility (mg/l)	12	200
MCL (mg/L)	N/A	0.005

Time-dependent samples were measured in triplicate with a Cannon-Feske Opaque (Reverse flow) viscometer and the interfacial tension of the mixtures was measured using the Pendant drop technique (Ambwani and Fort, 1979).

Since the DNAPLs selected were used in columns and test cells with a small dye concentration to allow visualization, all the properties were measured for the dyed DNAPLs.

PCE was dyed with a small concentration of Sudan IV (0.01%) and HFE had 1% of Blue Dye.

Attenuation coefficients of both DNAPLs were evaluated for the X-ray and gamma-ray systems. PCE has been previously used in our laboratory so attenuation coefficients have already been measured. However, attenuation techniques have not been used yet to determine saturation of HFE-7100 in porous media.

Studies conducted by Glover (2003) showed that a phase consisting solely of HFE is essentially indistinguishable from water using X-ray attenuation. In order to increase the differences in attenuation coefficients between water and NAPL, several mixtures of HFE with a doping agent were investigated. Iodoheptane was selected as the doping agent because it has attenuation characteristics that are distinctly different from water. However, the use of a multi-component DNAPL introduces certain complexity in the

evaluation of partitioning tracer behavior. The different solubility of the components in the mixture alters the value of the partition coefficient over time. Consequently, HFE was rejected as the representative DNAPL.

PCE was the chemical selected as the representative DNAPL for the following experiments. The physical and chemical properties obtained from this study are necessary for future input in numerical modeling analysis.

3.1.3 Tracers

In order to evaluate the tracer behavior for the selected NAPL, four partitioning tracers were tested. Tracer selection is a really important step in the design of the PITT. The criteria for the tracers included the following (Young et al., 1999):

- Readily available and relatively inexpensive
- Low analytical detection limit
- Insensitive to small spatial variations in the composition of the DNAPL
- Low sorption to aquifer materials

The following tracers fulfill these requirements; isopropanol, 2-methyl-1-butanol, hexanol, 2,2-dimethyl-3-pentanol, and 6-methyl-2-heptanol (see Table 3.3). These tracers were also selected based on the broad range of partition coefficients that they covered. The partition coefficient of the tracers between the NAPL and aqueous phases was determined by equilibrating the alcohol tracer in PCE-water system. These procedures are described in section 3.3.

Table 3.3. Tracers selected

Name	Abbreviation	Density
Isopropanol	IPA	0.785
2-methyl-1-butanol	2M1B	0.819
Hexanol	HEX	0.819
2,2-dimethyl-3-pentanol	DMP	0.825
6-methyl-2-heptanol	6M2H	0.803

Sodium bromide (NaBr, Fisher Scientific) was selected as the conservative tracer. Using this conservative tracer and any of the partitioning tracers, saturations can be calculated based on the retardation of the partitioning tracer with respect to bromide. Bromide breakthrough curves are also used to estimate flow and transport parameters (dispersivity and porosity) with the use of numerical models.

3.2 Measurements

Tracer and DNAPL concentrations were measured using Gas and Ion Chromatography.

3.2.1 Gas and Ion Chromatography

Concentrations of tracers and PCE in the aqueous phase were measured with a Gas Chromatographer (GC). The GC instrument vaporizes the sample and then separates and analyzes the various components. Each component ideally produces a specific spectral peak that is recorded electronically. The size of the peaks is proportional to the quantity of the corresponding substances in the specimen analyzed. A Hewlett Packard

HP 6890 Gas Chromatograph with Flame Ionization Detector (FID) equipped with HP7683 Autosampler/Injector was used in this investigation. The method consisted of the following parameters:

- Injector. The injection volume 1 µl and the syringe size is 10 µl.

- Inlet. The splitless mode is used. The carrier gas is Helium with a total flow of 67.9 ml/min. The pressure is set at 20 psi and the heater at 200°C.

- Column. The DB-624 GC column is set at a constant pressure of 20 psi. The flow through the column is 5 l/min.

- Oven. Set point 55°C, maximum temperature of 235°C and a ramp of 12 °C/min.

- Detector. The Flame Ionization Detector uses hydrogen at a flow rate of 45 ml/min and air flow at 450 ml/min. The nitrogen is set at a constant rate of 25 ml/min. The temperature is set at 250 °C.

Ion chromatography is a form of liquid chromatography that uses ion-exchange resins to separate atomic or molecular ions based on their interaction with the resin. A DIONEX DX 500 chromatographic system was used to analyze bromide. The method consisted in the following parameters:

- Column. A Dionex IonPac AS 14A, 4 mm analytical column (4mm x 250 mm) with an IonPac 14A (4mm x 50mm) guard column was used for the analysis.

- Mobile phase. The eluent solution contains 8mM Na_2CO_3 and 1mM $NaHCO_3$

- Pump. The GP50 pump used 100% of the eluent solution at a flow rate of 1.00 ml/min.

- CD25 detector. 50 mA. The DS3 temperature is set at 26 °C.

- AS50 Autosampler. Injection volume: 25 µl.

44

3.2.2 X-ray and Gamma-ray Scanning

Gamma-ray and X-ray attenuation techniques have been used to determine saturation of chlorinated NAPLs in laboratory settings (Hill and Illangasekare, 2004; Imhoff et al., 2000). Both techniques have been developed from the principle that different materials in a multiphase system of sand, air, water and NAPL attenuate energy by different amounts. They are non-destructive and non-intrusive and they can provide accurate and precise real-time information, and they are more affordable than competing technologies such as NMR/MRI techniques. As a result, photon attenuation instruments have been employed for numerous investigations in the field of environmental engineering (Imhoff, 1995; Okuda, 1996; Willson, 2000).

By evaluating the intensities of a collimated energy beam passed through a sample, phase saturation can be determined. For chlorinated NAPL in a sand sample of 5 cm thickness, NAPL saturation as small as 5 percent can be determined by gamma-ray attenuation (Illangasekare et al., 1994). Detection limits for X-ray attenuation methods may be an order of magnitude smaller (Hill et al., 2000). X-ray attenuation methods also can provide greater spatial resolution of material properties than gamma-ray methods.

The raw data is given in counts. Lambert's law for light transmission through an absorbing medium is used to relate the initial gamma energy counts (I_o) to the emerging gamma counts I. This relationship is given as:

$$I = I_o \exp\left[-\sum_{i=1}^{n} U_i \rho_i x_i\right] \qquad (3.1)$$

where I_o represents the incident count rate, I is the emerging count rate, U is the mass attenuation coefficient (cm^2/g) and x is the path length through the material. The

subscript i represents the phases, in this case PCE and water were the two phases present.

The X-ray system traverses a 3.5 m long by 1.5 m high plane with internal clearance for objects up to 0.36 m (Figure 3.1). LabVIEW software was developed for both systems to provide automated movements synchronized for data collection. Tests have shown that both systems have typical movement times of less than 30 seconds with sub-millimeter positioning accuracy and repeatability.

As with the positioning motors, hardware and software were developed to automate the data collection process. Custom programs continuously collect spectra at specified locations. A high-performance germanium crystal (HPGe) detector is employed in X-ray characterization. This technique was used for the 2D cell experiments described in Chapter 5.

Figure 3.1. X-ray system
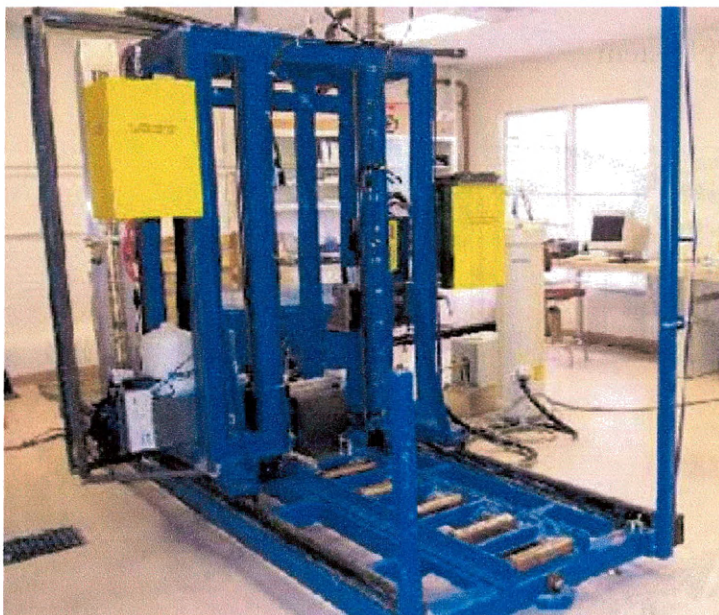
Gamma ray was used for the 2D intermediate scale experiment described in Chapter 6. The X-ray system was not used in this experiment due to the large size of the 2D tank that couldn't suit the requirements of dimensions for the X-ray system area.

The gamma system in our laboratory is capable of precise positioning in a vertical plane that is over 35ft long and 5ft high (Figure 3.2). The motor positioning is set and recorded by custom LabVIEW programs which communicate (over RS-232) with a Baldor embedded controller. Gamma rays are produced by two sealed radioisotope sources: 200 mCi of Americium-241 with a primary peak at 60keV and 50 mCi of Cesium-137 with a primary peak at 662keV which are contained within a collimated source enclosure. The relative strengths of the two gamma sources can be tuned through selective filtering to provide maximum accuracy/precision for the simultaneous measurement of water and oil saturations. More details about the methods, system description and operation can be found in Saba, 1999.

Figure 3.2. Gamma ray system

Attenuation coefficients for the water and dyed PCE were obtained for both sytems following procedures described in Saba, 1999.

3.3 Batch Experiments

Batch experiments were conducted to obtain the partition coefficients of all the tracers selected and the PCE.

The partition coefficient of the tracers between the NAPL and aqueous phases was determined by equilibrating the alcohol tracer in PCE-water system. The tracer solution was diluted in series of concentrations of 0-100% in different increments from the original concentration. Five 1.5 ml samples of each tracer solution were placed in 1.5 ml vials with 0.1 ml of PCE in three of them, capped and then placed in a shaker for 24 hours to allow equilibration of the system. Then, all the samples were centrifuged to achieve the separation of the two phases and then analyzed in a Gas Chromatographer. Concentrations of the tracers in the NAPL phase were plotted against the concentrations of the tracers in the water phase (Figure 3.3). A regression analysis of the plot provided values for the partitioning coefficient of each tracer for the different DNAPL concentrations.

Figure 3.3. Isotherms representing the partitioning between the NAPL and water phase, the partition coefficient is the slope of the linear fit.
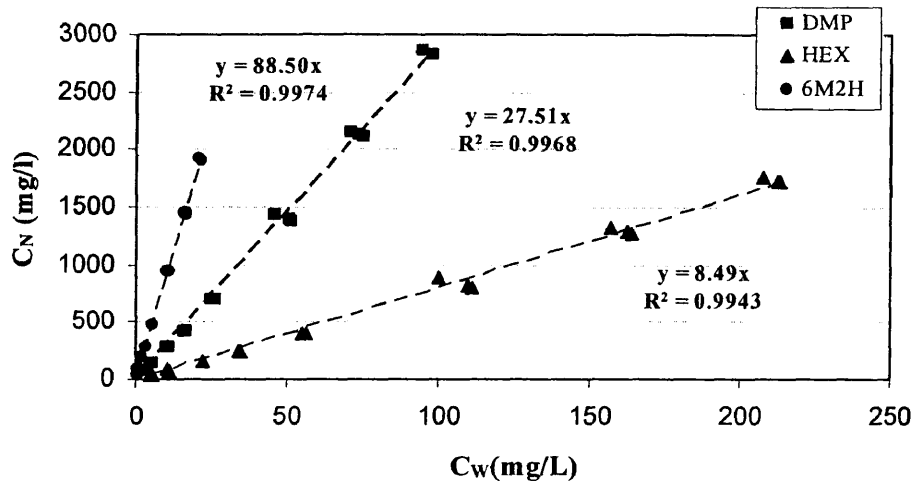
3.4 2D Cell Experiments

A series of experiments in a 2D test cell were conducted in the laboratory. The objective in this set of experiments was to evaluate the influence of pool morphology in tracer performance. Simple entrapment configurations of DNAPL were emplaced in a test cell to achieve a better understanding of fundamental processes and limiting factors. Information gained during these experiments is necessary to address later on more complicated DNAPL occurrences.

Flow experiments were conducted in a 30.5 cm x 22.8 cm x 2.54 cm test cell (Figure 3.4). The front wall of the cell was made of tempered glass to allow for observation. The back wall plate was made of aluminum to allow drilling of ports for sampling and pressure measurements. The glass and aluminum walls were attached to an

aluminum frame. Internal void volume of the cell was nominally 23 cm x 17 cm x 2.54 cm. The sampling ports were located in the cell along 11 horizontal lines, each containing 8 ports spaced 2.54 cm apart. These ports were used to extract aqueous samples for tracer analysis and to monitor the pressure in the tank.

Figure 3.4. Schematic of the flow cell.
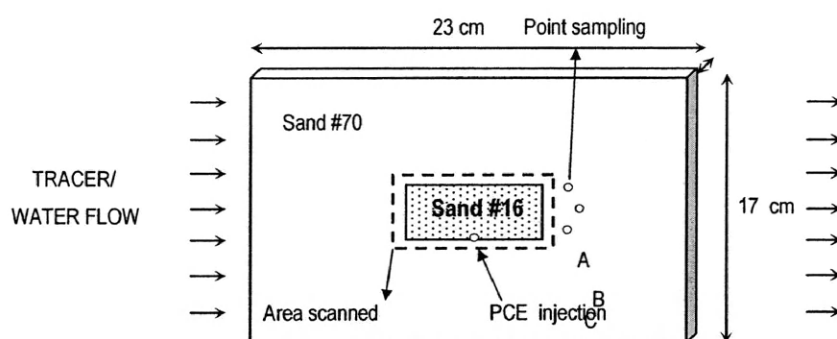
The simple heterogeneity consists of a coarse sand lens surrounded by a finer medium.

The flow cell was packed under water saturated conditions using silica sands. A sand with mesh size designation #70 was used as the background media and #16 sand was used to represent the coarser lenses block where the pool was placed. The coarser lenses block was 7.5 cm long and 3.0 cm in height (Figure 3.4). Table 3.1 gives the physical properties of these sands. This porous media configuration represents a contaminant zone entrapped in a two-dimensional confined flow domain.

An HPLC (Acuflow Series II) pump was used to provide constant water flow through the tank. Before the DNAPL injection, head, flow and conservative tracer concentrations observation were collected, to ensure that the cell was properly packed. This set of data was used later on for flow and transport calibration.

50

The test DNAPL (PCE) was injected into the coarse sand block through a sampling port and the PCE was fully contained due to capillary barrier effects. Initially, within the block, a high saturation PCE pool was created and then, PCE was drained out of the cell consecutively creating four different pool morphologies (defined by the fraction of PCE in the transition zone). The creation of the different pools was carried out following the same procedures developed in section 2.4 during preliminary experiments. X-ray characterization and tracer tests were performed for each of these pool configurations to evaluate the influence of different saturation profiles on the output from the PITT.

250 points were scanned over the contaminated zone area using X-ray attenuation techniques (Imhoff et al. 1995; Okuda et al., 1996). In the horizontal axis, scanned points were located every 1 cm and in the vertical axis every 2 mm in order to obtain an accurate profile of saturations with depth. To obtain PCE saturations, the flow cell was scanned before and after the PCE injection.

To observe the aqueous flow that carries the tracers, a small volume of food dye was dissolved in water and flushed through the system in steady state conditions for the same pore volume (PV) and flow rate as those used during actual tracer runs.

After the dye tracer test, a pulse of tracer solution was injected through the inlet port for 0.3 PV. The tracer solution contained 500 mg/l of DMP, 300 mg/l of 6M2H, 600 mg/l of HEX and 500 ppm of NaBr. A constant flow rate of 2 ml/min was maintained throughout the tracer test.

Samples were taken every 30 minutes, collected in 0.2 ml inserts placed in GC autosampler vials, and analyzed using a Flame Ionization Detector. After analysis of partitioning tracers, bromide concentrations were analyzed using Ion Chromatography.

The same procedure was repeated for the four different PCE saturation profiles.

Results, data analysis and discussion of this set of experiment are presented in Chapter 5.

3.5 Intermediate Scale Experiments

After the 2D cell experiment where the performance of the PITT was tested for simple heterogeneities, an intermediate scale experiment was set up to evaluate tracer behavior in more complex conditions of heterogeneity.

The large-scale experiment tank was made with four pieces 2.44 m long and 1.22 m high plates; three of them are clear polycarbonate and the other is aluminum plate. The polycarbonate plate opposite the aluminum plate is lined with tempered glass to prevent sorption of NAPL to plastic. The dimensions of the tank are 4.88 m × 1.22 m × 0.05 m.

Creation of the heterogeneous medium. Silica sand was used for packing the test tank. Five different mesh sizes of silica sand were selected to represent the heterogeneous field; the mesh sizes were #16, #30, #50, #70, and #110.

The design of a packing configuration for the 16 ft test tank using the five test sands (#16, #30, #50, #70, #110) was selected to represent a highly heterogeneous field. The parameters of the packing are: (1) mean of log K (K in m/day) 4.18, (2) variance of 1.22, (3) horizontal correlation length of 0.5 m and (4) vertical correlation length of 0.05 m. Multiple random field realizations were generated using these design parameters and one realization was selected for packing. Each realization was discretized into five categories spanning the range of hydraulic conductivity. Categories were associated with laboratory sands having known hydraulic properties. A realization suitable for entrapping a heterogeneous DNAPL source zone was then selected for packing the tank. The chosen configuration included zones within the target source area for DNAPL injection that were likely to produced a complex entrapment morphology while minimizing the possibility of vertical DNAPL migration to the bottom of the tank.

The upstream part of the source zone that was packed homogeneously with sand #8. The purpose of this homogeneous zone was to create a zone of high hydraulic conductivity for tracer injection that creates a uniform tracer front before entering the

source zone area. There were 6 pairs of arrays for concentration and head monitoring and one array for tracer injection. Each array had 40 sampling/monitoring ports spaced one inch vertically apart.

The tank was filled by hand according to the design. Sand volumes of approximately 80 ml where placed into the tank following the discretization that corresponds to the random field. A 5 cm PVC pipe was used to place each volume of sand into its specified location. In this manner, individual sand lenses approximate 15 cm long and 1 cm high were created in the test tank. By dropping the sand through the PVC pipe as the pipe was moved laterally along a 15 cm track, a discrete 'blocky' geometry was avoided and more realistic sand contacts were established. The resulting individual sand units were tapered at their boundaries rather than having sharp vertical fronts (Figure 3.5). Dry packing has been proven to be unsuccessful in this type of experiments due to the amount of air that is entrapped in packing procedures, so water saturated conditions were used in this experiment. The water level was maintained approximately 2 inches above the last layer packed.

Figure 3.5. Intermediate scale tank and details of the heterogeneous packing.
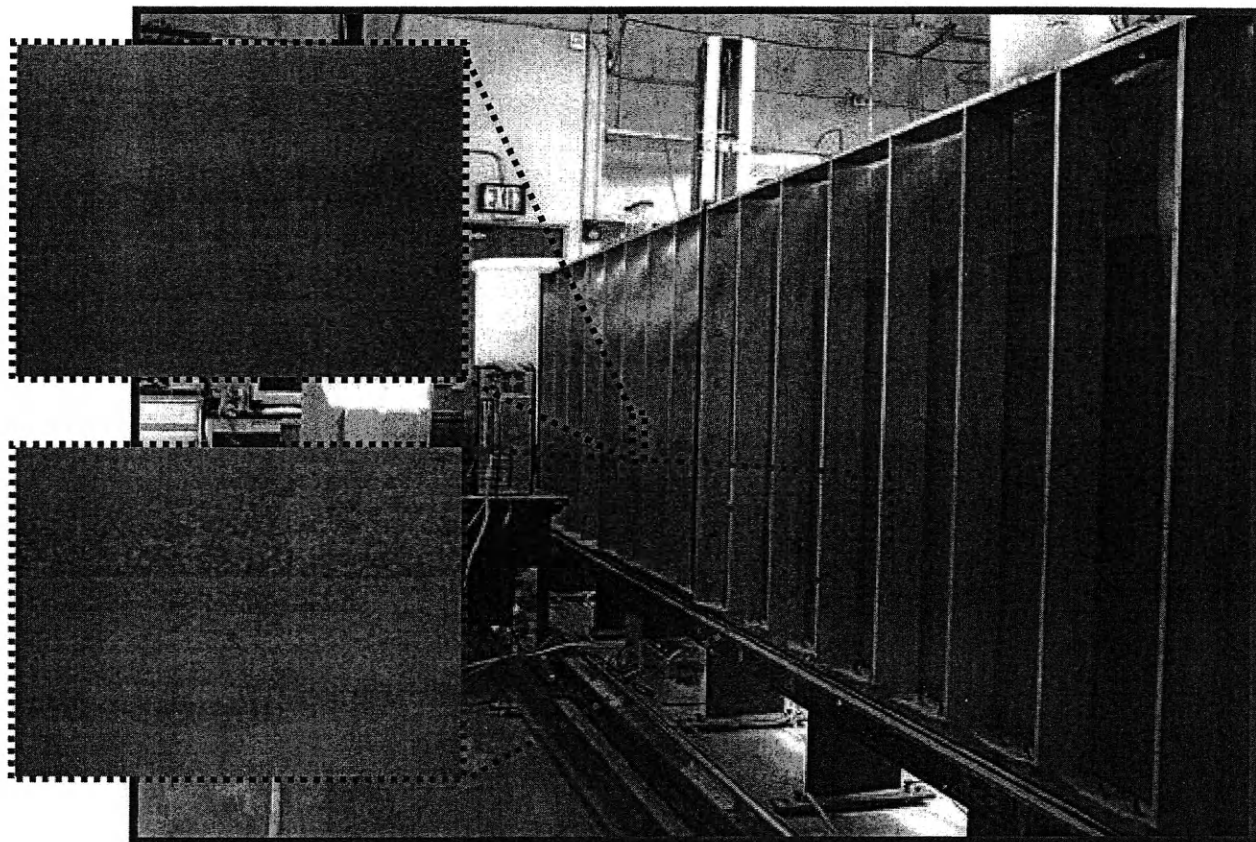
Figure 3.6. Schematic of the intermediate scale tank.
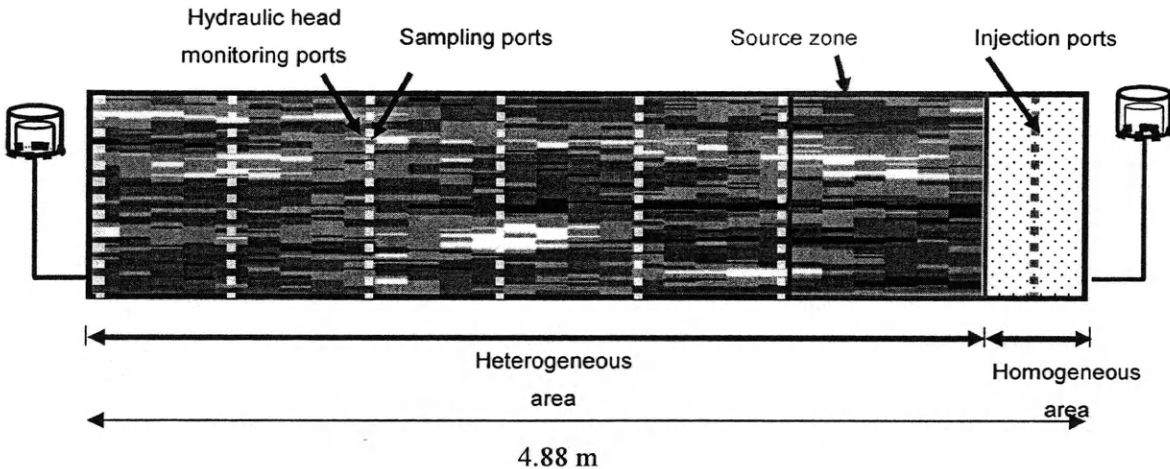
The Gamma-ray attenuation system was used to scan the source zone prior to and after PCE spill. It took approximately 8 days to scan the source zone area (an area of approximately 70 cm × 60 cm).

Head and flow measurements. Pressure in the tank was monitored using a differential pressure transducer that provided readings at 48 different locations distributed throughout the entire domain. The pressure transducer consists in a pressure sensing diaphragm and two coils. When a differential pressure is applied to the sensor, the diaphragm deflects away from one coil and towards the opposite. The change in coil impedance is directly proportional to the position of the diaphragm, so the amplitude of the signal is directly proportional to the applied pressure.

The transducer was connected to a head reservoir (the reference) and to a solenoid controller. This controller is connected to 48 ports in the tank (Figure 3.7). Lab-view software has been developed to automatically control the selector switch and provide

sequential input to the transducer from all the 48 ports. The output (voltage) was converted into head measurements using a linear fit created from calibration data.

Figure 3.7. Pressure transducer system.
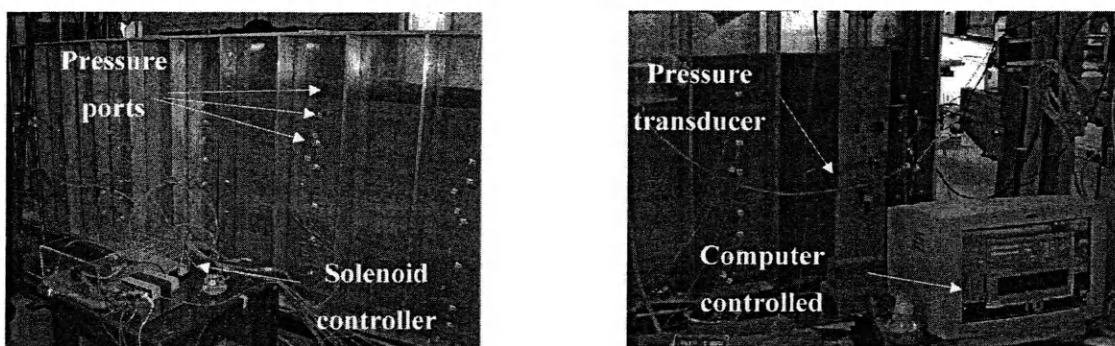
Flow measurements taken after packing and during head measurements showed a steady flow rate at 62.93 ± 0.50 ml/min. Figure 3.8 shows flow measurements during measurement of the head distribution with the pressure transducer system.

Flow and pressure measurements were taken at the same time. These observations were for flow model calibration. Figure 3.9 shows the results of the pressure transducer in the 48 head monitoring ports. Anomalies observed in ports 28 and 40 represent clogging of the needle during experiments.

Figure 3.8. Flow measured by weight.
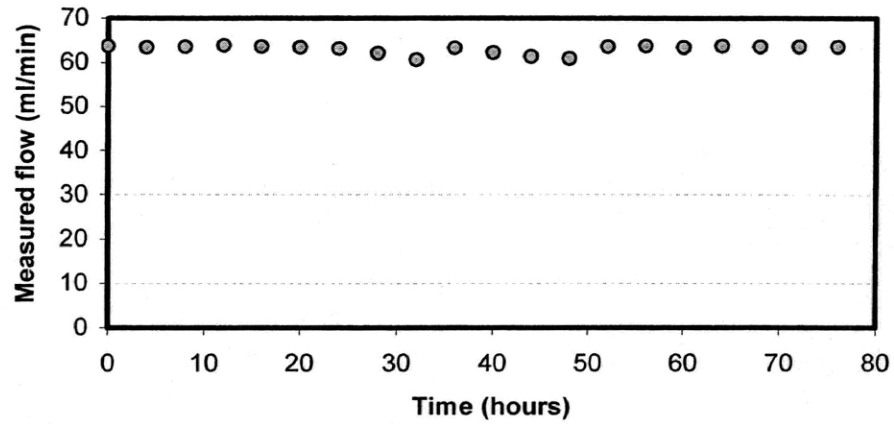
Figure 3.9. Results of the pressure transducer.
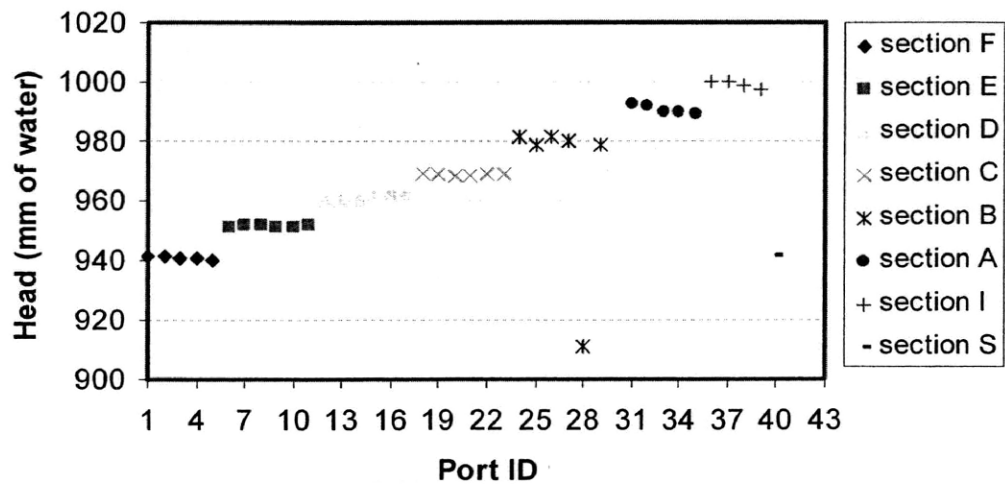
Blank tracer test. A bromide and partitioning tracer test was conducted prior to the spill. The objectives of this experiment were:

- To evaluate the uniformity of tracer injection through all the ports.

- To evaluate if the partitioning tracers were subject to retardation due to sorption into the soil.

- To test design parameters of the tracer test for post spill characterization: concentration of tracer, flow rate, injection time, sampling frequency and total sampling time.

- To obtain a conservative tracer data set for estimation of transport parameters using numerical models.

A solution of 500 pm of NaBr, 300 ppm of hexanol and 300 ppm of DMP was injected in the in tank using a multi-syringe pump. The total flow rate of water through the tank was controlled using two constant head reservoirs; the head difference created was approximately 8 cm. The flow rate of the injected solution was 0.25 ml/min in every port. Pressure was monitored during experiments (see Figure 10 for port location). Since the multi-syringe pump allows for injection in 32 ports, the total injection flow was 8 ml/min. The duration of the tracer slug was 10 hours.

Samples were taken manually in 29 locations located in 6 different arrays as specified in Figure 3.10. To reduce the sampling volume, 0.2 ml inserts were placed in 1.5 ml vials. A total of 596 samples were generated during the experiment and analyzed in the gas chromatographer.

Figure 3.10. Location of sampling ports.
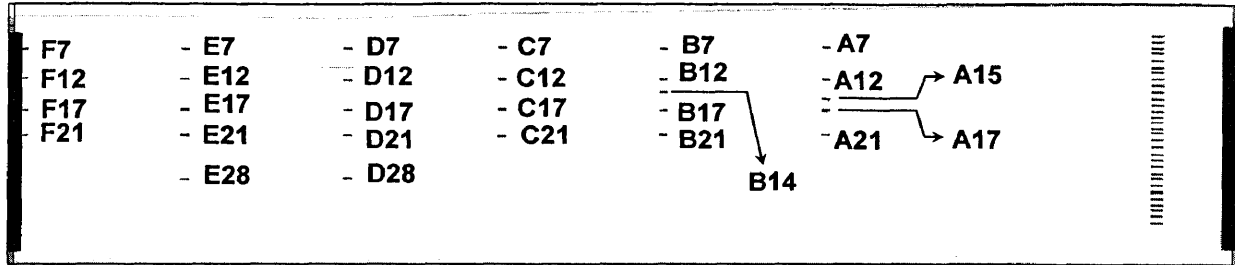
Figure 3.11. Tracer breakthrough curves for sampling ports in arrays A and B.
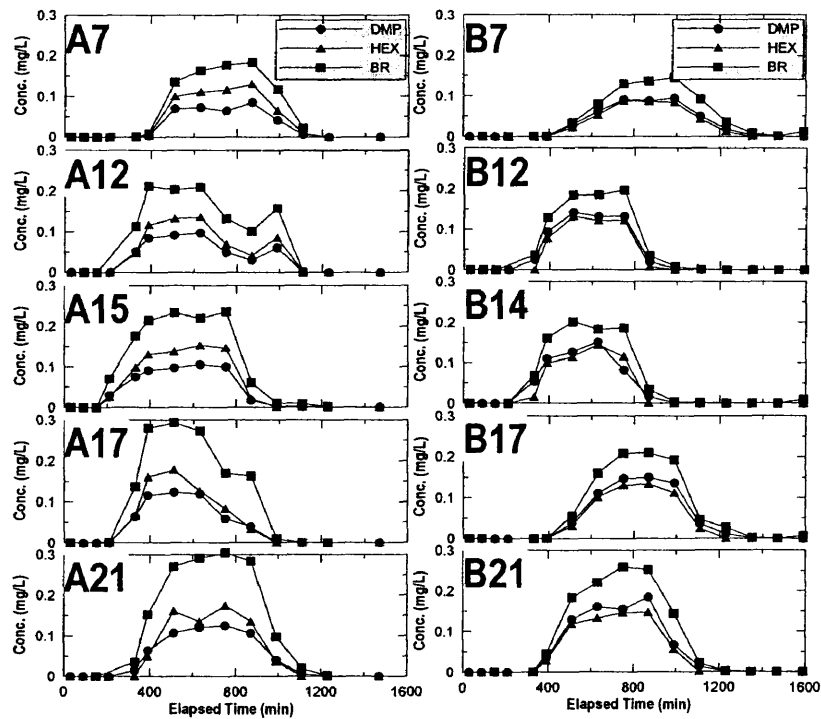
As observed in section A (Figure 3.11), some discrepancies between bromide and the partitioning tracers were observed. Since there is no NAPL in the tank, it was expected to obtain the same breakthrough curves from all the tracers. These discrepancies can be a result of the volatilization of the alcohols.

To evaluate if the difference in concentration values between the different tracers affected the travel time, the first centralized moments of the breakthrough curves were calculated. The travel time calculated from all the tracers at one port should be the same since there is no DNAPL present. As it is shown in the Figure 3.12; the center of mass remains the same so these differences do not affect travel times and subsequently retardation values obtained from partitioning tracers.

Figure 3.12. Travel times obtained using the breakthrough curves of the three different tracers at section A.
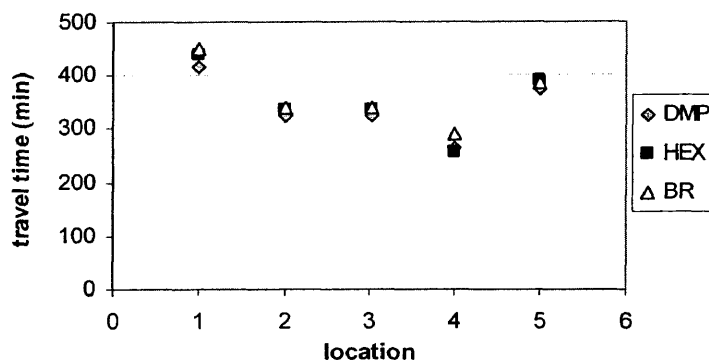
Based on the above tracer results, several conclusions can be drawn:

1. Tracer front seems to be fairly uniform in the vertical direction.

2. No retardation of the partitioning tracers was observed due to sorption into the soil.

3. Design parameters (concentration of tracer, flow rate, injection time, sampling frequency and total sampling time) seem to provide adequate results for the objectives of the test.

4. This set of tracer data set will be used for estimation of transport parameters using numerical models.

PCE spill. A total of 586.7 ml of PCE dyed with red Sudan IV (0.01%) was injected in the source zone through five ports (Figure 15). The amounts injected into each port are listed in Table 3.4. PCE was injected under constant head of PCE using Mariotte-bottle under no flow condition in the tank.

Table 3.4. Volume of PCE injected into each injection port

Source Location	Volume injected
1	272.0
2	71.9
3	41.4
4	93.3
5	93.2
Total	586.7

Figure 3.13. Injection of the PCE.
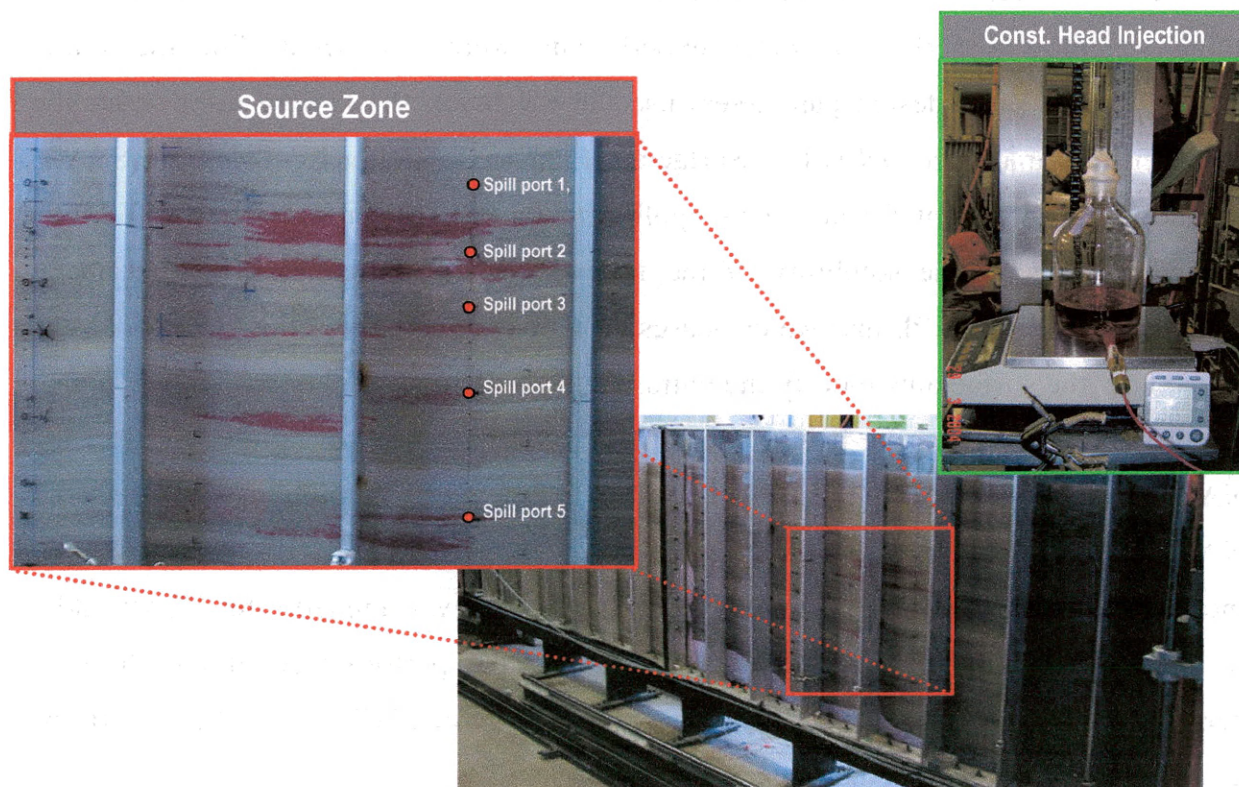
In order to evaluate the influence of the entrapment architecture on the performance of the partitioning tracer test, it was necessary to determine the actual saturation distribution in the cell. With the gamma system, the saturation distribution can be accurately characterized.

The gamma attenuation system was initiated when the static condition was achieved (i.e. no further NAPL migration is observed). After injection of the PCE and gamma scanning a series of tracer experiments were conducted. For the tracer experiments, the same design parameters used in the blank PITT were used. After the first tracer to characterize DNAPL, a Surfactant-Enhanced Aquifer Remediation (SEAR) also known as surfactant flushing was applied to the two-dimensional tank. SEAR is designed to enhance the solubility of the DNAPL phase by reducing the interfacial tension between the NAPL and water phases. For this investigation, the purpose was to observe how the surfactants modify the entrapment configuration, rather than to evaluate the remediation performance. It is expected that the surfactants will remove most of the DNAPL that is accessible by the surfactant flow lines. After remediation, we expected a DNAPL entrapment architecture where most of the DNAPL in the residual form has been removed and most of the pools still prevail. The gamma was applied after SEAR and a PITT was conducted again. In this way, not only the performance of the PITT to determine architecture is evaluated, also the performance of PITT as a tool to determine the effectiveness of the remediation can be assessed.

Results, data analysis and discussion of this set of experiment are presented in Chapter 6.

Chapter 4

NUMERICAL MODELS

As discussed in chapter one, there are two main approaches to obtain saturation of DNAPLs from breakthrough curves: method of moments and numerical modeling.

Numerical models can be used to interpret laboratory data. They require spatial and temporal discretization, and an approximate solution to the governing equations. A numerical model is a combination of a conceptual model, numerical formulation and a computer code with relevant input parameters derived from field and laboratory information (Moore, 2001).

To simulate flow and transport, the widely used groundwater and transport models MODFLOW (Harbaugh et al, 2000) and MT3DMS (Zheng and Wang, 1999) were selected. The partitioning behavior and the presence of NAPL were incorporated with the MODTRACER algorithm (Saenton, 2003). This Fortran preprocessor calculates effective parameters to account for the NAPL phase and simulates partitioning behavior as a sorption process. UTCHEM (Delshad et al., 1999) was selected as the multiphase flow model to generate the NAPL spills for all the realizations developed in Chapter 7.

Once a numerical model was selected to simulate a DNAPL spill (UTCHEM) and a set of models were combined to simulate tracer flow, transport and partitioning (MODFLOW/MT3DMS/MODTRACER), it was necessary to invert the model to estimate optimal parameters. UCODE (Poeter and Hill, 1998) and PEST (Doherty, 1994) were selected to solve the inverse problem.

A brief description of the models used in this study is presented in this chapter.

4.1 UTCHEM

UTCHEM (Delshad et al, 1999) is a multicomponent, multiphase, compositional model of chemical flooding processes which accounts for complex phase behavior, chemical and physical transformations and heterogeneous porous media properties. The model was originally developed to model surfactant oil recovery but has been modified for applications that involve the use of surfactants in aquifer remediation. The balance equations are the mass conservation equations, and overall balance that determines the pressure for up to four fluid phases and an energy balance equation to determine the temperature.

UTCHEM allows for variations in relative permeability and capillary pressure in each grid cell as well as variable density, viscosity, velocity dependent dispersion, molecular diffusion, adsorption, interfacial tension, and capillary trapping. Using the geochemical option, UTCHEM is able to model aqueous reaction chemistry including aqueous electrolyte chemistry, precipitation/dissolution of minerals, and ion exchange reaction with the media. Injection and extraction wells can be set up vertically and horizontally. The recent version 9.0 includes a dual porosity formulation and biodegradation of organic compounds.

Currently, UTCHEM is the only numerical simulator that includes partitioning behavior. However, previous experience with this code has shown considerable numerical difficulties and/or simulation times that are unnecessary long. This is an issue since one of the most important steps of the analysis is automated calibration; this process could lead to extremely long simulation times. Another constraint in the use of UTCHEM is that it simulates only equilibrium partitioning, whereas in some cases residence times will not be long enough to assume local equilibrium. Therefore, UTCHEM was rejected for simulation of partitioning behavior in this research, but it was selected as the multiphase code to create the set of NAPL spills discussed in Chapter 7.

4.2 MODFLOW and MT3DMS

A Modular Three-Dimensional Finite-Difference Ground-Water Flow Model initially developed by Michael McDonald and Arlen Harbaugh (1998), is the world's most used groundwater modeling code. The partial-differential equation of groundwater flow used in MODFLOW is:

$$S_s \frac{\partial h}{\partial t} = \frac{\partial}{\partial x}\left(K_{xx} \frac{\partial h}{\partial x}\right) + \frac{\partial}{\partial y}\left(K_{yy} \frac{\partial h}{\partial y}\right) + \frac{\partial}{\partial z}\left(K_{zz} \frac{\partial h}{\partial z}\right) + W \qquad (4.1)$$

where h is the potentiometric head, W represents fluid sources or sinks, Ss is the specific storage of the reservoir, K_{xx}, K_{yy}, and K_{zz} are values of hydraulic conductivity along the x, y, and z axes.

MODFLOW simulates: single phase, saturated flow of constant density in porous media (Darcy's Law applies) for 1, 2, or 3 dimensional systems in 2D areal or cross-section mode, or quasi-3D mode. MODFLOW simulates both steady state and transient flow in heterogeneous, anisotropic, layered units. It uses a block centered finite difference solution technique applied to variable grid spacing in the x, y, and z directions. Units can be confined, unconfined, or convertible. Boundary conditions include: Dirichlet, Neumann, Cauchy, and Phreatic Surface options. Simulated stresses include: Wells, Recharge, Evapotranspiration, Rivers, Streams, and Drains.

The outputs from this model used in this research are the hydraulic head distribution and flow velocity through each cell. MODFLOW generates the velocities necessary to simulate tracer transport when coupled with a contaminant transport code.

The contaminant transport model selected to represent conservative and partitioning tracer transport is MT3DMS (Zheng and Wang, 1999) with the addition of

the reaction package. The modular structure supports advection, dispersion, sinks, sources, mixing, sorption and reaction. The transport code solves the following equation:

$$\frac{\partial(\theta c)}{\partial t} = \frac{\partial}{\partial x_i}(\theta D_{ij}\frac{\partial c}{\partial x_j}) - \frac{\partial}{\partial x_i}(\theta \overline{v}_i c) + \sum R_n + q_s c' \qquad (4.2)$$

where c is the concentration of contaminant of interest, θ is the porosity of the medium, R_n is the reaction associated with the species, q_s represent sources and sinks and c' is the solute concentration associated with such source/sink.

The transport model is used in conjunction with the flow model with the assumption that changes in solute concentration will not affect significantly the water flow field. MT3DMS retrieves the hydraulic heads and the various flows saved by the flow model and incorporates this into the transport model to solve Equation 4.2.

4.3 MODTRACER

The contaminant transport model MT3DMS does not include the NAPL phase. In order to represent DNAPL and partitioning behavior another code developed by Saenton (2003) was incorporated as a preprocessor.

MODTRACER (Saenton, 2003) represents partitioning behavior assuming linear sorption. It is a pre-processor that calculates properties that change in the presence of DNAPL. These are hydraulic conductivity (K), porosity (ϕ), and density (ρ). The expressions use in this module to calculate the new or effective K, ϕ and ρ are:

Wyllie's equation was used to calculate relative permeability k_r:

$$k_r = \left(\frac{1 - S_N - S_{r,w}}{1 - S_{r,w}} \right)^3 \tag{4.3}$$

where S_N is the entrapped NAPL saturation and $S_{r,w}$ is the water residual saturation. This correlation has been used by Demond (1998) and selected by Geller and Hunt (1993) to analyze their data. Wyllie's equation was found to agree with experimental results and provided the best fit to the data.

Then, the effective hydraulic conductivity (K) can be calculated as:

$$K = k_r \cdot K_s \tag{4.4}$$

Where K_s is the saturated hydraulic conductivity of the porous media.

When linear sorption (equilibrium or rate limited) is represented in MT3DMS, the program requires four types of input parameters in the basic transport and reaction package: effective porosity, bulk density, distribution coefficient, and linear mass transfer coefficient (for equilibrium sorption, the mass transfer coefficient is zero). Based on NAPL saturation, the model calculates the required parameters as shown in equations 4.5, 4.6 and 4.7.

$$\phi_e = (1 - S_n) \cdot \phi \tag{4.5}$$

$$\rho_b = (1 - \phi)\rho_s + (1 - S_n)\phi\rho_w + S_n\phi\rho_n \tag{4.6}$$

$$K_d = \frac{\phi_e K_p S_n}{\rho_b(1 - S_n)} \tag{4.7}$$

where ρ_b, ρ_s, ρ_w, ρ_n represents bulk, solid, water, and NAPL density respectively, Φ_e is the effective porosity and K_d is the effective sorption coefficient.

The developed scheme is only valid if NAPL is static, assumption that is valid considering the duration of a tracer test, normally below 10 days (Annable et al., 1998, Meinardus et al., 2002, Divine et al., 2004).

A study conducted by Saenton, (2003) describes the details of model development and verification with the analytical solution. The simulator successfully represented partitioning behavior and simulations were completed in relatively short periods of time.

4.4 Inverse Modeling Codes: UCODE and PEST

Calibration is the process of adjusting parameter values, boundary conditions, model conceptualization, and/or model construction until the model simulation matches field observations. Calibration of a model allows for adjustment of the parameters to accommodate an integrated interpretation of the system. Once a model is calibrated, it can be used to make predictions and evaluate the importance of different parameters in the system.

In this work, inverse modeling was used to attain calibration of flow and transport parameters and to estimate saturation values from breakthrough curve tracer data.

Two universal inverse modeling codes were used for parameter estimation: UCODE (Poeter and Hill, 1998) and PEST (Doherty, 1994). Both algorithms use systematic parameter estimation based on non-linear least squares regression. Universal inversion codes allow pre-processors and post-processors to be included as application models.

UCODE solves the non linear regression problem by minimizing a weighted least-squares objective function with respect to the parameter values using a modified

Gauss-Newton method. The procedure begins by substituting starting parameters in the forward application, then, UCODE extracts the selected simulated values and compares them with observed values. The differences between both values are called residuals. These residuals are weighted, squared and summed to calculate the objective function. Parameter sensitivities are calculated by using the perturbation method based on forward, backward, or central difference methods. Once residuals and sensitivities are calculated, MRDRIVE updates the new parameter values using the Gauss-Newton method. If the changes in parameter values and the objective function are below a convergence criteria specified by the user (normally one percent), parameter estimation converges.

PEST solves the non linear problem in a similar way as the UCODE algorithm. The main reason of using PEST in the last stages of this investigation had to do with one of the features that PEST offers; the parameters-estimation can be constrained between the physical limits of the parameter to estimate. In this work, the saturation was limited to its physical values [0,1]. This was necessary because it was found that the estimation of the parameters during UCODE calibration could result in saturation values above or below its physical limits. This caused problems in the execution of the MODTRACER preprocessor as an application model; the effective K_d (equation 4.7) could become infinity or zero, creating anomalies in the flow model for both scenarios.

Chapter 5

INFLUENCE OF DNAPL POOL MORPHOLOGY ON THE PERFORMANCE OF PARTITIONING TRACER TESTS

5.1 Abstract

Partitioning tracer techniques, initially developed in the petroleum industry, are promoted as a way to determine entrapped dense non aqueous phase liquid (DNAPL) mass in source zones. A suite of chemical tracers, some of which partition into the DNAPL phase, is injected into the source zone to estimate the entrapped saturation of contaminant. Current application of the technique can determine DNAPL at residual saturation, but does not provide reliable mass estimates of DNAPL in high saturation areas (e.g. pools) that may occur in some source zones. To evaluate this technique's limitations in characterizing source zones with complex entrapment architectures that may contain pools, estimation errors associated with well characterized single-isolated DNAPL pools were investigated. Improvements in current methods of data analysis were explored with the goal of reducing estimation errors. X-ray attenuation was used to determine the spatial distribution of saturation within the pool under different total DNAPL mass entrapment while the DNAPL was subjected to tracer tests. Model analysis used to interpret the tracer data showed that the partitioning tracer breakthrough simulations based on equilibrium partition coefficient (Kp, from equilibrium batch tests) fit the experimental data poorly, suggesting rate-limited partitioning that is controlled by the water flow velocity through the NAPL entrapment zone. In order to relax the

requirement of partitioning to be at equilibrium, the use of "effective partition coefficients" (Kpe) was investigated. The Kpe was determined via inverse modeling and batch experiments. A comparison of the saturation estimates using method of moments, and inverse modeling with both equilibrium and rate-limited partitioning was conducted. Results demonstrated that the incorporation of rate-limited behavior in the analysis can enhance the performance of tracer tests for high saturation zones.

5.2 Introduction

Chlorinated solvents in the form of dense non aqueous phase liquids (DNAPL) exist in a large number of hazardous waste sites. The inherent geologic heterogeneity in most of the sites contributes to the complexity of DNAPL movement and subsequent entrapment (Schwille, 1988; Kueper et al., 1989; Illangasekare et al., 1995). Once the DNAPL enters the subsurface, its distribution is controlled by fingering (Held and Illangasekare, 1995), preferential channeling, and heterogeneity of the subsurface formation (Kueper and Frind, 1991). The final entrapment is commonly conceptualized as one of two idealized geometries: residual ganglia and blobs (regions of low saturation) and pools (regions of high saturation). Pooling may occur in different entrapment scenarios, such as accumulation on a low permeability layer (Kueper et al., 1989) or entrapment within coarse lenses (Saba and Illangasekare, 2000). The distribution of DNAPLs in the subsurface has also been called architecture; the architecture of a system could potentially be defined with moments that measure total mass, center of mass, and spreading of the spill in a quantitative manner (Saenton, 2003). Under conditions of complex architecture, delineating and characterizing source zones could be a challenge. If the mass distribution is unknown, effective remediation becomes difficult.

The Partition Interwell Tracer Technique (PITT) first used in the petroleum industry was extended for detecting and characterizing the distribution of NAPL contaminants in subsurface environments (Jin et al., 1995). This technique adapts and extends several existing detection and characterization methods from the fields of groundwater hydrology and petroleum reservoir engineering (Allison et al., 1991). The use of PITT for DNAPL characterization has increased in recent years. Most of the time, it has been used to assess remediation performance (Rao et al., 1997; Annable et al., 1998; Jawitz et al., 1998; Meinardus et al., 2002; Divine et al., 2004). Although this technique and its extensions have been applied with some success in a number of sites, its limitations under complex DNAPL entrapment morphologies have not been adequately evaluated. Tracer tests are expected to result in underestimation of mass when the tracer does not access the entrapped DNAPL or non-equilibrium partitioning occurs (Rao et al., 2000). The focus of this research study is the evaluation of the PITT for characterization of sites with unidentified NAPL sources; the final goal is to evaluate whether appropriate design of the technique can minimize estimation errors in high saturation zones.

The use of PITT involves injecting a tracer solution consisting of at least one conservative tracer and a mixture of chemicals with different partition coefficients (Kp) into the aquifer. Partitioning tracers undergo retardation while conservative tracers are unaffected by the presence of DNAPL; this temporary partition causes the partitioning tracers to lag behind the conservative tracers. The amount of DNAPL in the source zone swept by the tracer mixture can be estimated by analyzing tracer breakthrough curves observed down-gradient. The retardation (R) of the partitioning tracer is calculated directly from collected breakthrough curve data, and is given by the ratio of partitioning (t_p) and conservative tracer (t_{np}) travel times.

Assuming local equilibrium during partitioning for a water-NAPL system, the saturation of entrapped NAPL (S_N) in the tracer swept volume can be calculated using:

$$S_N = \frac{R-1}{R + Kp - 1} \qquad (5.1)$$

where Kp is used in the dimensionless form

The assumption of local equilibrium may be true for low saturations, but may not be applicable in situations where DNAPLs are entrapped under high saturations such in pools. Jin et al. (1997) used UTCHEM, a multiphase flow and transport model (Delshad et al., 1996) to estimate the relative error associated with NAPL detection in pools. These authors demonstrated that estimation errors never exceed 50% for the hypothetical conditions that were tested. Rao et al., (2000) pointed out that data from DNAPL sites suggest that the estimation errors are larger than the estimates based on numerical modeling analysis for hypothetical conditions.

Laboratory experiments were conducted in a two-dimensional cell to generate a data set of tracer breakthrough for different morphologies of an isolated pool with different saturation distributions (e.g, saturation profiles) created by controlling the total entrapped mass within the pool. In these controlled experiments, it was possible to accurately determine the saturation profile using in situ measurements and to associate this profile with the corresponding tracer response; a situation that would not be possible in the field. Using this approach, we could investigate fundamental processes of partitioning behavior under different pool morphologies and methods of data analysis. Our objectives were to identify the sources of estimation error and to refine the application of tracer methods under complex entrapment architecture. For data analysis, we investigated a methodology that uses inverse modeling in conjunction with a new transport simulator based on MODFLOW-MT3DMS (MODTRACER) developed by Saenton (2003). Sensitivity analysis performed using this set of numerical models demonstrated the effect of the local equilibrium assumption in the estimation errors. We investigated the incorporation of effective parameters in the analysis to reduce these major inaccuracies. The knowledge gained from these investigations can be used to

improve design protocols and data interpretation of tracer methods at geologically complex field sites.

5.3 Conceptual Pool Model

In numerous simulation studies, DNAPL pools have been conceptualized as homogeneous blocks of high saturation with sharp boundaries (Jin et al., 1997; Sale and McWhorter., 2001; Roy et al., 2002; Imhoff and Pirestani, 2004). The pool, as conceptualized in this study, is recognized as consisting of a zone of high saturation that does not have a defined sharp upper boundary; rather, the high saturation zone is bounded by a transition zone where the saturation changes from high to residual values (Figure 2.6) (Moreno-Barbero et al., 2002). This conceptual model derives from the processes leading to pool formation and is supported by laboratory studies (Kueper et al., 1989; Gerhard and Kueper, 2003), field observations (Kueper et al., 1993), and theoretical analysis (McWhorter and Kueper, 1996).

The saturation profile of a pool will depend on many factors; volume and rate of spill, porous media properties, type of the DNAPL, time duration of the release, and other subsurface flow conditions (Feenstra and Cherry, 1998).

A number of studies have been reported in the literature on the limitations of tracer methods when used to estimate volumes of DNAPLs in high saturation zones (Nelson et al., 1999; Willson et al., 2000; Dai et al., 2001; Jalbert et al., 2003; Imhoff and Pirestani, 2004), but pool morphology and its influence in PITT effectiveness has been overlooked. Recently, Jayanti, (2003) evaluated the accuracy of PITT when hydrodynamic inaccessibility occurs. However, equilibrium partitioning was assumed in all the simulations. In this study, the validity of the equilibrium assumption was explored.

The hypothesis developed after extensive literature review and preliminary experiments (see Chapter 2) is that as the DNAPL saturations in the lower portions of the pool are high, the bypassing of the tracers in combination with rate-limited partitioning would constrain residence time of the tracer that comes in contact with the DNAPL phase. This limits the tracer partitioning and causes underestimation of DNAPL mass in the high saturation zone of the pool. Conversely, the transition zone has lower DNAPL saturations resulting in higher aqueous relative permeabilities, which allow the tracers to flow through this zone. Hence, when the saturation profile of the pool is such that a larger fraction of the total mass in the pool is in the transition zone, the estimation error becomes less. A set of experiments with different saturation profiles (defined by the relative mass fraction in the transition zone) were conducted to obtain quantitative data to test this hypothesis. Use of this conceptual model (see Figure 2.6) in the analysis of PITT data led to the investigation of factors that influence the saturation profile of a pool and how different saturation profiles would influence the partitioning behavior. This pool conceptualization was applied in two-dimensional test configurations to establish relationships between pool morphology and performance of the PITT. The pool morphology was accurately measured using X-ray attenuation methods (Imhoff et al., 1995; Okuda et al., 1996).

5.4 Materials and Methods

A series of experiments in a two-dimensional test cell was conducted in the laboratory. A description of the materials used is followed by a description of the methodologies for tracer and X-ray characterization.

Tetrachloroethylene (PCE) was used as the test DNAPL for these experiments (Aldrich Chemical). It was dyed with a small fraction of Sudan IV (0.01%) to allow

observation through the transparent wall of the test cell. Table 3.2 provides the relevant chemical and physical properties of PCE.

A mixture of 2,2-dimethyl-3-pentanol (DMP), n-hexanol (HEX) and 6-methyl-2-heptanol (6M2H) (all from Sigma Chemical) was used as the partitioning tracer solution. Kp between PCE and water measured from batch tests are 27.51, 8.49 and 88.50, respectively. Selection criteria of the tracers were based on general guidelines defined by Young et al. (1999) and on their partition coefficients: low enough to allow a reasonable time for breakthrough and high enough to ensure separation between partitioning and non-partitioning tracers. Bromide (in the form of NaBr) was selected as the conservative tracer.

Silica sand was used for packing the test tanks to create the pools. A sand with mesh size designation #70 was used as the background media and #16 sand was used to represent the coarser lenses block where the pool was placed. Table 5.1 gives the physical properties of these sands.

Table 5.1. Properties of the sand used for the experiment.

Properties	#16	#70
Hydraulic conductivity[a], cm/min	25.8	1.44
Porosity[a], Φ	0.48	0.48
Dispersivity[a] α, cm	0.07	0.08
Mean grain size d_{50}[b], mm	0.88	0.19
Brooks and Corey [1964] [b], Pe,	7.6	25
Brooks and Corey [1964][b], λ, cm	3.5	1.9
Residual water saturation[b]	0.07	0.30

[a] Parameters estimated by numerical modeling
[b] Calculated values from [*Illangasekare et al., 1995*]

Flow experiments were conducted in a 30.5 cm x 22.8 cm x 2.54 cm test cell. The front wall of the cell was made of tempered glass to allow for observation. The back wall plate was made of aluminum to allow drilling of ports for sampling and pressure measurements. The glass and aluminum walls were attached to an aluminum frame. Internal void volume of the cell was nominally 23 cm x 17 cm x 2.54 cm (see Figure 5.1). The sampling ports were located in the cell along 11 horizontal lines, each containing 8 ports spaced 2.54 cm apart. These ports were used to extract aqueous samples for tracer analysis and to monitor the pressure in the tank.

The flow cell was packed under water saturated conditions using the silica sands. The coarser lenses block was 7.5 cm long and 3.0 cm in height (see Figure 5.1). This porous media configuration represents a contaminant zone entrapped in a two-dimensional confined flow domain. An HPLC (Acuflow Series II) pump was used to provide constant water flow through the tank.

Before the DNAPL injection, head, flow and conservative tracer concentrations observations were collected, to ensure that the cell was properly packed. This set of data was used later on for flow and transport calibration.

The test DNAPL (PCE) was injected into the coarse sand block through a sampling port and the PCE was fully contained due to capillary barrier effects at the coarse/fine sand interface. Initially, a high saturation PCE pool was created within the coarse sand block by injecting a known volume of PCE. A fraction of the injected PCE was drained out of the cell, consecutively creating four different pool saturation profiles (defined by the fraction of PCE in the transition zone. X-ray characterization and tracer tests were performed for each of these pools to evaluate the influence of different saturation profiles on the mass estimates obtained from the PITT. To be able to observe the aqueous flow that carries the tracers, a small volume of food dye was dissolved in water and flushed this through the system in steady state conditions for the same pore volume (PV) and flow rate as those used during actual tracer runs.

Figure 5.1. Schematic of the flow cell and area scanned by X-ray.
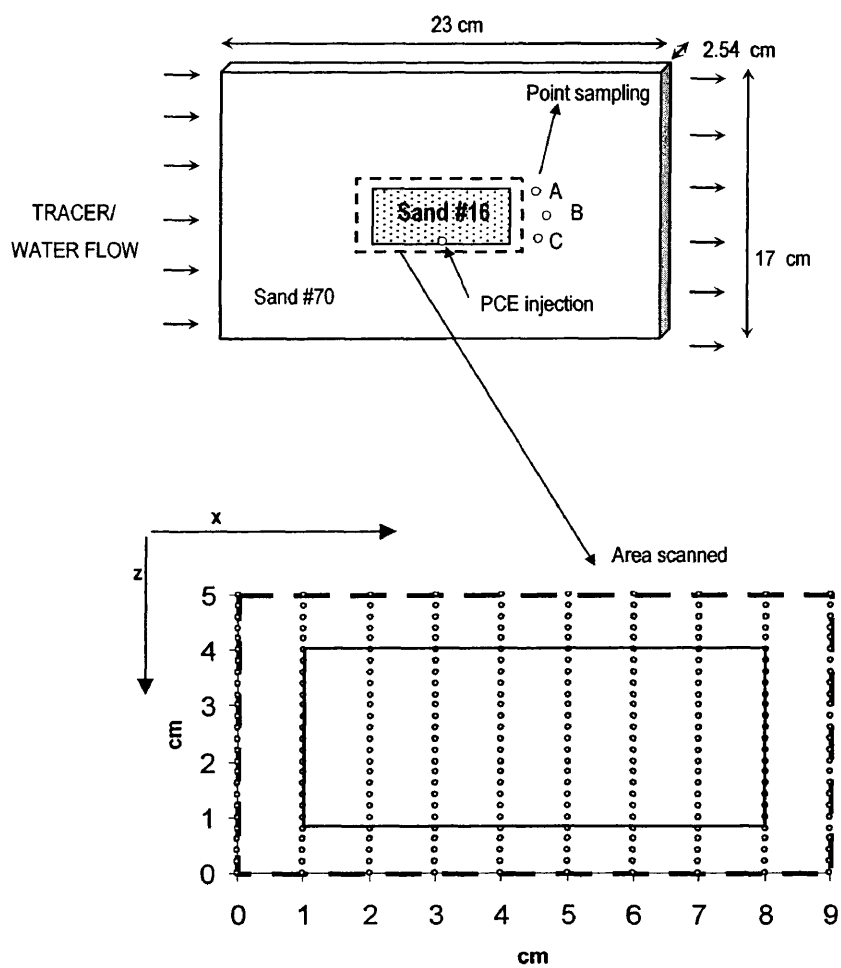
After the dye tracer test, a pulse of tracer solution was injected through the inlet port for 0.3 PV. The tracer solution contained 600 mg/l of 2,2-dimethyl-3-pentanol, 300 mg/l of 6-methyl-2-heptanol, 600 mg/l of n-hexanol and 500 ppm of NaBr. A constant flow rate of 2 ml/min was maintained throughout the tracer test.

Samples were taken every 30 minutes, collected in 0.2 ml inserts placed in GC autosampler vials, and analyzed using a Flame Ionization Detector. After analysis of partitioning tracers, bromide concentrations were analyzed using Ion Chromatography.

The same procedure was repeated for the four different PCE saturation profiles. Breakthrough curve data for all the tracer experiments are presented in the APPENDIX.

5.5 Results

PCE saturations were obtained from X-ray scans. The details of the X-ray attenuation methodology as applied to DNAPL saturation measurements can be found in Hill et al., (2002) and Hill and Illangasekare, (2004). A total of 250 points were scanned over the area contaminated with PCE. X-ray scanning was performed every 1 cm in the x axis and every 0.2 cm in the z axis. The different spacing in x and z axes was assigned based on the assumption that the distribution is fairly homogeneous in the x direction and the saturation variation is significant on the z direction, as it is expected from our pool conceptual model. Saturation profiles shown in Figure 5.2 represent the average saturation in the x direction of the 10 vertical sections where the saturation was measured. The error bars are the standard deviation of the average value.

Figure 5.2. Saturation profiles for the four configurations obtained by X-ray characterization. Error bars represent the spatial variability along the x axis.
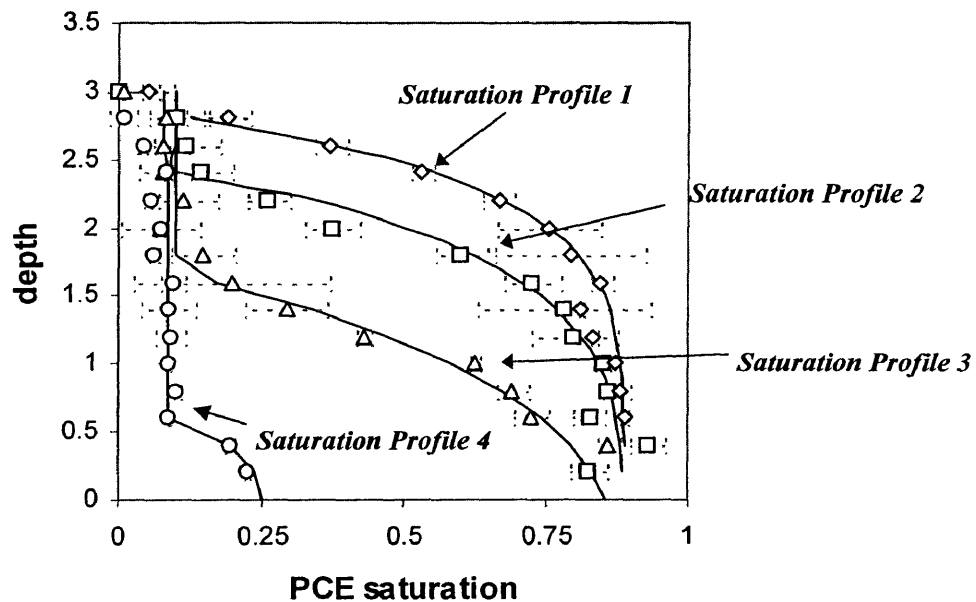
Scanning was performed for each of the four saturation profiles; X-ray attenuation results agreed with the mass of PCE estimated gravimetrically, as shown in Table 5.2.

Table 5.2. Total mass of PCE injected and measured by X-ray for each of the pool configurations.

Experiment ID	PCE (g)	
	Mass	X ray
Saturation Profile 1	27.0 ± 0.1	27.7 ± 0.3
Saturation Profile 2	21.9 ± 0.1	21.6 ± 0.3
Saturation Profile 3	16.7 ± 0.1	13.3 ± 0.2
Saturation Profile 4	8.2 ± 0.1	6.8 ± 0.4

5.5.1 Observed Tracer Behavior

During the dye tracer test, digital images were taken every 1 minute to record the tracer flow patterns within the cell. Four of these images are presented in Figure 5.3; as shown, the tracer bypasses the high saturation zone at the bottom of the pool and primarily migrates through the transition zone. This qualitative observation of migration paths of the dye validates the hypothesis that the tracers will mostly partition within the transition zone, and when the fractional mass of the DNAPL within this zone is high, the total mass estimation accuracy improves.

Figure 5.3. Dye tracer test through the flow domain.
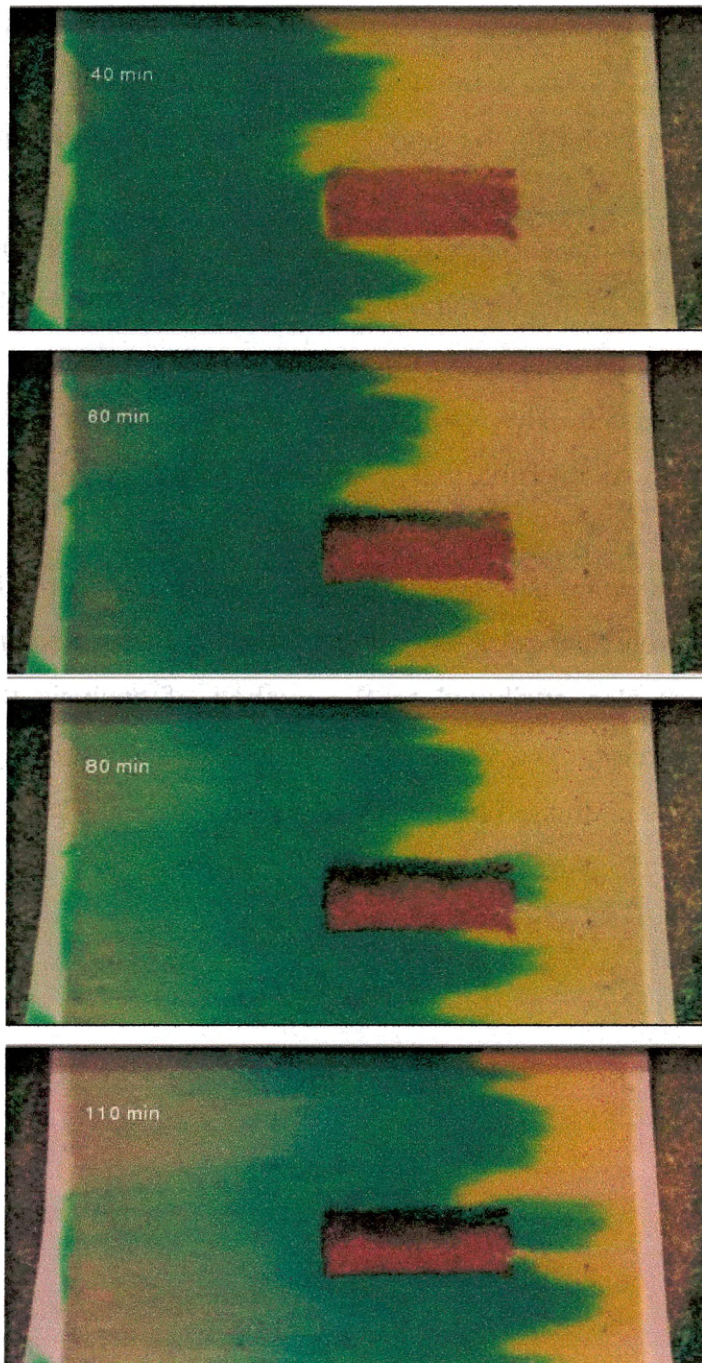
For each saturation profile, two tracer tests were performed. In one test, aqueous samples were collected from the outlet (simulating an extraction well) and in the other, sampling was done at different vertical distances immediately down-gradient of the pool (Ports A, B and C in Figure. 2). Mass estimates obtained from the moments of tracer breakthrough curves were compared to the actual mass of PCE present. In Saturation Profile 1, tracers estimated only 20% of the total PCE mass that was placed in the pool. For Saturation Profiles 2, 3, and 4; the depth of the high saturation zone became smaller in relation to the entire thickness of the pool, and tracers estimated 29, 39, and 57% of the total mass, respectively. These results were obtained using breakthrough curve data obtained from the outlet of the cell. The results of partitioning tracer tests for the PCE configurations studied are shown in Table 5.3. Saturation values were obtained using method of moments.

Although these results demonstrated the influence of pool morphology on the performance of the test; the relevant mass estimation discrepancies associated with the four saturation profiles were also attributed to the method of analysis that assumes equilibrium partitioning behavior. The influence of the method of analysis on the estimation errors of the PITT is addressed in the following section.

Table 5.3. Saturation values obtained by PITT for each of the saturation profiles.

Experiment ID	Sampling location		Saturation		
			DMP	hexanol	6M2H
Saturation Profile 1	Outlet		0.004	0.006	0.002
Saturation Profile 2	Outlet		0.005	0.007	0.002
	Ports	A[a]	--	--	--
		B	0.038	0.041	0.017
		C	0.051	0.099	0.020
Saturation Profile 3	Outlet		0.005	0.007	0.004
	Ports	A	0.009	0.099	0.001
		B	0.017	0.122	0.002
		C	0.045	0.186	0.004
Saturation Profile 4	Outlet		0.003	0.001	--
	Ports	A	0.008	0.075	0.001
		B	0.023	0.143	0.004
		C	0.012	0.106	0.002

5.5.2 Numerical Modeling Analysis

Recognizing the limitations of the tracer data analysis using moments, a second method of tracer data analysis was tested using numerical modeling. The purpose was to evaluate the errors of underestimation that can be attributed to the assumption of equilibrium inherent in the Kp. The flow and transport parameters of the test cell were calibrated using observed heads, total flow through the cell, and bromide concentrations measured over time at different locations of the flow domain. The flow model

---

[a] Port was clogged during experiment.

MODFLOW (Harbaugh et al., 2000), transport model MT3DMS (Zheng and Wang, 2000) and the inversion code UCODE (Poeter and Hill, 1998) were used in the parameter estimation.

Once the flow and transport parameters were estimated, the program module MODTRACER (Saenton, 2003) was used for tracer breakthrough data analysis. The method of analysis incorporated into MODTRACER enables existing flow and transport codes, MODFLOW and MT3DMS, to account for the presence of NAPL phase and partitioning behavior. The reduction in relative permeability of the aqueous phase and the retardation of partitioning tracer due to the presence of NAPL are taken into account. Inputs to this module include NAPL saturation (S_N) and Kp. The module simulates partition behavior assuming linear sorption and performs calculations to modify the parameters that are affected by the presence of entrapped DNAPL. It calculates a set of effective parameters, such as effective hydraulic conductivity, effective porosity, bulk density, and sorption coefficients corresponding to a given NAPL saturation in a computational cell. After MODTRACER generates the effective parameters, they are input in MODFLOW and MT3DMS. The model was verified against the analytical solution and validated using experimental data (Saenton, 2003). The scheme used in this module is only valid under the assumption that NAPL distribution is in static equilibrium.

Using the saturation profiles obtained from X-ray scanning (see Figure 5.2), MODTRACER generated the effective flow and transport parameters that were input in MODFLOW and MT3DMS. The model-simulated tracer breakthrough curves in the computational cell were compared with experimental data obtained from sampling ports B and C in Saturation Profile 2.

In this first simulation, the Kp determined in batch tests under equilibrium conditions was used. Simulations showed that while the computed conservative tracer breakthrough curves matched the experimental data well, the computed partitioning tracer breakthrough based on equilibrium Kp (from equilibrium batch tests) showed poor fit. The model outputs were found to be extremely sensitive to the assumed Kp. To relax

the requirement of partitioning to be at equilibrium, the use of an "effective partition coefficient" or "distribution coefficient" was investigated. This effective partition coefficient Kp_e was obtained through inverse modeling. UCODE was used to estimate Kp_e by minimizing the square residuals between the simulated and observed breakthrough curves. Figure 5.4 shows the model fit to the breakthrough curves from Ports B and C located at different depths. These effective parameters were lower than the ones obtained in batch experiments. Since the contact time between the tracer and the DNAPL decreases with increasing DNAPL saturation; the Kp_e is different for each region. These values were obtained using UCODE because the DNAPL saturation profile is known (from X-ray data). In the field, the saturation distribution is unknown so the Kp_e cannot be determined in this manner. A method developed to estimate Kp_e independently from DNAPL saturation in the laboratory follows.

Figure 5.4. Fitting of experimental values by inverse modeling relaxing the equilibrium condition.
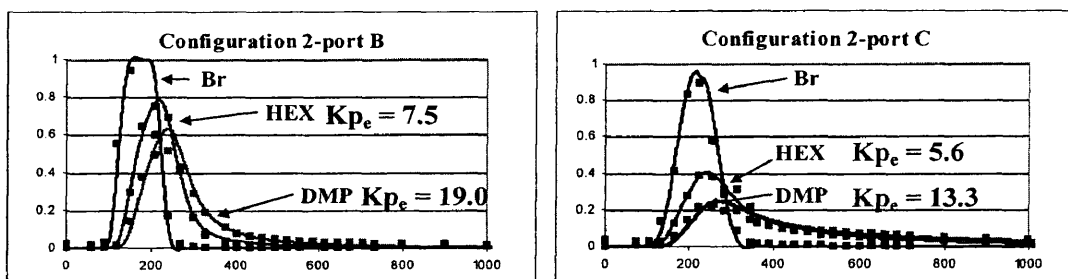
5.5.3 Nonequilibrium Batch Experiment

After obtaining the effective partition coefficients by inverse modeling, we performed a batch study to obtain a range of Kp_e in the laboratory.

The parameter Kp, assumes that the sorbed concentration ($\hat{C}$) is directly proportional to the dissolved concentration (C), as it is given from the linear sorption isotherm.

$$Kp = \frac{\hat{C}}{C} \qquad (5.5)$$

If the local equilibrium assumption is not valid, a mass transfer coefficient could be applied and sorption could be modeled as a first-order reversible kinetic reaction using a mass transfer coefficient (β) between the sorbed and dissolved phases. However, in complex entrapment architecture, where permeability contrasts control the local water velocities, it is difficult to assign a single value of mass transfer to the entire source zone (Saenton, 2003). Instead, a specific distribution coefficient applied to different areas was used, reflecting the local degree of deviation from equilibrium.

The objectives of this batch study were: i) to evaluate whether effective partition coefficients can be obtained independently in the laboratory instead of through inverse modeling, ii) to evaluate the influence of different residence time periods on the distribution coefficient, and iii) to analyze the behavior of different tracers under nonequilibrium conditions.

The nonequilibrium batch experiments followed the same procedure that was used in the equilibrium batch tests, except that the partitioning process was stopped at different times (15 min, 1 hour, 2 hours, 6 hours, 12 hours and 24 hours) by separating the aqueous and NAPL phases. The last time period of 24 hours corresponded to the equilibration time in the previous batch experiment.

Equilibration was achieved in two ways; one series of experiments was conducted with equilibration in an orbital shaker and another series was manually tumbled every 15 minutes. The samples were tumbled in the second series of experiments to maintain the integrity of DNAPL blobs throughout the experiments. Changes in the distribution coefficient over time are shown in Figure 5.5. For the three selected tracers, equilibrium was reached around 24 hours.

In the two-dimensional cell experiments, tracers with smaller partition coefficients provided a more accurate estimate of DNAPL volume, as observed by Brooks et al. (2002) in field tracer tests and by Imhoff et al. (2003) in laboratory experiments. This behavior can be explained by observing the plots in Figure 5.5; 6M2H (Kp = 88.50) presents very low values of Kp at early times, far different from its equilibrium partitioning value. As a consequence, if equilibrium is assumed when rate-limited behavior is present; the use of the equilibrium coefficient introduces significant error in the mass estimate. On the other hand, tracers with greater hydrophobicity (e.g. hexanol, Kp = 8.49), have an equilibrium coefficient that is not drastically affected by rate-limited behavior at early times, introducing less error in the analysis.

The Kp_e obtained by inverse modeling fell within the range of Kp_e determined in the laboratory. Both of these independent methods provided a clear indication of the importance of kinetic limitations in the partitioning process.

Figure 5.5. Values of Kp_e at different equilibration times for the three partitioning tracers.
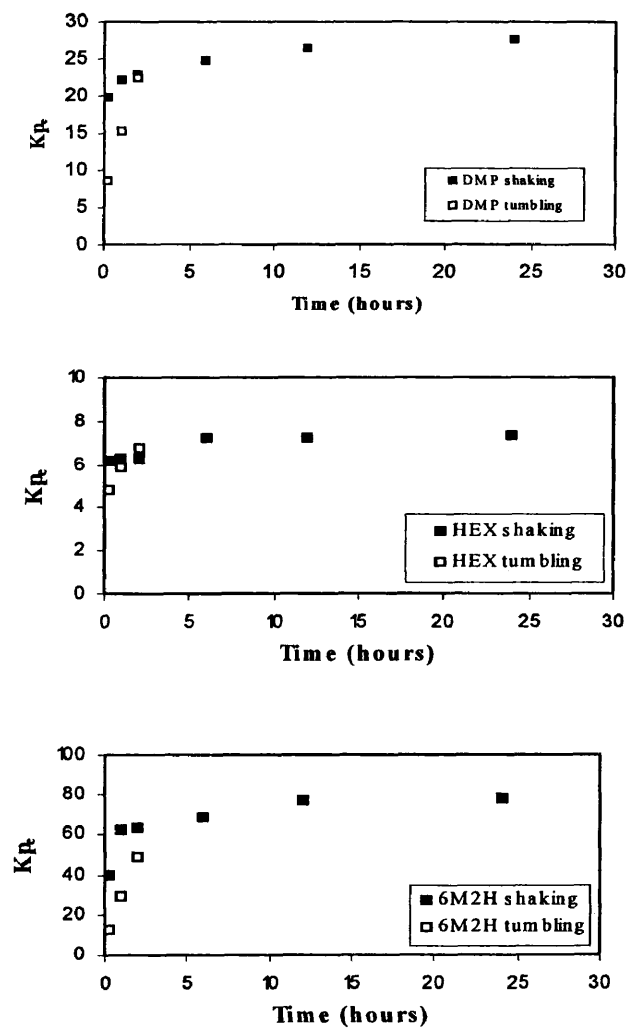
5.5.4 Saturation Estimation

Saturation distribution in the source zone can be estimated using inverse modeling. In previous simulations, the saturation profiles obtained from X-ray characterization were used to calibrate the partition coefficients. In these simulations, the information obtained by X-ray was not used in the inversion. The purpose is to use tracer data to estimate DNAPL saturation as is done in the field. Finally, results obtained from numerical analysis were compared with the saturation profiles obtained by X-ray and with estimations obtained using method of moments.

Although different researchers have used inverse modeling as a way to obtain saturations from tracer data (Jin et al., 1995), our approach used inverse modeling with additional information contained in the breakthrough curves. When zones of lower relative permeability are encountered, tailing and asymmetry appear in the breakthrough curves, reflecting rate-limited partitioning. The hypothesis is that these features could be used in the analysis to improve the quality of the saturation estimation. In order to apply this methodology, a set of distribution coefficients over time was required for each tracer (as conducted in the previous section).

Each of the breakthrough curves were used to estimate the saturation of the zone swept by the tracers, therefore a different Kp_e was assigned for each of the three zones based on the plots obtained through batch experiments.

In Figure 5.6 breakthrough curves collected at three different vertical locations of the source (A, B and C) are shown for Saturation Profile 3. Increased tailing with depth is observed when the concentrations are plotted in the semi-log scale. As tailing increases with permeability reduction in the vertical direction, smaller Kp_e values (farther from equilibrium) should be applied.

Figure 5.6 Breakthrough curves collected at three different locations after the source zone for Saturation Profile 3. Increasing tailing is observed as a result of increasing NAPL saturation.
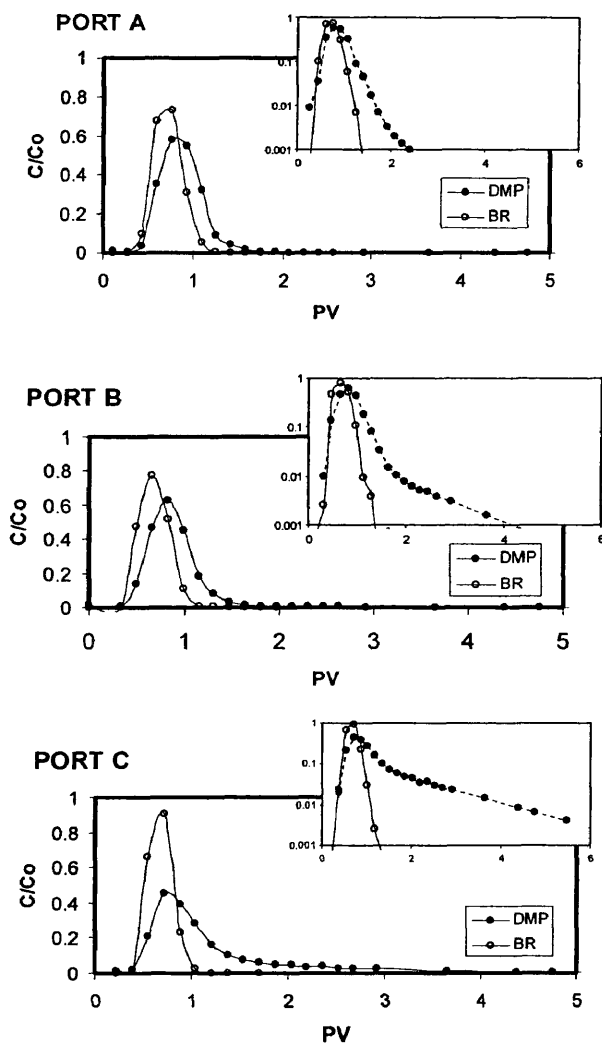
First, the Kp obtained from equilibrium batch test (27.51) was used to back-calculate saturation (one value of saturation for each zone). In a second simulation, three different Kp_e were applied to the three different zones. With the range of Kp_e obtained in the nonequilibrium batch tests for DMP (Figure 5.5), three different values were selected for the three swept zones. Zones 1, 2 and 3 represent the three areas of the source zone that correspond to the breakthrough curves obtained from Port A, B and C.

The estimation of saturation using MODTRACER/MODFLOW/MT3DMS coupled with UCODE for the three different zones is represented in Figure 5.7. The use of Kp_e provided a more accurate estimate. The total mass estimated using equilibrium Kp is 59.8%, whereas the use of Kp_e resulted in a total mass estimation of 87.7%. The use of Kp_e not only improved the estimation of PCE mass, but also the enhanced the quality of the regression.

Figure 5.7 Comparison of mass estimates obtained by numerical analysis, method of moments and X-ray characterization in Saturation Profile 3.
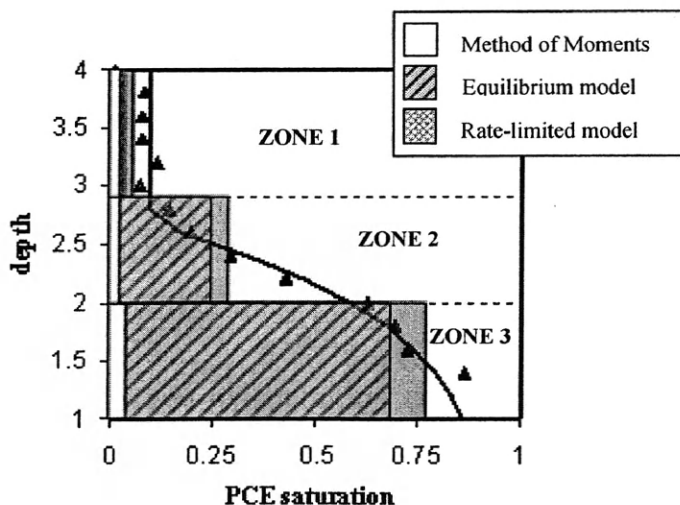
The difference between the three breakthrough curves obtained experimentally for this saturation profile Figure 5.6 are reflected in the computed values for the moments, where increasing tailing with depth results in increasing values of the second centralized moment (Valocchi, 1985). This characteristic could be used to incorporate tracer breakthrough curve features (e.g. signatures) as indicators of nonequilibrium conditions. The second centralized moments of the breakthrough curves versus the effective partition coefficients appear to follow a linear relationship. Decrease in relative permeability due to increasing DNAPL saturation with depth shows a linear relationship with the deviation from the Kp (see Figure 5.8). This type of empirical representation could be useful in field studies, since it would allow for extrapolation to determine values of Kp_e that correspond to specific breakthrough curves.

Figure 5.8. Linear relationships between effective partition coefficients with second moment (left) and average relative permeability (right).
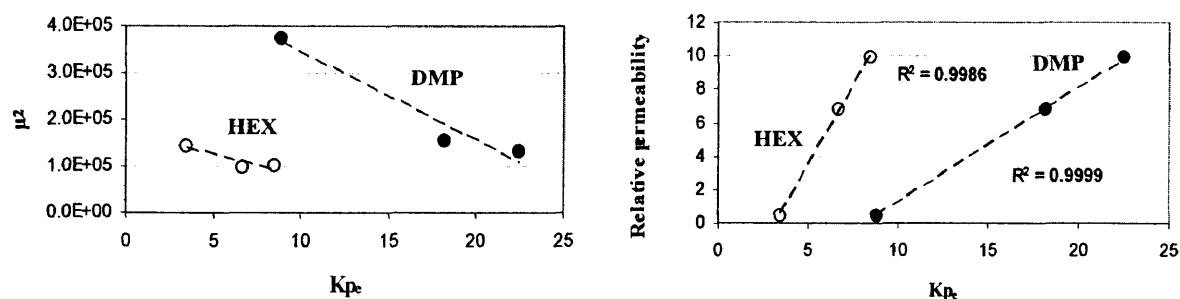
Estimated values of saturation via inversion with Kp_e will correct the effect of nonequilibrium partitioning. However, this method does not account for underestimation caused by hydrodynamic inaccessibility of the tracers to all DNAPL mass in the pool. The tracers do not respond to certain zones of the pool that are not accessed due to low

aqueous permeabilities. Under these conditions, streamlines of water carrying the tracer tend to diverge from the entrapment zone (as shown in Figure 4 for Saturation Profile 1).

5.6 Conclusions

Several conclusions can be drawn from this study. The pool morphology has an effect on the performance of the partitioning test. The influence of the NAPL saturation on the performance of the test has been evaluated by different researchers (Jin et al., 1997; Nelson et al., 1999; Dai et al., 2001). In those investigations, pools were considered homogeneous with a single value of saturation assigned to the high saturated zone. In this study, we investigated a broad spectrum of saturations that are present within a pool, demonstrating the macroscopic concept of a pool and its influence on the performance of the test. Variable permeability led to nonuniform DNAPL saturation, which resulted in the differing tracer breakthrough curves we observed at different vertical locations from the source zone.

This has several implications in field applications where the type of the DNAPL and the geological heterogeneity control the entrapment. The specific gravity of the DNAPL spilled determines the formation of thick or thin pools (McWhorter and Kueper, 1996). The transition zone is controlled by the type of DNAPL as well. The type of pools that are expected in the field will determine the performance expected by the PITT.

The tracer breakthrough curve data were analyzed using the traditional moment method and a calibrated numerical model. A "measured versus known" assessment was performed for both methods with respect to the actual DNAPL distribution obtained by X-ray data. In this way, the validity and limitations of both methods were established. Although method of moments severely underestimated the DNAPL mass, the use of first

and second moments yields valuable information about unique breakthrough curve signals that are related with the DNAPL architecture of the system.

The numerical model selected for this investigation successfully represented tracer transport providing useful information about the effect of the local equilibrium assumption in the final mass estimates. The purpose of this study was to evaluate simple, isolated pools to understand fundamental processes, but since the analysis is based in inverse modeling, more complicated architectures encountered at field sites could lead to non uniqueness of the solution and parameter estimates that are not robust. A validation of the presented procedures is presented in Chapter 6 for more complicated entrapment scenarios in an intermediate scale tank.

Modeling analysis suggested that more accurate DNAPL volume estimates could be obtained using Kp_e representative of nonequilibrium scenarios. However, depending on the saturation distribution, Kp_e are different; the tracer residence time depends on the degree of saturation that varies with depth, as shown in Figure 5.8. This study suggests that a unique Kp_e may not be applicable to an entire source zone.

Even though this is a disadvantage in the current use of PITT, the use of multilevel samplers (sampling at different depths) provides breakthrough curves that contain information about entrapment architecture and kinetic limitations. These signals indicate that Kp_e and/or mass transfer coefficients could be applied at different depths to estimate saturation with inverse modeling. Evaluation of signatures from breakthrough curves is crucial in the assessment of deviation from equilibrium. If the degree of nonequilibrium is still uncertain, the range of Kp_e obtained in batch experiments could provide values for conducting quantitative error analysis.

Incorporation of results from this investigation into tracer design and data analysis protocols may amplify the extent of the partitioning tracer technique for DNAPL characterization at heterogeneous sites.

Chapter 6

INFLUENCE OF DNAPL SOURCE ZONE ARCHITECTURE ON THE PERFORMANCE OF PARTITIONING TRACER TESTS

6.1 Abstract

This study represents the first intermediate scale experiment to investigate partitioning tracer behavior in experimental settings that could reproduce some of the features of the complexity of heterogeneous field sites. The purpose of this work is to examine the effect of DNAPL architecture on the performance of PITT in conditions of heterogeneity. Tracer experiments were conducted in a (4.87 m x 1.21 m x 0.05 m) flow cell with a heterogeneity defined by a log-normal distribution of hydraulic conductivity with a mean value of $\mu_{lnk} = 4.18$ cm h^{-1}. PCE was spilled into the heterogeneous media in controlled conditions but the DNAPL phase was allowed to distribute naturally, creating entrapment zones with residuals, transition and pool zones. Gamma attenuation methods were used for in-situ measurement of DNAPL saturations. Once the saturation distribution was accurately characterized, a set of tracer tests was conducted. The extensive data set gathered in this experiment was analyzed to evaluate the potential of tracers to determine complex DNAPL architectures. Method of moments and inverse modeling were both applied to evaluate how different methods of interpretation affect the final results.

Inverse modeling offered an integrated interpretation of the system and tracer behavior and it allowed the incorporation of effective "effective partition coefficients"

(Kp_e) to relax the requirement of equilibrium. Even though underestimation of the high saturation zones is expected, the incorporation of information contained in the breakthrough curves (e.g. tailing) in data interpretation enhances the mass estimation by the tracers.

The procedure developed in Chapter 5 for a single pool was tested here for a more realistic DNAPL source zone architecture containing both residuals and pools. The final goal was to determine the potential of PITT to characterize NAPL architecture in heterogeneous sites and to provide a set of guidelines that could improve current application of the technique in conditions of heterogeneity.

6.2 Introduction

It is widely recognized that the inherent complexity of DNAPL sites increases the difficulty of effective site remediation. Innovative research has been conducted in the last years to improve and develop techniques that can successfully determine the distribution of the DNAPL in the subsurface.

The Partition Interwell Tracer Test (PITT) was developed for environmental applications by Jin et al. (1995). This technique was originally developed by petroleum engineers in enhanced oil recovery. It consists of the injection of a set of reactive and non-reactive tracers that travel through the source zone located between the injection and extraction wells. The transport of the reactive tracers is delayed with respect to the non-reactive tracers due to partitioning into and out of the DNAPL phase. If equilibrium conditions are present then the retardation depends only on the DNAPL saturation and the partition coefficient of the tracer (Kp).

The limitations of the PITT in conditions of heterogeneity have been identified in several studies (Nelson et al., 1999; Rao et al., 2000; Brooks et al., 2002; Jalbert et al.,

2003). The non-uniform distribution of DNAPL as a consequence of the natural heterogeneity results in hydrodynamic inaccessibility that may lead to underestimation errors.

Different studies in the literature have been conducted to explore this issue. Willson et al. (2000) evaluated the assumption of local equilibrium in one-dimensional columns and observed the effect of rate limited absorption in tracer breakthrough curve data. Dai et al. (2002), evaluated the sole influence of entrapment architecture (pools versus residuals) where estimation errors were measured in one-dimensional columns. In a recent investigation, Imhoff and Pirestani, 2004 proposed a set of guidelines to interpret breakthrough curve data to ascertain the importance of mass transfer limitations. With respect to two dimensional studies; Nelson et al. (1999), evaluated the influence of heterogeneity and sampling methods in an experimental tank where two different block geometries were created, but the NAPL distribution was homogeneous within the block which may not be a realistic model (as discussed in Chapter 5). Jalbert et al. (2003) performed an experiment that also demonstrated the general difficulty of tracer tests to detect NAPL located in pool or large lenses.

All the investigations above considered one dimensional or two dimensional studies with discrete and simple inhomogeneities. Two types of entrapment configuration have been considered so far: residuals and pools. In chapter five the issue of a pool that contains a broad spectrum of saturations was introduced and explored in a two dimensional test. Results showed the importance of including the transition zone in the final output of the test.

It is necessary to observe tracer behavior in simplistic scenarios of DNAPL distribution to understand mass transfer mechanisms. However, it is also important to up-scale the findings from previous investigations to more complicated settings that could resemble natural, heterogeneous field systems. Several tracer tests studies have been conducted in the field (Annable et al., 1998; Cain et al., 2000, Jawitz et al., 2000; Meinardus et al., 2002; Divine et al., 2004). The problem in field investigations comes

from the difficulty in understanding fundamental processes since the DNAPL distribution is unknown.

This investigation attempts to fill the gap between too simplistic heterogeneous settings in the laboratory scale and full-scale studies. An intermediate scale tank was used as an artificial two-dimensional aquifer. A stochastic heterogeneous random field was generated to represent the effect of field heterogeneity; in this way, tracer performance could be evaluated in more complex entrapment morphologies. This is the largest controlled experiment to evaluate PITT performance that has been conducted so far.

The objective of this research experiment was to develop data to validate techniques that could delineate and determine DNAPL saturations in heterogeneous entrapment configurations. Previous experiments described in this thesis were conducted to quantify estimation errors of partitioning tracers and to improve existing tracer technologies; this experiment was used to validate these improvements in tracer protocols for more realistic heterogeneous settings.

6.3 Materials and Methods

A set of tracer tests experiments was conducted in an intermediate scale flow tank. Since the purpose of this investigation is to evaluate PITT under heterogeneous conditions, packing configuration and procedures were design to resemble the complexity of heterogeneous field sites. To create the permeability domain, the turning bands method was used to generate a random field. The input parameters were mean of log K (K in m/day) 4.18, variance of 1.22, horizontal correlation length of 0.508 m and vertical correlation length of 0.0508 m. Then, the hydraulic conductivity was discretized into five categories that correspond to five Unimin laboratory sands (Barth and Illangasekare, 2000). Out of the twenty realizations generated with the selected statistical parameters,

only one was selected to be physically created in the tank. The criterion established to select one particular realization was based on the protection of the bottom of the cell from DNAPL migration, by choosing a realization with a lower permeability layer located between 0.5 and 1.5 ft distance from the bottom of the tank. In this way, enough vertical distribution of DNAPL in the source zone was allowed while the bottom of the cell was still protected from DNAPL that could deteriorate the joints and leak through the tank seals.

Two main regions were defined in the tank: a homogeneous zone created out of a coarse material used for tracer injection, and a heterogeneous zone where DNAPL is injected and observations ports are distributed downstream of the source zone to monitor tracer transport. Constant head reservoirs controlled the boundaries and they could be raised or lowered to set the desired gradient through the cell.

A PVC pipe was used for delivery and placement of the sands according to the selected permeability distribution. The pipe allowed for settling of the grains and created more realistic boundaries, avoiding the formation of sand blocks. The packing was conducted under water-saturated conditions to avoid air entrapment; the water level was maintained 1 or 2 inches above the top layer. A total of 2800 cells were packed in 100 layers and 28 columns.

After packing, water was flushed through the tank and a series of experiments was conducted once that steady state flow condition was achieved. The chronology of all these activities is presented in Table 6.1 and a description of all the PITT experiments follows.

102

Table 6.1. Chronology of all the experimental tasks.

Task ID	Description
Scanning 0	Gamma scan prior to spill
PITT 0	Blank tracer test to check design parameters, background retardation and to obtain transport parameters for model calibration
PCE spill	586.7 ml of PCE were spilled into the tank
Scanning 1	Gamma scan to determine PCE saturations
PITT 1	Partitioning tracer test to determine DNAPL architecture
SEAR	Surfactant flushing
Scanning 2	Gamma scanning to determine new saturations after remediation
PITT 2	Partitioning tracer test to determine DNAPL architecture and remediation performance

6.3.1. PITT 0

A background tracer test was conducted primarily to evaluate retardation of the conservative tracers due to other mechanisms such as sorption into the medium. With this test it was also possible to (1) check the uniformity of tracer injection through all the ports, (2) test design parameters like flow rate, injection time, sampling frequency and total sampling time, and (3) obtain a set of conservative tracer data for calibration of transport parameters.

A solution of 500 ppm of NaBr, 300 ppm of hexanol and 300 ppm of DMP was injected into the upstream tank using a multi-syringe pump located in the center of the homogeneous zone. The pump used 32 injection ports that were set to create a total injection flow rate of 8 ml/min during a total injection time of 10 hours. The water flow

rate through the tank was controlled using two constant head reservoirs connected to each end of the tank.

After tracer injection, samples were taken manually at 29 ports located at 6 different vertical arrays located downstream from the source zone (Figure 6.1). To reduce the required sample volume, 0.2 ml inserts were placed in 1.5 ml vials. A total of 596 samples were collected during the experiment and analyzed in the gas chromatograph.

Figure 6.1. Schematic of the flow cell. On the top, the permeability field is represented, on the bottom, the location of all the sampling ports is specified.

104
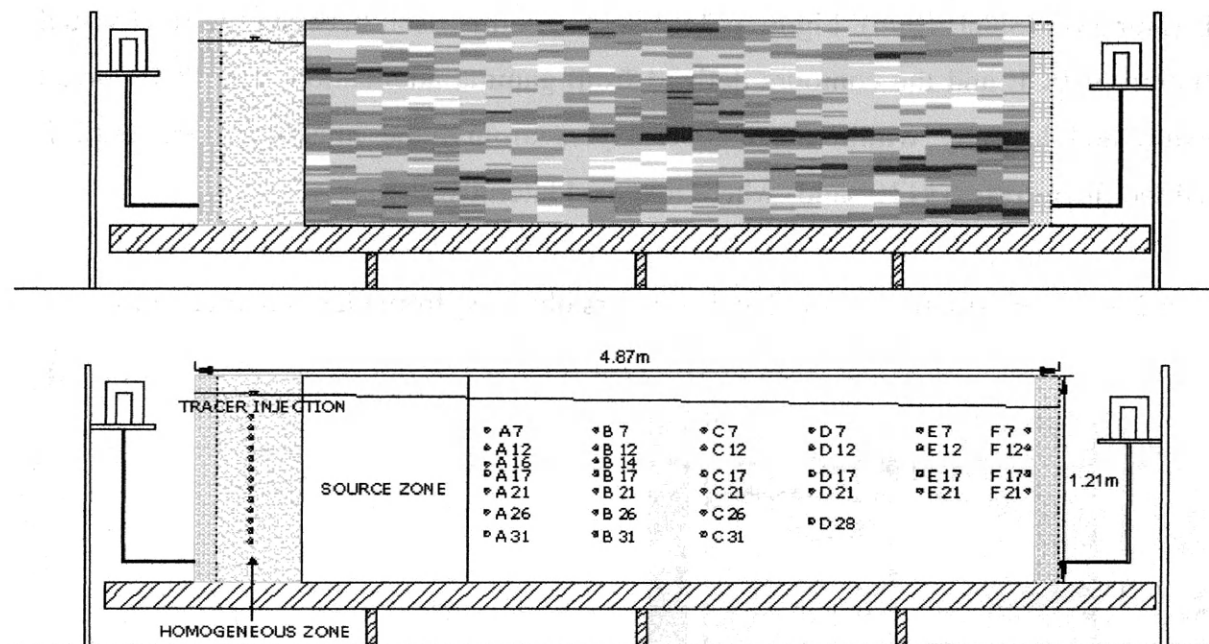
6.3.2. PCE Spill.

Once the porous media were packed in the tank and steady state flow was established through the cell, the PCE source zone was created. A Mariotte bottle was used to inject PCE under constant head. To avoid lateral migration of the contaminant beyond the area scanned during background gamma scanning, the PCE was injected at five different vertical locations in the same vertical array, each of them located at a different depth. During injection, the flow rate and the volume of PCE injected were monitored using an electronic scale. A total volume of 586.7 ml was injected and allowed to achieve static conditions.

After the spill, the saturations of PCE in the source zone were determined using gamma attenuation. Results from Scanning 0 and Scanning 1 were combined to obtain NAPL saturation (Saba, 1999). Figure 6.2 shows the comparison between the final visual distribution of PCE and the contours defined from gamma attenuation. The PCE spread downward and laterally within the coarser layers around the injection ports until it reached the finer layers (#110 sand) where it spread laterally.

Figure 6.2. Final distribution of PCE and contours obtained from Gamma attenuation.
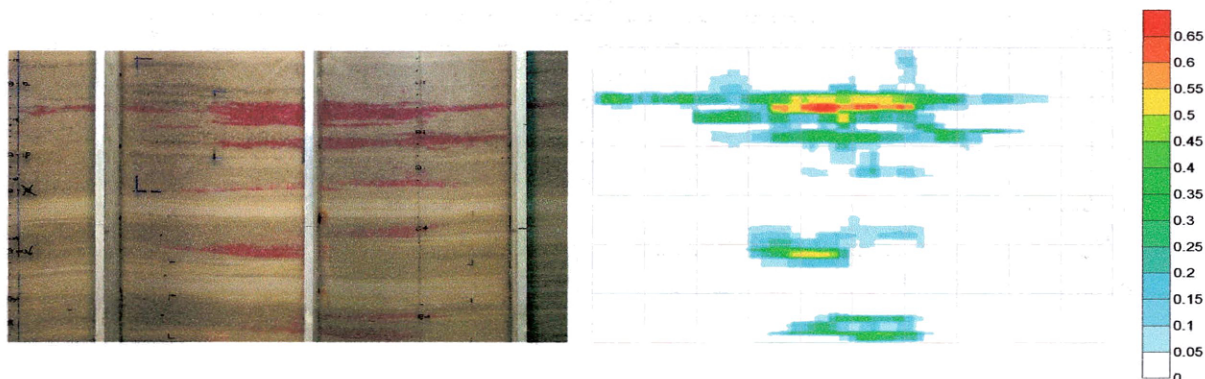
6.3.3. PITT 1

After injection of PCE and scanning of the source zone, flow conditions were reestablished and the second partitioning tracer (PITT 1) was conducted with the same design parameters applied in PITT 0. During the test, flow was monitored at the tank outlet to verify steady state flow conditions throughout the experiment. The samples were collected in 1.5 ml vials with 0.2 ml inserts, then capped and stored for gas and ion chromatography analysis. A total of 900 vials were collected during this experiment. The total time of the experiment was increased to 4 days since a delay in partitioning tracer transport due to the presence of DNAPL was anticipated.

6.3.4. PITT 2

After the first tracer test to characterize DNAPL, a Surfactant-Enhanced Aquifer Remediation (SEAR), also known as surfactant flushing, was applied to the two-dimensional tank. SEAR is designed to enhance the solubility of the DNAPL phase by reducing the interfacial tension between the NAPL and water phases. For this particular investigation, the purpose was to obtain a new distribution of PCE with the use of surfactants, rather than to evaluate the performance of the SEAR technology. It is expected that the surfactants will remove most of the DNAPL that is accessed by the water flow lines. After remediation, a DNAPL entrapment architecture was presumed where most of the DNAPL in the residual form was removed and most of the pools still prevailed. Another gamma scan was conducted afterwards to obtain precise information about the saturation distribution after SEAR.

A second partitioning tracer test was then conducted with the same design parameters as the previous ones.

6.4 Results

Results obtained from all the tracer tests are discussed in the following section.

6.4.1 Observed Tracer Behavior

A series of experiments comprising three tracer tests were conducted in the tank. Results from experiment PITT 0 showed no background retardation of any of the tracers in the system (see section 3.5 for results and details). Breakthrough curves (BTC) also demonstrated that the injection pump was generating the appropriate flow patterns in the domain, so a uniform tracer front was created in the homogeneous zone before entering the heterogeneous zone. The location of the injection and extraction ports was found suitable for future tests since the tracers swept the area that was supposed to delineate the future source zone (after DNAPL spillage). The data obtained in PITT 0 also showed the influence of heterogeneity reflected in the variability in breakthrough curve shapes collected at the same vertical section.

Results of PITT 1 demonstrated the presence of DNAPL. During data analysis, the Ion Chromatograph experienced some technical difficulties, which caused the loss of some bromide samples. This technical problem resulted in bromide breakthrough curves that are nonexistent or incomplete (A26 and A31). The breakthrough curve data obtained at all the locations in the tank can be found in Appendix A.

Before the data were examined using method of moments, the breakthrough curves were analyzed qualitatively to evaluate signatures or features that contain information about the vertical architecture of the system.

In Figure 6.3, the breakthrough curves collected in array A are presented. All the locations captured some retardation by the partitioning tracers. The breakthrough curves collected during PITT 1 demonstrated the presence of high saturation zones of PCE.

Tailing observed in A16 and A17 indicates that the DNAPL is not distributed uniformly since a uniform distribution would produce a simple offset (Brooks et al., 2002; Jawitz et al., 1998b). This feature could also be the result of non equilibrium conditions that reflect permeability contrasts in the source zone. These permeability contrasts control the local velocities, and tracer may not reside for a sufficient time to partition with all the DNAPL mass. Tracers just partition with the DNAPL located in the transition zone of the pools as described in the conceptual model developed in previous chapters.

In these scenarios of high heterogeneity and rate-limited partitioning, the retardation is reflected in the tailing portion of the breakthrough curve and may not be entirely captured due to the detection limit of the analytical instruments. The BTC tail was extrapolated using an exponential decay function (Pope et al., 1994; Annable et al., 1997) in the cases where truncation was observed (A16 and A17). Those BTCs are plotted in Figure 6.3 in both natural and semi-log scale to show the trend at low concentrations.

The issue of tailing becomes more problematic as the distance from the source zone increases since tails are not detected due to concentration values below detection limits. In array F (located at 3.5 m from the source zone) the retardation becomes very small compared with the retardation obtained at array A (at 0.5 m of the source zone) due to mixing and dilution of tracers.

Figure 6.3. Breakthrough curves collected in array A.
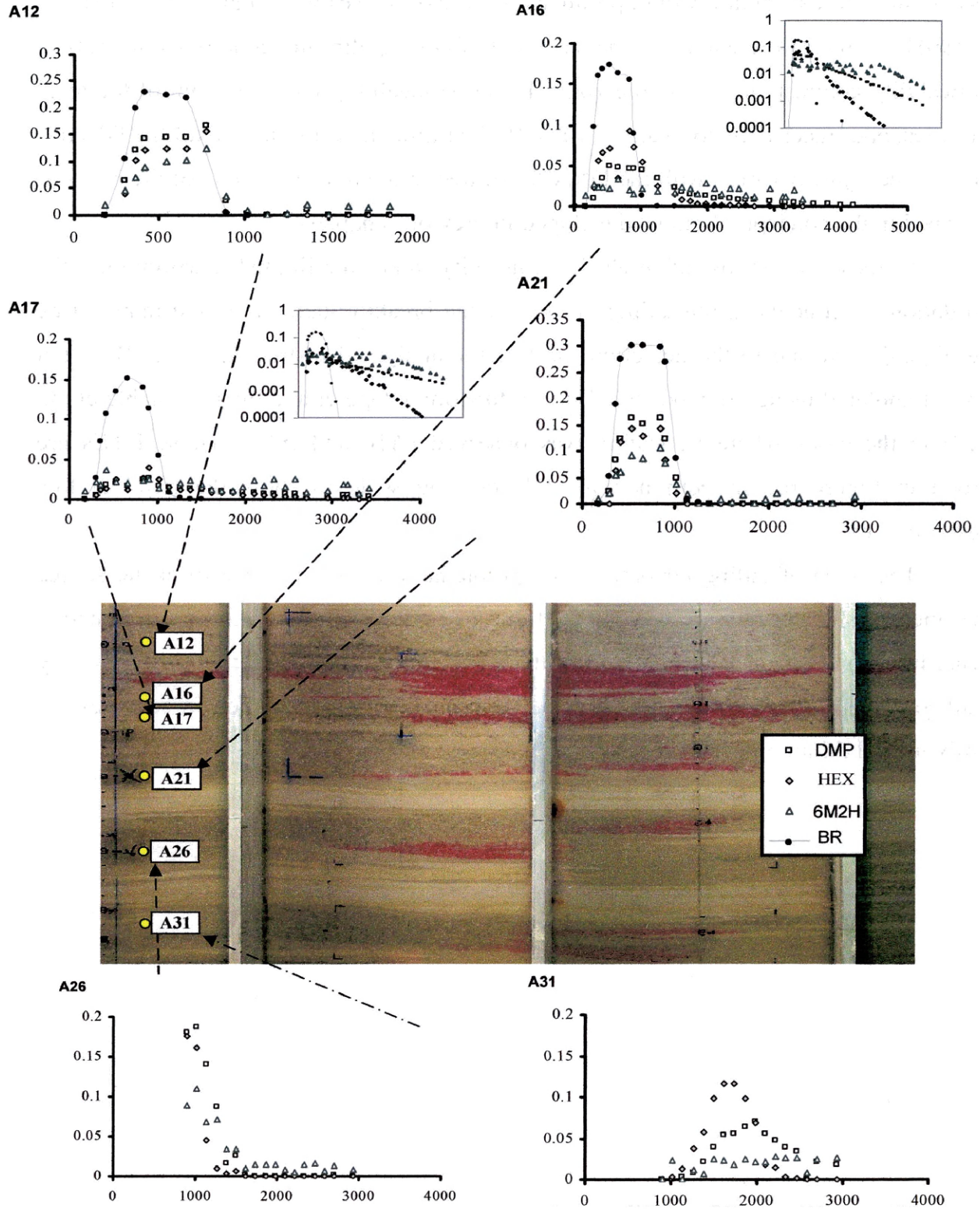
6.4.2 Method of Moment Analysis

After qualitative analysis of the breakthrough curves, arrival times of all the tracers were calculated using numerical integration. The average saturation can be obtained with equation 2.6.

For the sampling ports that did not contain sufficient bromide observations, hexanol observations were used as the reference to calculate retardation values using Equation 6.1 (Jin et al., 1995). Equation 6.1 is the simplification of Equation 2.6 for conservative tracers as reference tracers.

$$S_N = \frac{\bar{t}_2 - \bar{t}_1}{(K_{N,W}^2 - 1)\bar{t}_1 - (K_{N,W}^1 - 1)\bar{t}_2}$$

(6.1)

The saturation values obtained at each location are represented in Table 6.2.

Three partitioning tracers were injected in the tracer solution which implies that breakthrough curves and retardation obtained from the three tracers were evaluated to select the tracer that provides the most reliable data. Since hexanol was used as a reference tracer in the breakthrough curves that lack bromide data, and 6M2H seems to deviate more from equilibrium conditions (see Figure 5.6), DMP was selected as the "best performer tracer". Numerical modeling analysis used DMP data for inversion procedures.

Table 6.2. Average saturation values obtained using method of moments for all the sampling ports.

PORT	SATURATION		
	DMP	HEX	6M2H
A7	0.0038	0.0121	0.0049
A12	0.0027	0.0041	0.0048
A16	0.0703	0.0800	0.0374
A17	0.0646	0.1352	0.0267
A21	0.0019	*	0.0085
A26	0.0185	*	0.0144
A31	0.0121	*	0.0022

PORT	SATURATION		
	DMP	HEX	6M2H
B7	0.0003	*	0.0111
B12	0.0016	*	0.0165
B14	0.0142	0.0058	0.0156
B17	0.0207	0.0177	0.0105
B21	0.0437	0.0527	0.0238
B26	0.0012	*	0.0051
B31	0.0121	0.0149	0.0031

PORT	SATURATION		
	DMP	HEX	6M2H
C7	0.0005	0.0084	0.0049
C12	0.0087	*	0.0161
C17	0.0136	0.0004	0.0070
C21	0.0081	0.0045	0.0029
C26	0.0234	0.0256	0.0138
C31	0.0360	0.0765	0.0146

PORT	SATURATION		
	DMP	HEX	6M2H
D7	0.0023	*	0.0097
D12			
D17	0.0111	0.0036	0.0035
D21	0.0110	*	0.0013
D28	0.0083	*	0.0024

PORT	SATURATION		
	DMP	HEX	6M2H
E7	0.0001	*	0.0084
E12			
E17	0.0085	*	0.0024
E21	0.0037	*	0.0003
E28	0.0042	*	0.0034

PORT	SATURATION		
	DMP	HEX	6M2H
F7	0.0141	*	
F12			0.0028
F17	0.0073	*	0.0015
F21	0.0114	*	0.0018

---

* It indicates that hexanol data was used to calculate retardation

As expected, with increased distance from the source zone, the retardation values were smaller since the signal attenuated due to mixing. Figure 6.4 shows the comparison between method of moment estimates and the gamma-measured distribution of PCE. The method over or underestimates the vertical saturation profile depending on the tracer flow around the source zone and downstream. In array A, B and C, the signals contain some information about the vertical architecture. On the contrary, results obtained at array D, E and F did not contain enough information about the DNAPL vertical distribution. In arrays located at a distance greater than 2 meters from source zone, the heterogeneity controls the mixing of the signals downstream and dissipates the information about the vertical architecture.

Figure 6.5 shows the average saturation values obtained at each array: the error bars represent the variability of the values obtained from all the ports located in the array. Array A (the closest to the source zone) has more variability since the ports collected strong signals with information about the vertical architecture of source zone. As the distance from the source zone increases, the signal attenuates and the information about vertical architecture dissipates (low variability in array F). This figure shows the importance of well location in the design of the PITT.

Figure 6.4. Actual PCE saturation (line) and PCE saturation calculating using moments (dots).
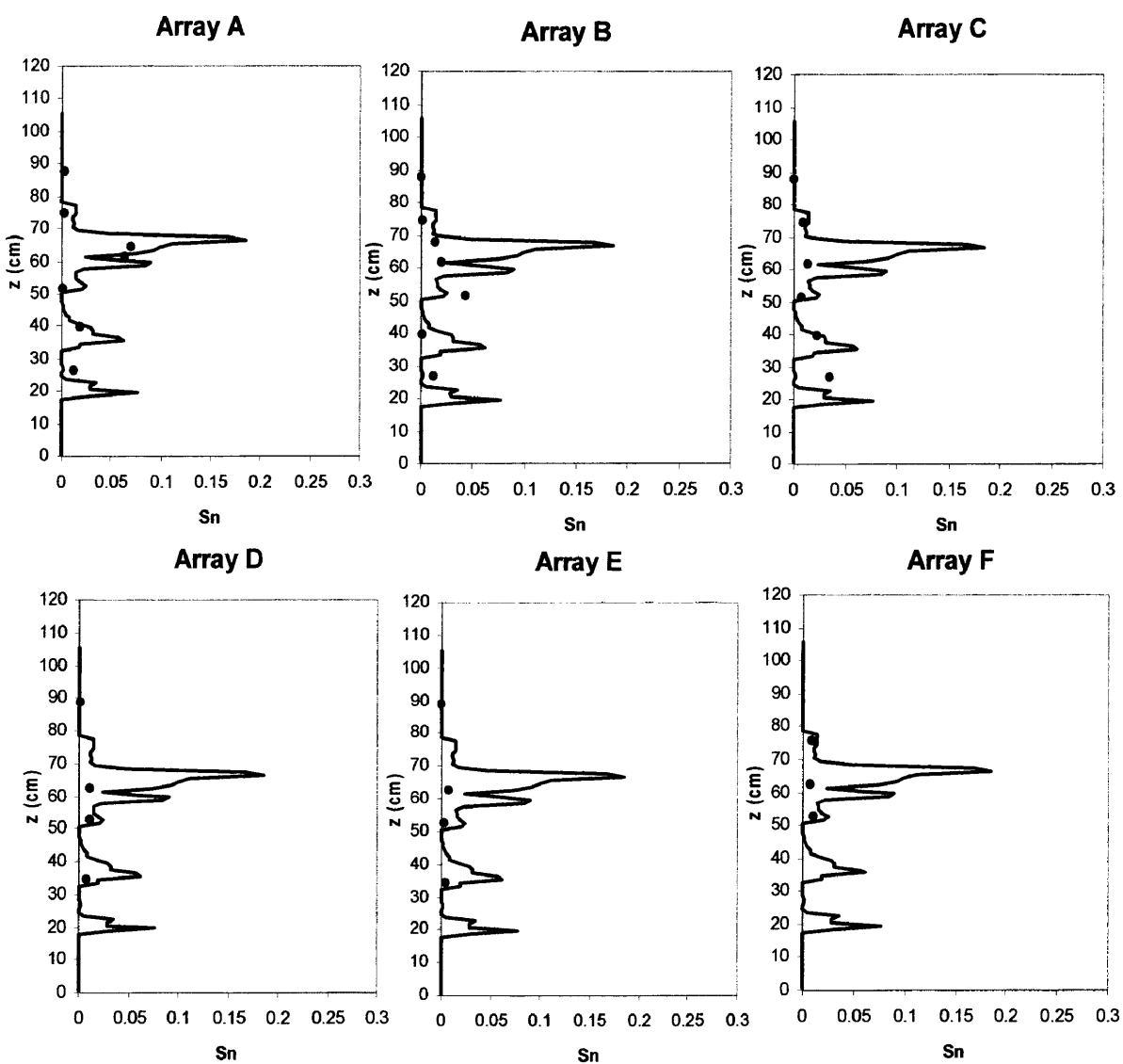
Figure 6.5. Saturation values obtained with increasing distance from the source zone.
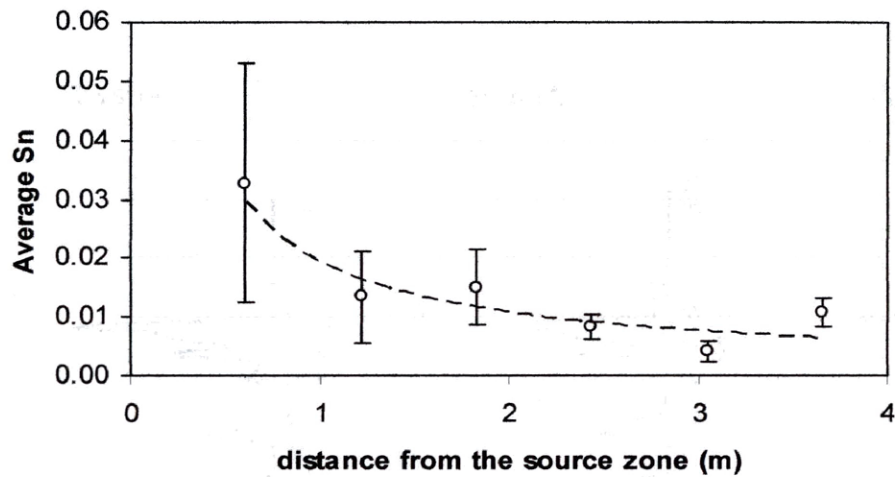
The gamma measurements were performed after SEAR and a second PITT was conducted (PITT 2). In this way, not only can the performance of the PITT to determine architecture be evaluated, but also the performance of PITT as a tool to determine the effectiveness of the remediation can be assessed. From the saturations obtained by gamma attenuation, high saturations zones of PCE were still present (Figure 6.6).

Figure 6.6. Final distribution of PCE and contours obtained from Gamma data after SEAR.
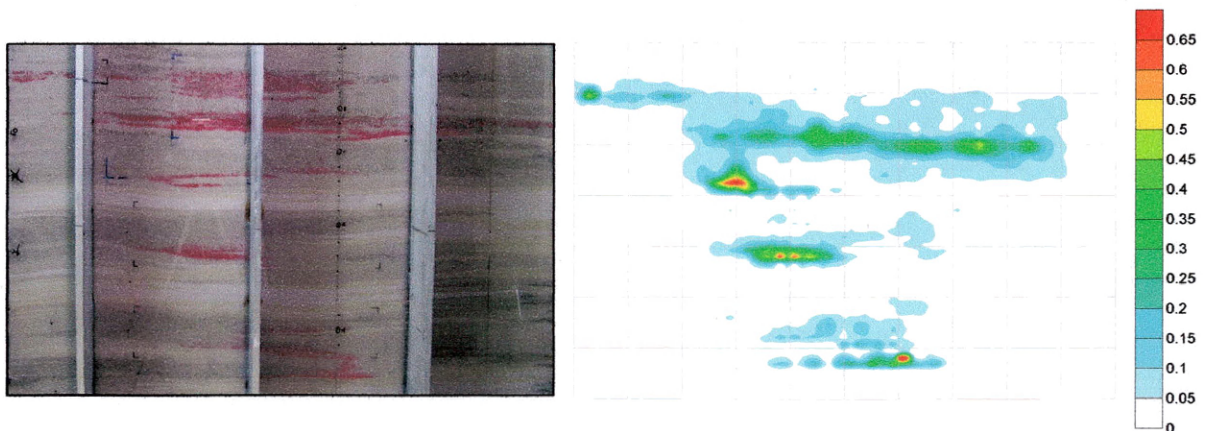
The qualitative observation of breakthrough curves obtained in PITT 2 shows the lack of tailing in all the locations (see Figure 6.7). Since it was hypothesized that the tracers do not flow through the high saturation zones due to the permeability contrasts, tracers are not reflecting retardation from most of the PCE mass still present. The remaining PCE zones are disconnected from the tracer flowpath due to the inefficiency of the surfactant in removing pool areas. This problem could have severe effects when PITT is applied to assess remediation performance; the test shows that most of the DNAPL mass has been removed, when in reality, tracers are bypassing the remaining DNAPL.

After qualitative analysis of the breakthrough curves, arrival times of all the tracers were calculated using numerical integration following the same procedures use in PITT 1 to obtain saturation values. Underestimation of the DNAPL saturation is observed in all the arrays. For this architecture, the signal dissipates by the time it reaches array B such that it contains almost no information about the vertical DNAPL architecture.

116

Figure 6.7. Breakthrough curves collected in array A after surfactant flushing.
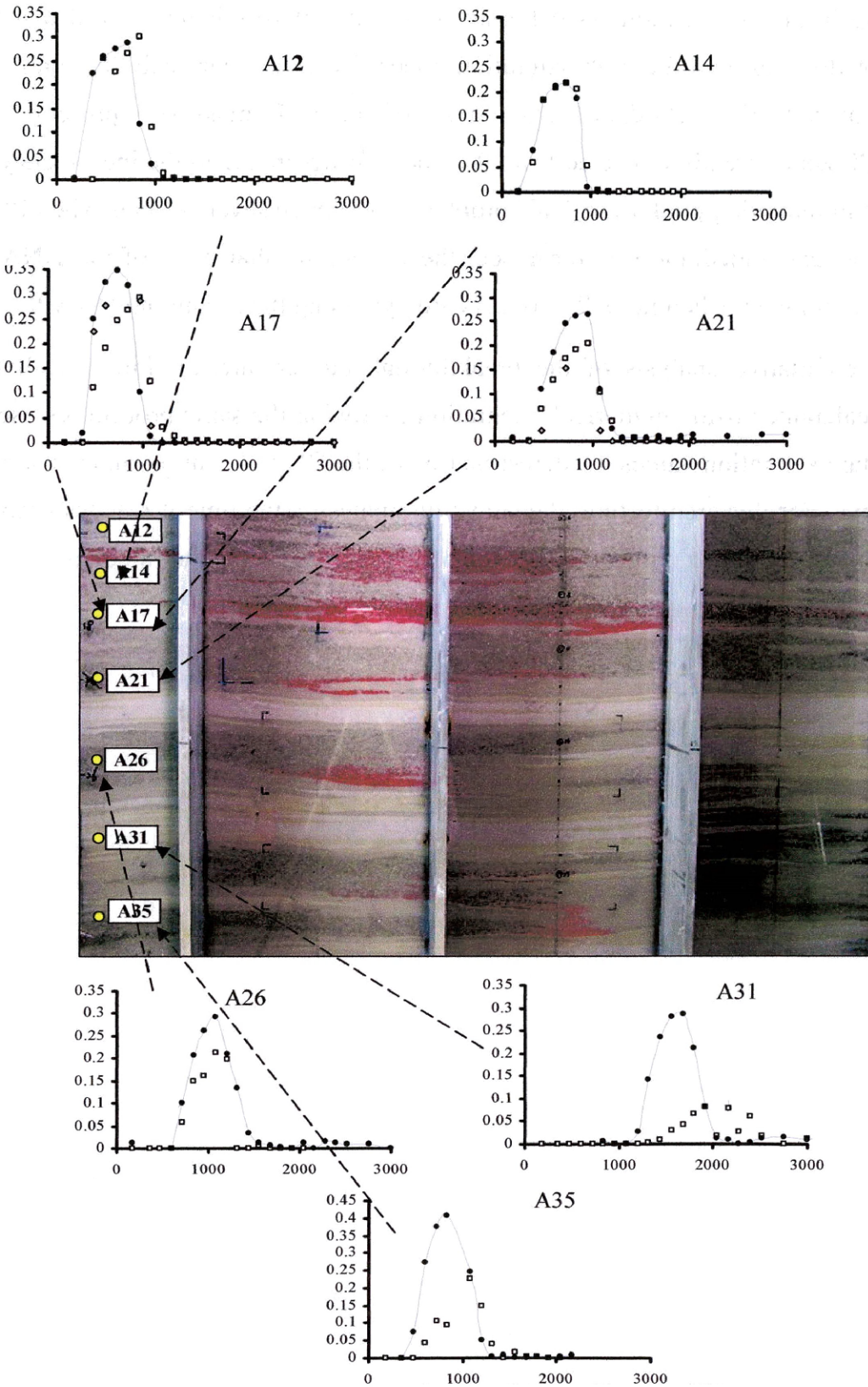
Figure 6.8. Actual PCE saturation (line) and PCE saturation obtained by moments (dots) at each of the arrays after surfactant flushing.
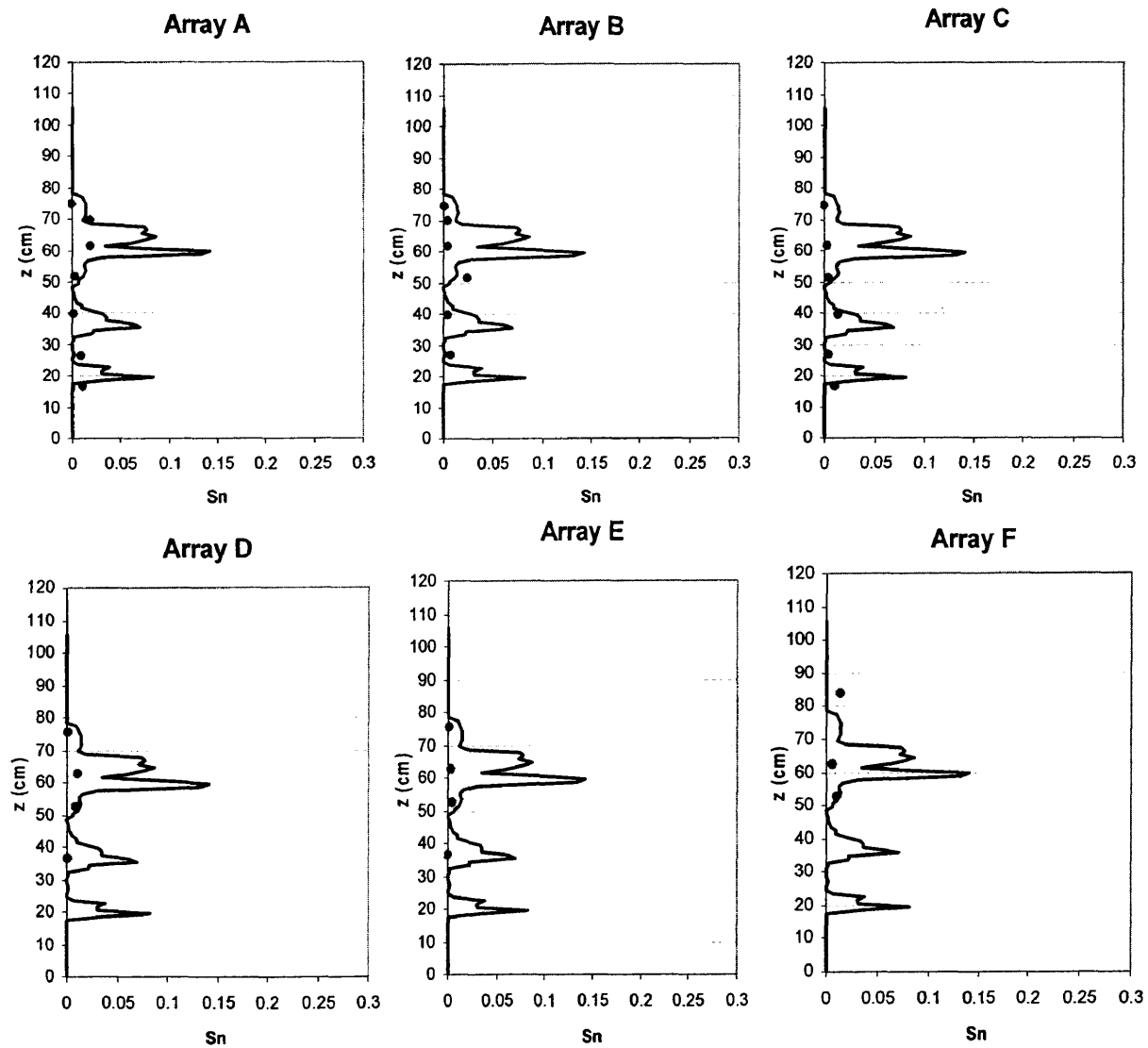
The difference between the saturations obtained from PITT 2 and the saturations obtained from PITT 1 should hypothetically represent the PCE removed by the SEAR technology. Figure 6.9 represents saturation results from both tests at each of the six vertical arrays. On first inspection, array A and B show a decrease in saturation in the portions of the source zone that contain most of the PCE mass (between A14 and A17). However, the contour plots in Figures 6.2 and 6.6 show that a considerable amount of PCE remained in those locations where PITT showed a decrease in saturation (A16 and A17).

Figure 6.9. Saturation obtained from PITT 1 and PITT 2 in all the arrays.
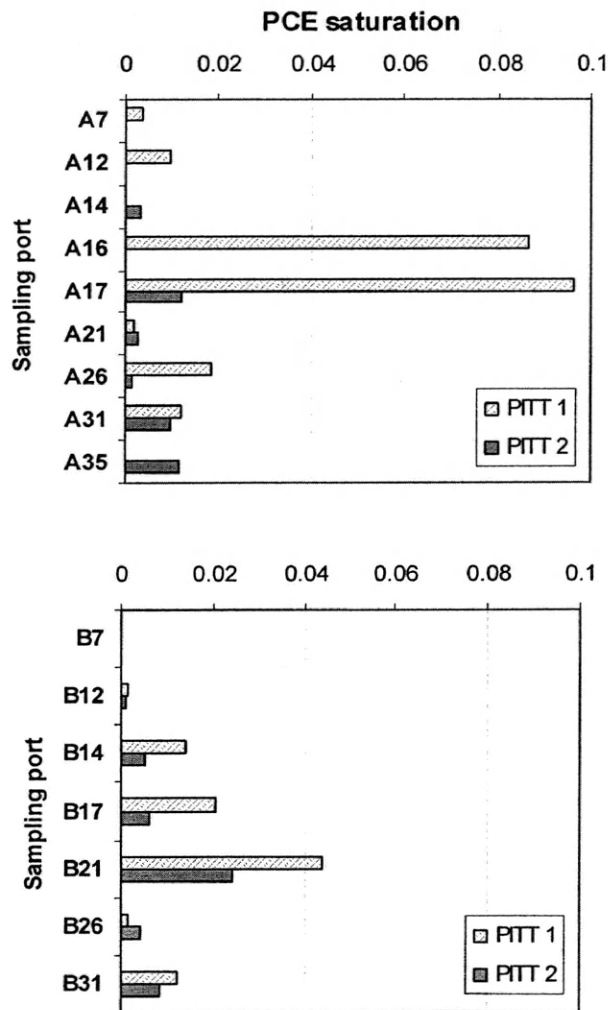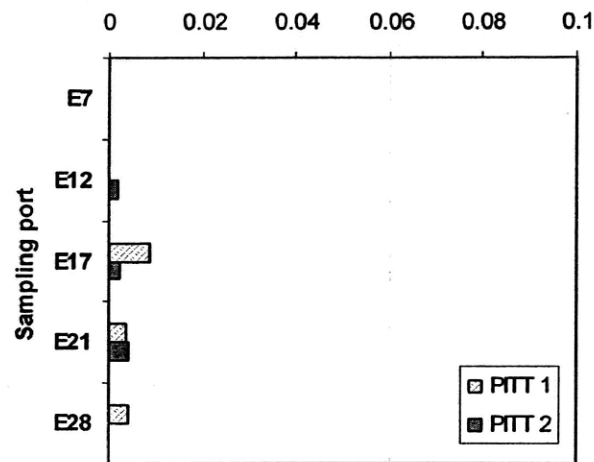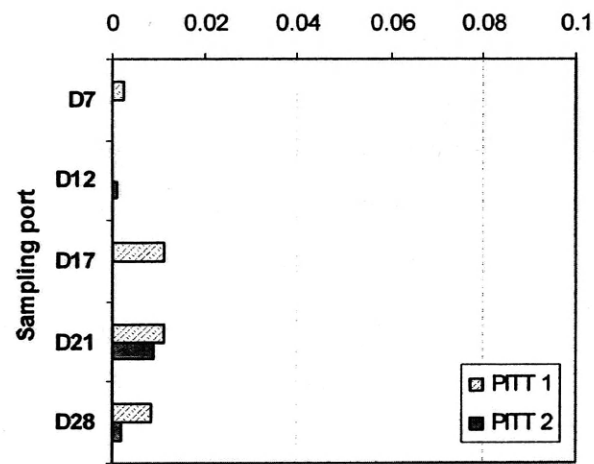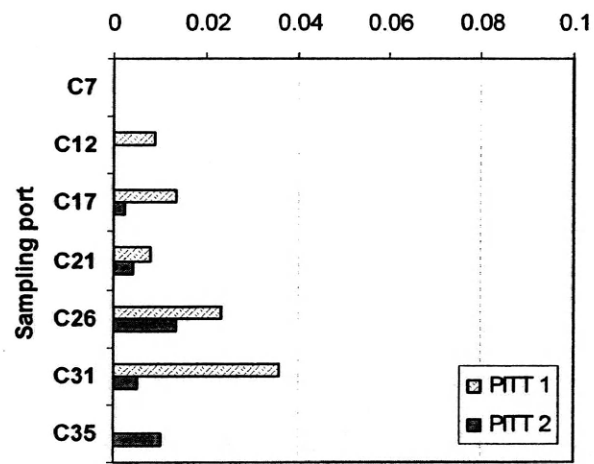
According to method of moment analysis of PITT data, the percentage of saturation removed varies from 79% and 47%. The wide difference between both values comes from the location of the array used to estimate saturation. The comparison of gamma data before and after remediation shows a reduction in PCE mass of 39%. The substantial disparity between results of method of moments (79% reduction) and gamma attenuation (39% reduction) concerning remediation performance represents a major drawback of PITT. The underestimation of PITT to calculate DNAPL mass in heterogeneous media has been pointed out by many researchers; however, the potential of PITT as a method of evaluating remediation performance in high saturation zones has never been evaluated. This study shows that in conditions of heterogeneity the combination of pre and post-remediation tracer data could miscalculate the percentage of mass removed.

The overestimation of mass removed by remediation using tracers can be explained by evaluating the processes that take place in pool areas. Before surfactant flushing, the tracers could not access the high saturation zones due to their lower permeability (Figure 6.10 A). During surfactant flushing, the surfactant flow lines did not contact the high saturated zone at the bottom of the pool either. As a result, only the residuals and transition zones were removed (Figure 6.10 B). Both tracers and surfactants did not come in contact with all the DNAPL volume. After remediation, the second tracer test was conducted through a source zone where just high saturation zones were left. Since most of the transition and residuals zones were removed, the tracers did not provide much retardation. Combining both tracer tests, an apparent result of high remediation efficiency was computed when high saturation zones of PCE were still present as demonstrated in gamma contours.

Figure 6.10. Schematic of tracer flow through a pool before and after surfactant.

A) Before   B) After surfactant
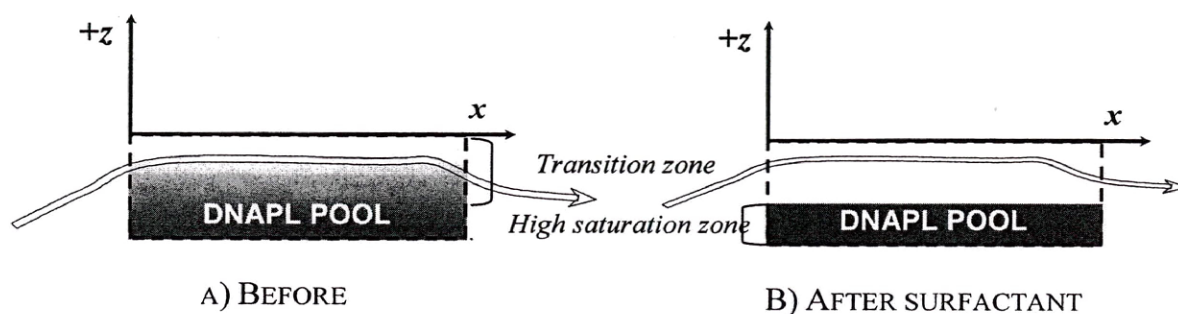
6.4.3 Inverse Modeling Analysis to Determine Source Zone Architecture

In Chapter 5, a method to improve saturation estimates by tracers was developed. This method uses inverse modeling combined with information contained in the breakthrough curves. This method was tested for a single well characterized pool. With the intermediate-scale set of data generated in the two-dimensional tank, it is possible to evaluate the potential of the method to determine DNAPL architecture in more complicated heterogeneous settings.

The method couples a set of application codes with an inverse modeling code. The finite difference groundwater model MODFLOW (Harbaugh et al., 2000) was used to simulate flow through the cell. This model can work in concordance with MT3D (Zheng and Wang, 2000) to simulate transport. The DNAPL phase and the partitioning behavior were incorporated in the transport using the preprocessor MODTRACER (Saenton, 2003). The governing equations of these models can be found in Chapter 4.

The tank was discretized into 106 layers, 154 columns and 2 rows. The flow and head observations and the tracer test data collected prior to the DNAPL spill were used

for model calibration of flow and transport parameters. The assignment of saturation values to the source zone to produce numerical values that match the experimental breakthrough curves was formulated as an inverse problem that can be solved by non linear square regression. The computer program PEST (Doherty, 1994) was used to conduct parameters estimation.

Initial inverse modeling set up. The first inverse modeling set up incorporated measured relative concentrations of partitioning and conservative tracers collected at arrays A, B and C. The parameter estimation was defined using seven different areas with seven parameters to define the saturation distribution (S1, S2, S3, S4, S5, S6 and S7). For N observation points in each array, the source zone was discretized into N different zones and each them had a constant saturation value (Saenton, 2003). Figure 6.11 shows the re-conceptualization of the source zone for inverse modeling.

Parameter estimation is an iterative process; on each of the iterations, the model and the observed breakthrough curves are compared. The evaluation of the objective function and the parameter changes allows the inverse model to determine if a new iteration is necessary, and if so, the whole process is repeated. Nonlinear regression begins with starting parameter values, so it is necessary to input an initial set of saturations for the seven areas. Results from method of moments in array A were used as the initial set of saturation values.

It is obvious that the high degree of heterogeneity of the domain created a more complicated source zone than the one reconceptualized for inverse modeling, as seen from the saturation values obtained from gamma attenuation. However, just the information that was observed during the PITT was used in the inversion problem which created a more simplistic source zone due to the limited information available from tracer tests. The purpose was to determine if this information is sufficient to characterize the location of "hot spots" and the main features of the source zone. After parameter

estimation, results from the inversion were compared with the saturation distribution obtained from gamma attenuation.

Figure 6.11. Re-conceptualization of the source zone area for parameter estimation.
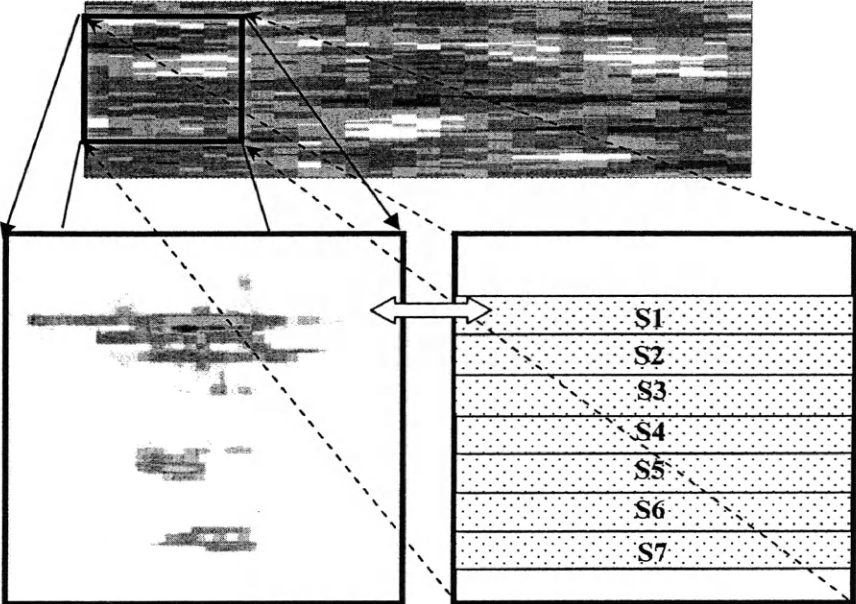
When conducting regression analysis, it is necessary to evaluate the uniqueness of the solution, which is the set of parameter values at which regression converges regardless of the starting values (Poeter and Hill, 1998). This could be accomplished by initiating regression with a different set of values. Lack of uniqueness could be a consequence of a local minima or extreme parameter correlation. In this case, initial results from inverse modeling demonstrated a high correlation between parameters. The fact that the initial saturation parameters are set based on results from method of moments could solve this problem, but to improve regression analysis, the head data collected from the pressure transducer and outflow measured during PITT 1 were

incorporated in the inverse model as observations. With the additional information about flow and head distribution in the tank, the inverse model converged to a unique solution.

The DNAPL architecture obtained by inverse modeling and its comparison with actual data is represented in Figure 6.12. Results from inverse modeling mimic the distribution of saturation obtained from gamma attenuation. This method of analysis improves the saturation estimation with respect to method of moments. Tracer breakthrough curves analyzed by inverse modeling captured the distribution of the source zone.

Figure 6.12. Comparison of the saturation distribution obtained from inverse modeling and actual data.
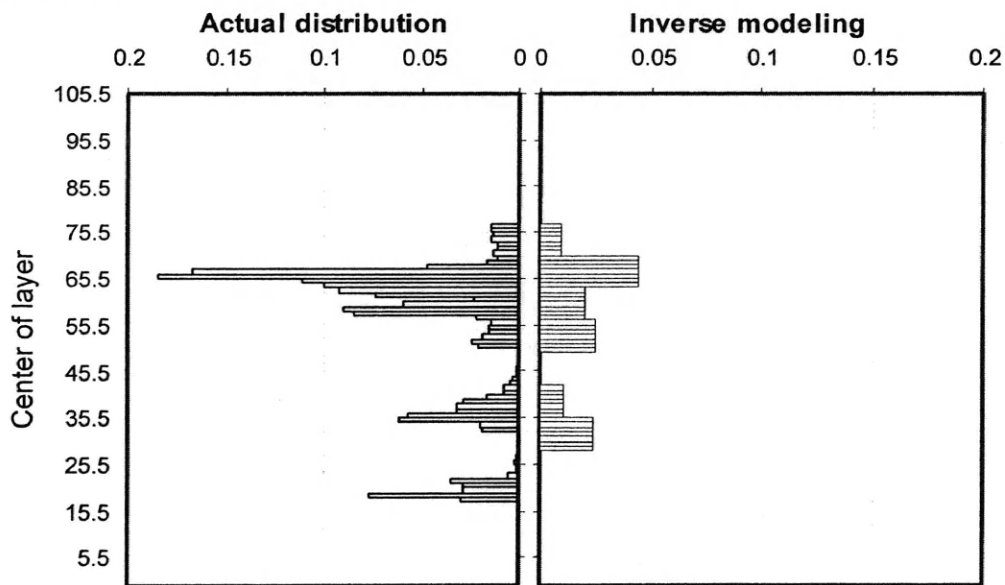
The simulated breakthrough curves at the end of the simulation were compared to the experimental data to evaluate whether the models mimic the long tailing observed in the experimental tracer responses. Figure 6.13 shows how the simulated bromide data fit well the experimental data. Both curves show the same time for breakthrough as well as the same degree of spreading. However, DMP simulated values do not provide a good fit

as observed in Chapter 5 when equilibrium was assumed in the analysis. The simulated DMP breakthrough curves show a single offset instead of the asymmetric and long-tailed curve obtained during experimentation (Figure 6.13). If local equilibrium is not attained, local equilibrium-based models will predict a breakthrough response that occurs too late and exhibit too little dispersion (Valocchi, 1085). This is an indication that the model is not capturing the behavior of the tracers and this miscalculation could affect final results.

Figure 6.13. Experimental and simulated breakthrough curves for ports A16 and A17.
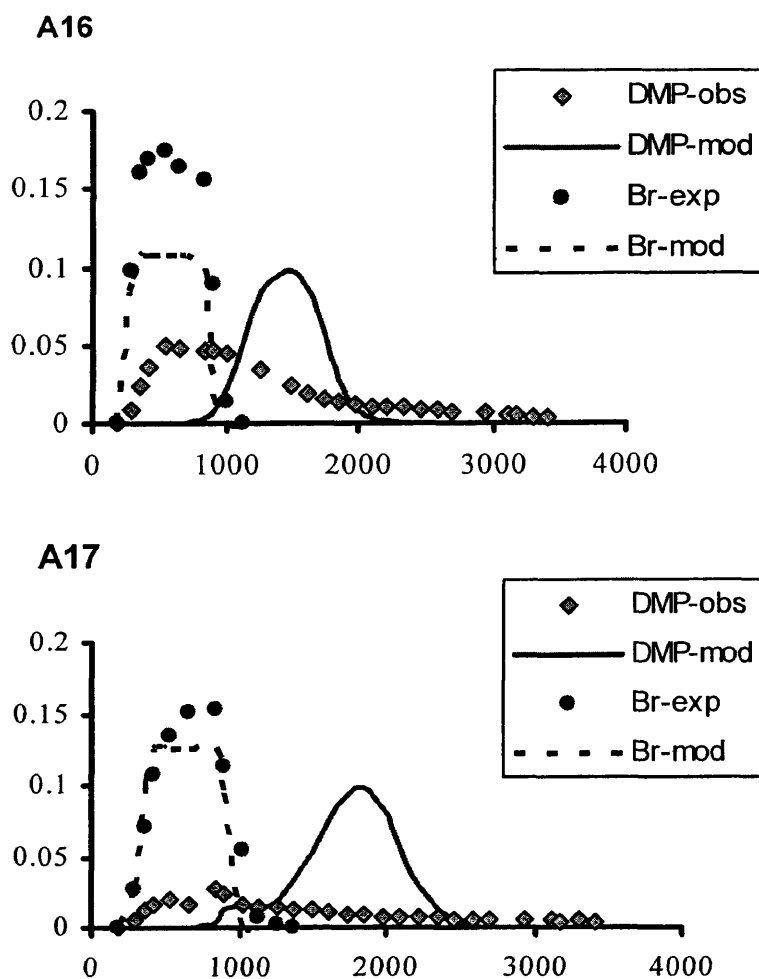
In an attempt to overcome these problems, effective partition coefficients were incorporated in the inversion analysis.

Incorporation of effective partition coefficients. The issue of nonequilibrium was addressed using a method proposed by Valocchi (1985) to measure the deviation from equilibrium. The differences among the simulated and experimental breakthrough curves for DMP are reflected in the computed values of moments. Considering that the numerical models provide a breakthrough curve that represent local equilibrium and that the experimental data represent a breakthrough curve under non equilibrium behavior, the deviation from equilibrium could be measured using the second moment of the two data sets. ε_2, the fractional change in the second central moment, is defined as:

$$\varepsilon_2 = \frac{\mu_2^K - \mu_2^E}{\mu_2^E} \tag{6.2}$$

Superscripts K and E refer to the kinetic (i.e. nonequilibrium) and equilibrium models, respectively. μ refers to the nth central moment:

$$\mu_i = \frac{\int (t - \mu_1)^i C(t)dt}{\int C(t)dt} \tag{6.3}$$

If the fractional change of the second moment is calculated for the breakthrough curves collected and simulated at all the ports (Figure 6.13), large ε_2 values are obtained, representing large deviations from equilibrium (see Figure 6.14). To relax the condition of equilibrium, nonequilibrium coefficients obtained in batch experiments were substituted for the equilibrium values. These values were selectively applied to the areas

that were subject to nonequilibrium behavior represented by high values of fractional changes in the second central moments.

Figure 6.14. Fractional change of the second moment in array A
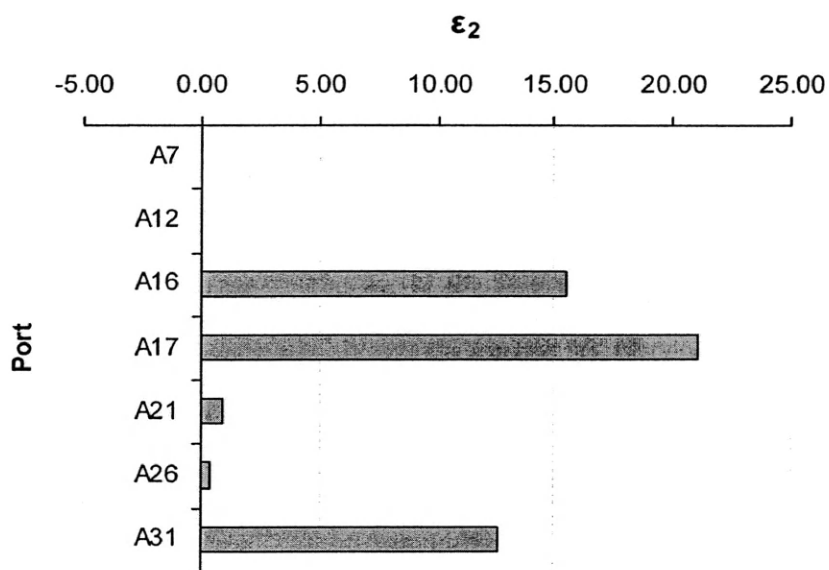
After evaluation of the fractional change of the second moment, the non equilibrium batch experiments for DMP developed in Chapter 5 were applied to the inversion analysis. Figure 6.15 shows three distinctive zones, based on the deviation from equilibrium. The values of the equilibrium partitioning were modified with "effective partition coefficients" for the zones that correspond to breakthrough curves A16, A17 and A31. Values of $Kp_e=25$, $Kp_e=20$ and $Kp_e=25$ were applied to zones S3, S4 and S7 respectively based on the deviation from equilibrium.

128

Figure 6.15. Kp as a function of time for DMP.

Time (hours)
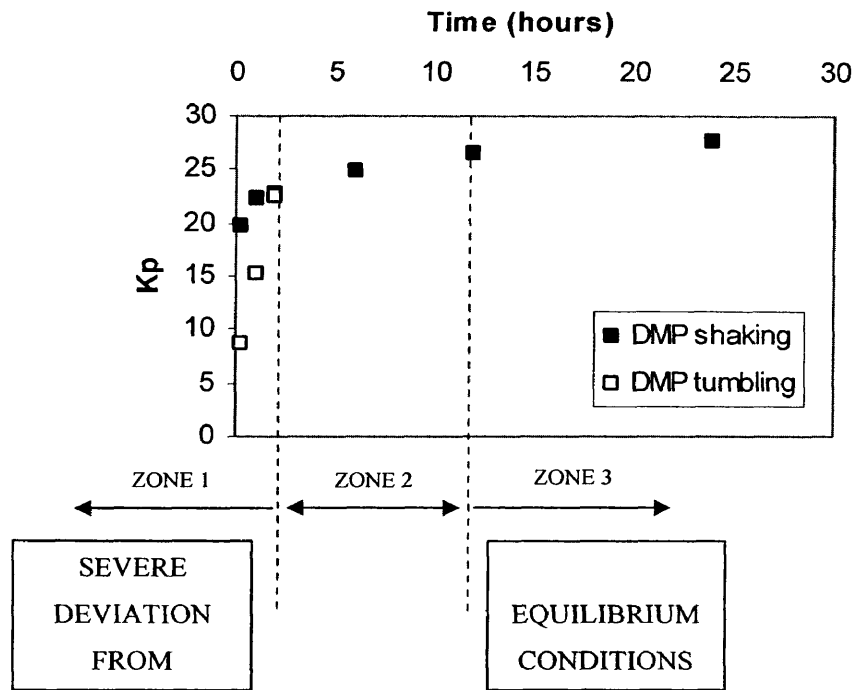
With the incorporation of Kp_e the model not only provided a source zone closer to the actual value (Figure 6.16), it also provided a higher quality regression.

The use of ε_2 to assign Kp_e gives rise to two fundamental issues: what is the cut off value for ε_2 to presume rate-limited behavior and how does ε_2 depend on other transport parameters like dispersion. The first issue is addressed by simply comparing quantitatively fractional change results for all the breakthrough curves and then qualitatively evaluate if these results agree with tailing observed in breakthrough curves.

The second issue depends on the quality of the transport model. In this scenario, the model was calibrated for flow and transport, so the difference between experimental

and simulated DMP breakthrough curves comes only from the saturation distribution and partitioning behavior.

Figure 6.16. Comparison of saturation distribution between actual PCE distribution and results from inverse modeling with Kp_e.
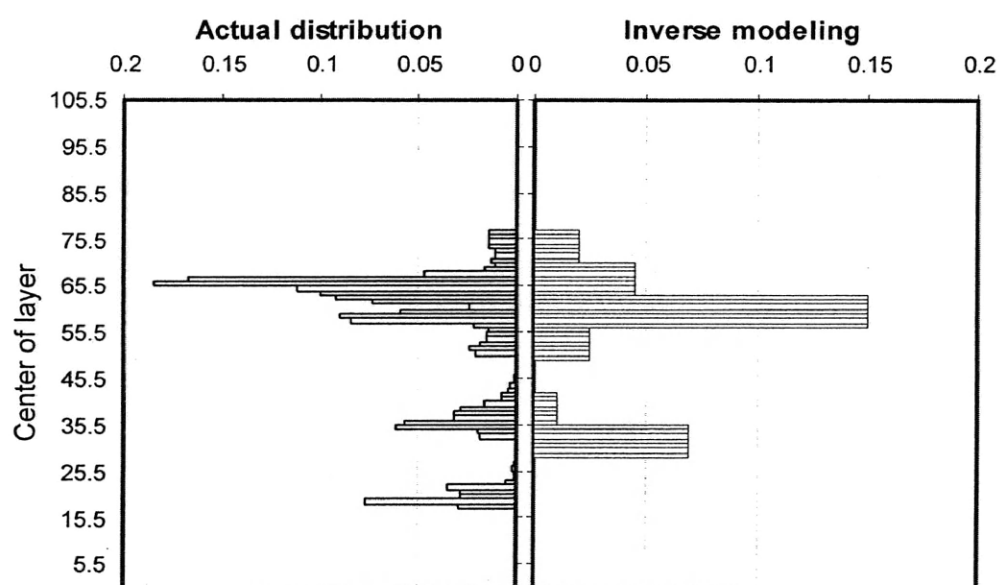
One of the advantages in this correction method is that even though the exact value of Kp_e is not specified for each situation, it allows for a determination of DNAPL distribution in the best and worst case scenario. This is, if equilibrium is assumed in the analysis, the underestimation will reach its highest value. Conversely, if a value of Kp_e =10 (far from the equilibrium condition) is input in the analysis, the maximum value for the saturation at that location will be obtained. In this way, the method can provide a range of saturation values to account for miscalculations caused by the local equilibrium assumption.

6.5 Conclusions

This is the first experimental study to evaluate the influence of heterogeneity on tracer performance in settings that resemble heterogeneous sites. Since it was demonstrated in Chapter 5 that extraction wells provide underestimation of the mass under conditions of heterogeneity, only multilevel samplers were used in this study. Multilevel sampling is also the only sampling method that can potentially provide information about the vertical architecture.

After collecting tracer breakthrough curves, method of moments was conducted to determine DNAPL saturation. This method offers limited information about the vertical distribution of DNAPL. It underestimated or overestimated saturation distribution due to the following factors:

- Flow bypassing due to heterogeneity
- Monitoring distance from the source zone
- Source zone architecture (pool or residual)
- Limited tracer solution accessibility to source zone

After method of moments, inverse modeling analysis was conducted to apply the new data interpretation method developed in Chapter 6. Results demonstrated that inverse procedures provided better results than method of moments: the source zone obtained by inversion was similar to the actual saturation distribution provided by gamma attenuation. Despite the computational effort that inverse modeling requires compared to method of moments, it allows for an integrated interpretation of the tracer behavior in the system. Results in this chapter demonstrated how the inversion exercise provided valuable information about the validity of equilibrium partition coefficients in situations where tracer partitioning is controlled by non equilibrium behavior. Inverse modeling also

showed the importance of collecting different type of observation data like heads or flows during PITT to facilitate regression analysis.

Even though method of moment analysis of breakthrough curves at multilevel samplers has several limitations, it is still a quick and easy procedure that should always be applied to breakthrough curves. It is also a necessary step for the inverse modeling set up that requires an initial guess of the saturation distribution.

While the use of tracers as a remediation metric in heterogeneous conditions has never been questioned, this study has shown how the tracers can overestimate remediation performance in the presence of pools. Divine et al., 2004 discussed the problems encountered in using PITT to assess remediation performance when remediation activities where highly effective: they could result in low remaining saturation distribution that could not be detected by PITT. Results from this study yield to the same conclusion for ineffective remediation activities in heterogeneous sites: the difficulty of remediation techniques to completely remove pool areas creates the problem of remaining high saturation zones that are disconnected and difficult to access by tracer flowpaths. In this case, tracers could lead to an overestimation of remediation performance that could have severe repercussions if these pool areas are not detected by the PITT.

Although this inverse modeling procedure was tested for a two dimensional setting, it can be extrapolated to three dimensional field settings. However, it is important to recognize that due to the two dimensional nature of the experiment, it might be the case that pools created here are thicker compared to what we could find in the field due to spreading in the third dimension. The "thicker" DNAPL morphology created in this two dimensional setting could lead to larger estimation errors than may be expected in the field. The next chapter describes a series of three dimensional simulations conducted to explore this issue.

Chapter 7

NUMERICAL SIMULATION STUDY TO DETERMINE THE INFLUENCE OF DNAPL ARCHITECTURE, WELL LOCATION AND HETEROGENEITY ON PITT PERFORMANCE

7.1 Abstract

Characterization of DNAPL in heterogeneous media represents a major challenge in the remediation process due to the complexity of DNAPL entrapment architecture. Non intrusive characterization techniques such as partitioning tracer tests offer the potential to determine the DNAPL distribution of the source zone. However, the effects of the heterogeneity on the performance of this technique have not been examined in a complete manner and the traditional application of the technique could lead to major estimation errors.

A systematic modeling study was conducted to obtain a broader view of the influence of heterogeneity on the partition interwell tracer test response by using two and three dimensional numerical simulations.

Using the same geostatistical parameters representative of well characterized heterogeneous sites, several synthetic realizations were generated in an attempt to capture some of the characteristics of a heterogeneous aquifer. In the previous chapter, one of these synthetic realizations was physically created in a two dimensional tank and a set of tracer experiments were conducted. Results demonstrated the effect of heterogeneity, well location and rate limited behavior on the performance of the tracer test. Yet, to

evaluate the influence of heterogeneity on tracer performance, the experimental study of just one occurrence may not be enough.

A two-dimensional simulation study was utilized to evaluate the influence of DNAPL vertical distribution and well location on the performance of the tracer test for a number of realizations with the same geostatistical parameters. Different geostatistics were also applied to measure tracer efficiency for different degrees of heterogeneity. The heterogeneity was quantified based on the variance of the hydraulic conductivity field.

Next, a three-dimensional case study was conducted to evaluate the influence of different injection-extraction patterns in tracer sweep efficiency. Results of this study can be used as guidelines in the design of the PITT for characterization of DNAPL at heterogeneous sites.

7.2 Introduction

Just a few numerical modeling studies have been conducted in the last years to evaluate partitioning tracer transport in heterogeneous aquifers. James et al. (1997) used stochastic methods to obtain optimal estimates of the spatial distribution of residual NAPL. The approach consisted of assuming that the heterogeneous aquifer properties are random space functions from an ensemble of physically plausible functions. After adopting that assumption; the authors demonstrated that tracer behavior can be predicted using the ensemble statistics of hydraulic conductivity, hydraulic head and NAPL distribution of a stochastic subsurface transport model. However, the creation of the DNAPL distribution was performed using a spatial correlation field that had uncorrelated hydraulic conductivity. Also, the maximum value of saturation was constrained at 0.3. Findings of this study showed how the analysis of the estimation errors was consistent with the true estimation errors. However authors recognized the limitations of the method

due to the uncorrelated structure of K and residual NAPL saturation. Also, the input of a synthetic DNAPL saturation distribution may have not been representative of the effectiveness of the technique in real applications that could lead to saturations above 0.3 and more inaccessible areas such as pools.

The same authors (James et al., 2000) conducted another study to determine the sensitivity of method of measured temporal moments to three different pumping configurations. Results of this study showed that convergent and divergent flow patterns provided slightly superior data than a typical line-drive pattern. In this case also the log K field was uncorrelated to the NAPL field.

Another investigation conducted by Zhang and Graham, 2001 evaluated different degrees of correlation between the fields of natural log conductivity and natural log volumetric NAPL content. Results demonstrated how a higher degree of correlations leads to a decreased prediction uncertainty over the uncorrelated case. Our concern is that the non correlation of the NAPL distribution field with respect to the hydraulic conductivity field assumed in previous work may have a considerable impact in the simulation results. The distribution of the DNAPL phase according to the porous media properties could create even larger differences in performance between line drive and five-spot patterns.

Jayanti (2003), studied the effect of heterogeneity on sweep efficiency during a PITT. He used different random permeability fields with a layered DNAPL saturation distribution obtained from field data and independent of the permeability field. The maximum DNAPL saturation was assumed to be 0.1. The estimation error for a typical alluvial aquifer with a standard deviation of 1.2 was 6 percent. We believe the higher estimation errors occur in the field, where the heterogeneity dictates the DNAPL distribution creating zones of saturation higher than 0.1 (Kueper et al., 1993).

The quality of tracer estimation for different DNAPL spills in conditions of heterogeneity has not been completely evaluated yet. In this study, a highly heterogeneous aquifer was created using spatial correlated random field for the hydraulic

136

conductivity. The DNAPL distribution was created using a multiphase flow simulator to generate an entrapment configuration controlled by the permeability field.

In the previous chapter, an experiment was conducted where a high degree of heterogeneity was physically created in a two dimensional cell. A series of PITT tracer tests were conducted to evaluate the performance of the test. Also, a method was tested to improve underestimation of mass by the tracers. This method uses inverse modeling in combination with Kp_e estimated from non equilibrium batch tests. Results from that experimental study showed that the incorporation of non equilibrium behavior in the analysis enhanced the performance of the test. In this chapter, a numerical simulation study is conducted to evaluate the influence of heterogeneity on tracer accuracy.

The study is divided into two-dimensional and three-dimensional simulations. The objective of the two-dimensional study was to evaluate the influence that entrapment architecture and field heterogeneity play in the mass estimation by the tracers. Different degrees of heterogeneity were chosen based on values obtained at three well characterized field sites; the MADE Site (Rehfeldt et al., 1992), the Cape Cod site (LeBlanc et al., 1991) and the Borden site (Sudicky, 1986). The MADE site geostatistics were used as reference values of a very heterogeneous site and Borden and Cape Cod were used as prototypes of less heterogeneous sites. A summary of the relevant properties of these sites can be found in Fernandez-Garcia (2003).

Following the two-dimensional simulation study, a three-dimensional study was conducted to test the sweep efficiency of line drive versus divergent and convergent tracer tests. The same multiphase flow simulator (UTCHEM) was used to create the DNAPL saturation distribution; in this way it was possible to upscale findings from the 2D studies where pools could be constrained by the two-dimensional domain, developing higher saturation values than those expected in 3D settings where a greater degree of spreading is allowed.

7.3 Two-dimensional Numerical Modeling Simulations

In this section, the simplified Monte Carlo approach used to evaluate the importance of entrapment architecture and heterogeneity in the PITT is described.

First, the geostatistical parameters to create a hydraulic conductivity field were selected. Initially, similar statistics of the MADE site were used. The statistical components necessary are the mean (μ_{lnK}), the variance (σ^2_{lnK}) and the vertical and horizontal correlation lengths (λ_v and λ_h). Twenty permeability fields were created with this set of statistical parameters using a random seed for each realization.

The second step involved the use of UTCHEM as a multiphase flow simulator. It was used to generate systematically a spill of PCE for all the stochastic permeability fields. The same volume was spilled for all the realizations. Details about the source zone creation can be found in section 7.3.1.

The third step involved the selection of a few realizations based on their distinctive source zone distribution. Six realizations were selected out of the twenty permeability fields based on the degree of DNAPL spreading in the vertical direction. This feature can be quantitatively measured using spatial moment analysis of the DNAPL spill (Saenton, 2003). The scope of this study is to evaluate the impact of source zone architecture on tracer test performance, so permeability distributions that generated similar architecture were rejected for future tracer transport simulations. The six realizations selected represented a broad spectrum of DNAPL architecture for the same degree of heterogeneity.

The fourth step consisted in the simulation of partitioning tracer transport using MODTRACER/MODFLOW/MT3DMS for the selected realizations. Since this study is purely numerical, method of moment analysis was conducted to analyze tracer responses and to determine the saturation detected by tracers. This assumption implies that the error in the DNAPL saturation by tracers here does not come from the method of analysis; the

138

underestimation arises from the sole influence of the hydrodynamic constraints due to the permeability field and DNAPL architecture.

Three different aspects were considered in this analysis:

- The effect of the degree of spreading of DNAPL mass on performance of PITT.
- The effect of the distance of the well from the source zone on performance of PITT.
- The effect of the variance of K on the performance of the PITT.

7.3.1 Generation of Permeability Fields

The two-dimensional model domain was 4.95 m x 1.00 m x 0.05 m. It was divided into 66 columns, 1 row and 100 layers (Figure 7.1). The tank consisted of two distinctive zones: a homogeneous zone for tracer delivery and a heterogeneous zone that contained the permeability field obtained from the random field generation. The heterogeneous field approximated a log-normal distribution of the hydraulic conductivity with a mean value of 4.18 m/day and a variance of 1.22. The lateral and vertical correlations were 0.5 and 0.05 m respectively. The distribution of K was discretized into five categories that represented five different sieve sands (#16, #30, #50, #70, #110).

A total of 20 realizations were generated.

Figure 7.1. Simulation domain.
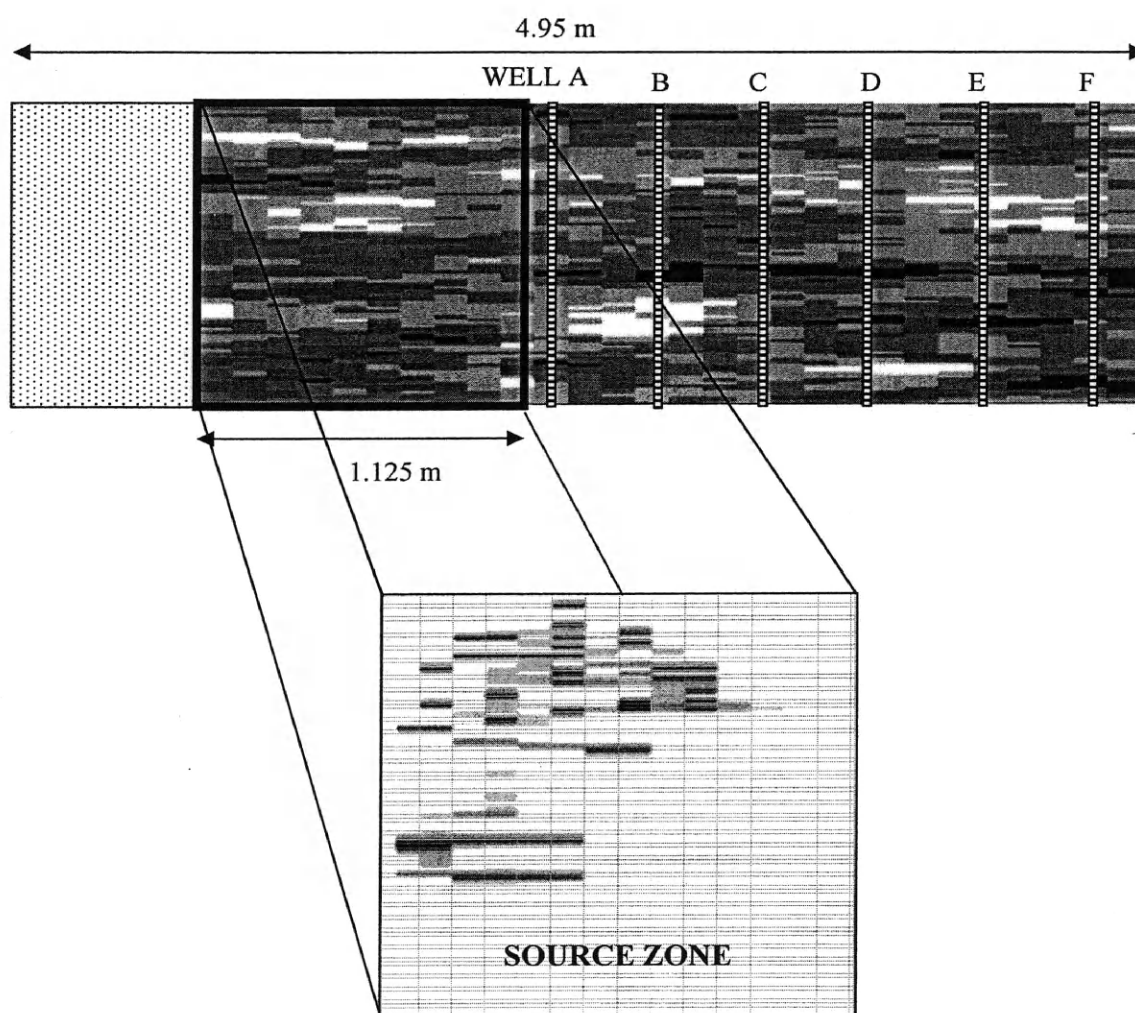
7.3.2 Source Zone Creation

To create the source zone, an area of 1.125 m x 1.00 m x 0.05 m was selected between the homogeneous zone and the area designated for all the monitoring wells. This region of the model domain was extracted and input in UTCHEM as a sub-domain where the DNAPL injection and migration was simulated. 600 ml were spilled from the center of the top layer. During UTCHEM simulations, there was no gradient between the top and left boundary, the PCE injection flow rate was $1.67 \, E10^{-3} \, m^3/day$. The total injection time was 3.6 days and 0.4 days were given for the PCE to stabilize. In the source zone, the sand #110 was replaced with clay to create permeability barriers that allowed the formation of pools.

Since UTCHEM was used to simulate the DNAPL source zone for all the realizations, a realistic saturation distribution was created allowing the heterogeneity of each realization to determine the distribution of NAPL throughout the domain. PCE was used as a representative DNAPL for consistency throughout this dissertation. The fluid physical properties used in the model are described in Table 2.2.

The source zones for all the realizations were classified based on the spread of the DNAPL mass. The spreading can be measured quantitatively using spatial moment analysis (Saenton, 2003). The zeroth moment (M_{000}) provides an estimate of the DNAPL mass. The first normalized moment in the x and z direction is a descriptor of the center of mass of the contaminant in both transversal and vertical direction. The second centralized moments in both directions provide a measurement of the degree of spreading of the contaminant from the center of mass. Spatial moments can be calculated using the equations below:

$$M_{ijk} = \iiint (\rho \cdot \phi \cdot S_N x^i y^j z^k) \, dxdydz \qquad (7.1)$$

$$\bar{x} = \hat{M}_{100} = \frac{M_{100}}{M_{000}} \qquad \bar{z} = \hat{M}_{001} = \frac{M_{001}}{M_{000}} \qquad (7.2)$$

$$M_{200} = \iiint \rho \cdot \phi \cdot S_N (x - \bar{x})^2 \, dxdydz \qquad M_{002} = \iiint \rho \cdot \phi \cdot S_N (z - \bar{z})^2 \, dxdydz \qquad (7.3)$$

Using these descriptors, the distribution of DNAPL in the model domain was measured for all the realizations. Since the simulations for flow and tracer transport could increase the computational effort substantially, seven realizations were selected for the tracer studies. The criterion for the selection was based on the coverage of a broad range of saturation distribution in the z axis. The hypothesis is that the value of the second moment in the vertical direction is an indicator of the spreading of DNAPL mass. Small values of the second moment in z direction indicate that the source zone is more likely to contain pools, since the DNAPL does not spread from the center of mass. On the other hand, a high value for the second moment in the z direction represents a source zone where the DNAPL is distributed throughout and more likely to contain residual zones.

In order to evaluate the sole influence of the vertical spreading, six realizations were selected with almost the same value of M_{200} and distinctively different values for M_{002}. In this way a broad range of distribution could be evaluated with a limited number of simulations. The selection of the realizations based on the value of the second moment can be evaluated in Figure 7.2. The rectangle represents an area where M_{200} is in the (0.057, 0.070) interval for all the realizations selected.

Figure 7.2. Second moment in vertical direction (M002) and horizontal direction (M200) for all the realizations.
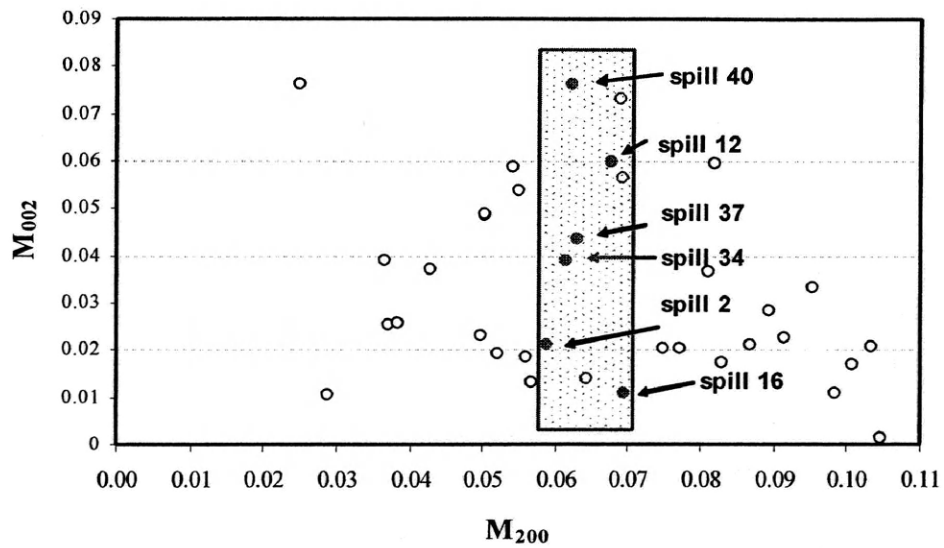
The DNAPL distribution of the selected realizations is shown in Figure 7.3.

Figure 7.3. The six selected source zone distributions.

144
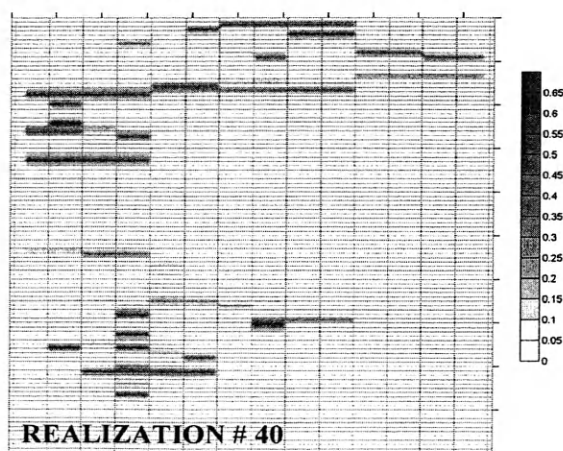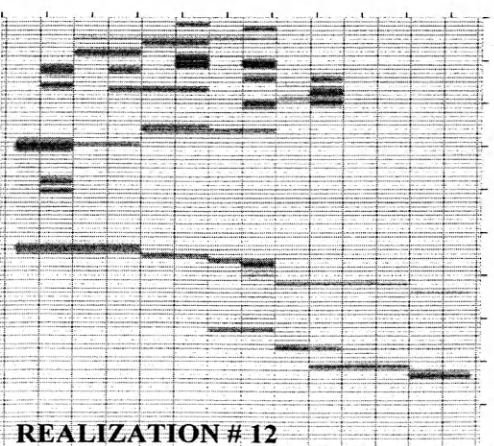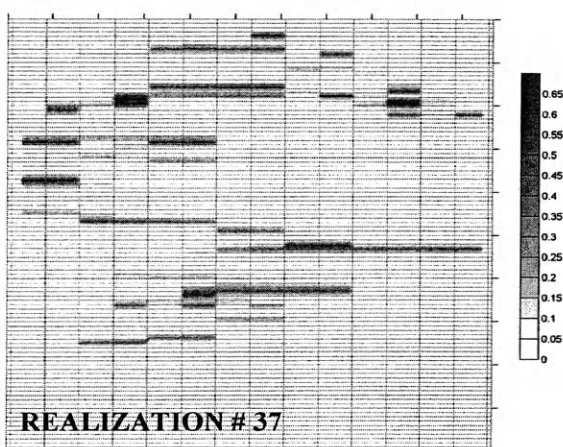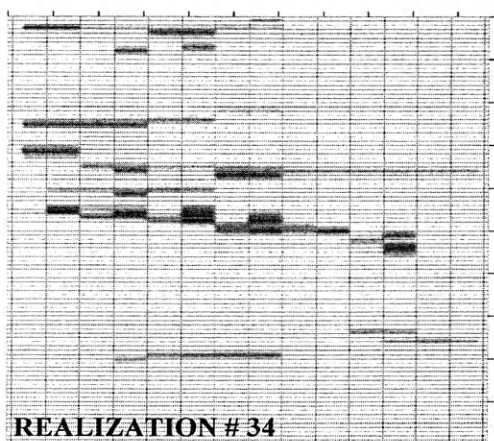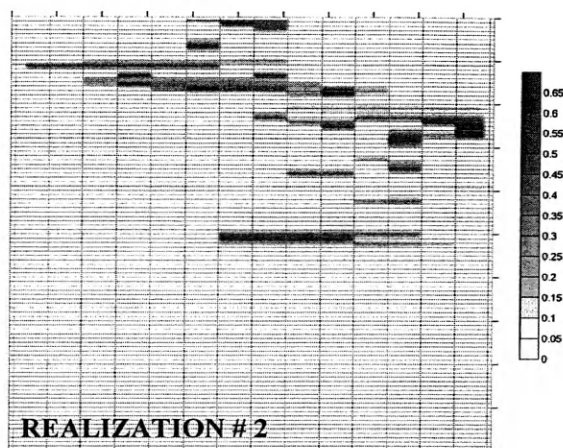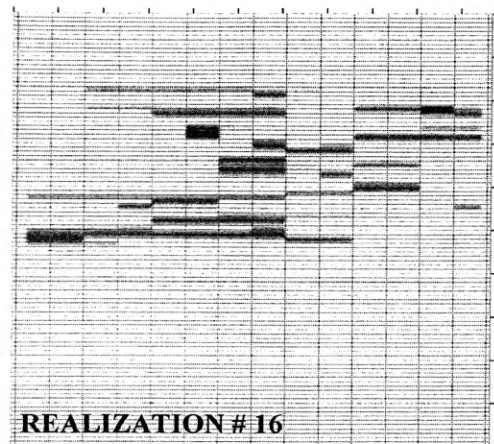
Table 7.1 represents the spatial moments of the selected realizations. The calculated mass from moments showed the same amount for all the simulations. The value of the second moment in z direction shows increasing spreading of the DNAPL mass from spill 16 to spill 40. This feature can be qualitatively visualized in Figure 7.3.

Table 7.1. Spatial moments of the selected realizations

Spill ID	M_{000} (kg)	M_{100} (m)	M_{001} (m)	M_{200} (m^2)	M_{002} (m^2)
16	0.9624	0.3731	0.7806	0.0694	0.0112
2	0.9624	0.6432	0.7384	0.0586	0.0211
34	0.9624	0.4499	0.5966	0.0614	0.0392
37	0.9624	0.4687	0.6332	0.0629	0.0437
12	0.9624	0.4179	0.6495	0.0675	0.0601
40	0.9624	0.3887	0.6304	0.0622	0.0764

7.3.3 Tracer Transport Modeling

Once the desired realizations were selected, the source zone sub-domains were incorporated into their respective full permeability fields. The same application models used in previous chapters to simulate tracer transport were applied here: the finite difference groundwater model MODFLOW was used to simulate flow through the cell. This model works in concordance with MT3DMS to simulate transport. The DNAPL phase and the partitioning behavior were incorporated in the transport using the preprocessor (MODTRACER). The governing equations of these models can be found in Chapter 4.

Once appropriate design parameters were selected, they were applied consistently to all the realizations. In this way, it was possible to evaluate solely the influence of permeability distribution in the remediation performance. DMP and bromide were used as the selected tracers. The tracers were injected through an array of 32 ports centered in the homogeneous zone at a rate of 8 m³/day. Observations were taken in a series of arrays located downstream. Each array has 37 ports which are located in every other cell in the vertical direction. The left and right boundaries were constant heads with a head difference of 0.085 m that determined a flow of 55 ml/min through the cell. A tracer injection pulse was applied for 600 minutes. The total simulation time of the experiment was 9000 minutes.

7.3.4 Estimation of PITT Performance

To evaluate the performance of tracer test for each of the realizations, the following methodology was used: the DMP and bromide breakthrough curves obtained at each of the locations in each array were analyzed using method of moments. This method of analysis is described in detail in Chapter 2. For each realization the saturation obtained at each cell by the UTCHEM simulator was averaged into a total saturation value for the whole source zone. This value of saturation was compared to the value of saturation obtained by applying method of moments to the simulated breakthrough curves.

The estimation percentage was calculated using the following expression:

$$\text{Estimation percentage} = \frac{S_c \cdot 100}{S_a} \tag{7.4}$$

where S_c represents the total value of calculated saturation from breakthrough curves and S_a represents the value of average saturation generated by UTCHEM.

7.3.5 Results

The conservative and partitioning tracers were collected at each of the 32 sampling points in each of the six arrays. The tracer response in the different arrays was evaluated to determine the saturation estimation as the distance from the source zone increases.

The tracer response curves collected at the same array showed the effect of heterogeneity on tracer breakthrough curves. As expected, each port in the vertical direction showed different arrival times. For each pair of conservative and partitioning tracer responses, a saturation value was calculated.

The effect of the degree of DNAPL spreading on performance of PITT. To illustrate the importance of the entrapment architecture, a partitioning tracer test was conducted for each of the six realizations. The estimation percentage of the six realizations was plotted against their value of the second spatial moments (Figure 7.4). In Array A, higher values of the second moment in the z direction correspond to better estimation of PCE mass by tracers; the mass is more uniformly distributed in the source zone which implies that there are more residuals than pools. Conversely, low values of the second moment translate into less spreading. It is important to note that this trend is just observed for signals collected in array A (the closest to the source zone). As the distance from the source zone increases, the estimation percentage has almost the same

value for all the realizations. Due to the mixing caused by the heterogeneity, the separation of the conservative and partitioning responses is minor by the time it reaches well F. The information about the architecture of the system dissipates with distance. This pattern indicates the importance of well location in tracer performance.

Figure 7.4. Estimation percentage as a function of DNAPL mass spreading (2nd moment) for all six realizations.
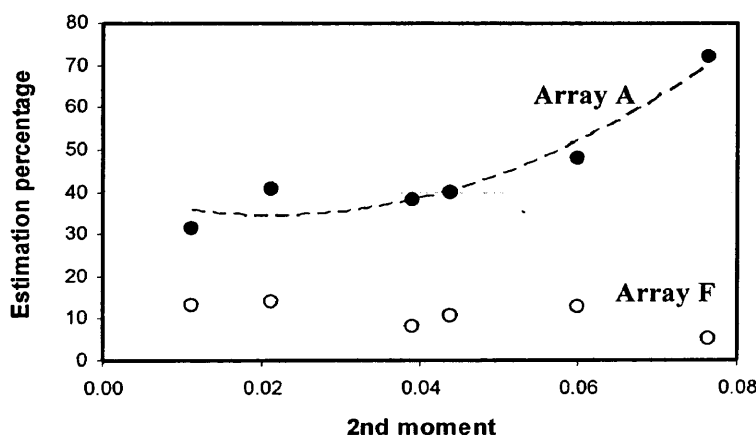
The effect of the distance of the well from the source zone on performance of PITT. Figure 7.5 shows the estimation percentage for all the realizations for all the signals collected in the different arrays. For architectures with a more uniformly distributed DNAPL (higher centralized second moments) the influence of well location is higher. This pattern suggests that when the DNAPL is distributed mostly in the residual form, it is feasible to obtain accurate mass estimation if the wells are located close enough to the source zone. As the distance from the source zone increases, the signal attenuates more for configurations that have more residuals than pools. Figure 7.7 shows

the average of results for all the realizations. Mass estimation errors increase up to 35% from well A to well F.

Figure 7.5. Estimation percentage for the six selected realizations.
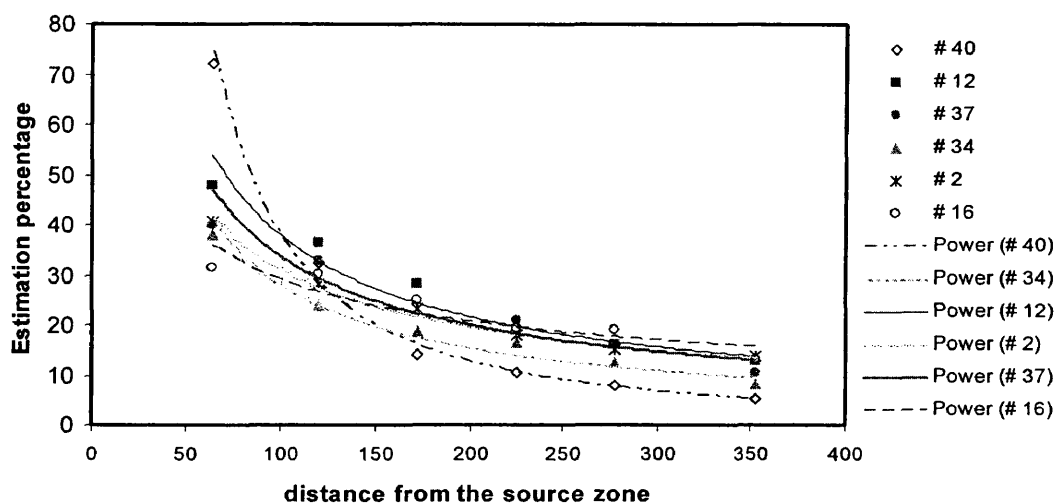
Figure 7.6. Average values of estimation percentages for all the realizations
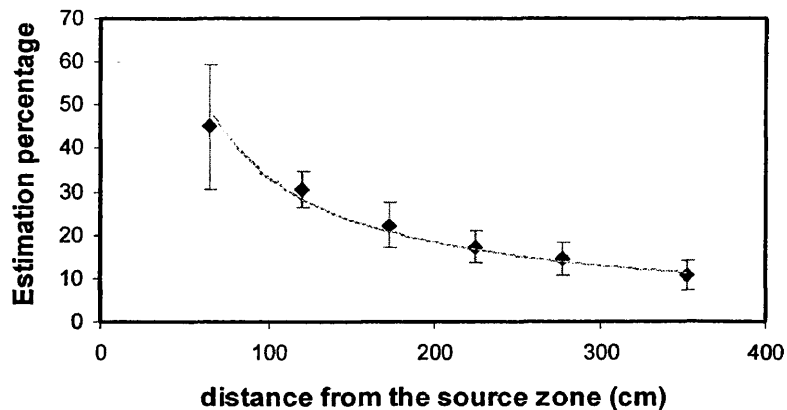
The effect of the degree of heterogeneity on the performance of the PITT. The variance is the geostatistical parameter that determines the degree of heterogeneity. The simulations above were all performed for a value of $\sigma^2 = 1.22$. To evaluate the effect of the variance of permeability on tracer performance, a set of realizations were generated using two different values for the variance; 0.75 and 0.25. These values correspond to less heterogeneous sites.

Twenty realizations were generated for the medium and low heterogeneity case with the parameters of $\sigma^2 = 0.75$ and $\sigma^2 = 0.25$ respectively. The other geostatistical parameters (mean and correlation length) remained the same.

The same amount of PCE (0.6 L) was spilled for all the realizations, and spatial moment analysis was conducted to determine quantitatively the features of the DNAPL entrapment for all the simulations. The second moment in both vertical and horizontal direction is represented in Figure 7.7 in the form of histograms. For the low heterogeneity case, the second centralized moments in the vertical direction have higher values for all the realizations than the second moment in the horizontal direction. As the value of the variance increases, the distribution of the M_{002} shifts to lower values. This result is in concordance with the fact that field heterogeneity controls the DNAPL entrapment. Less heterogeneous sites provide more DNAPL in residual form with respect to more heterogeneous sites, given that the rest of the geostatistical parameters remain the same.

150

Figure 7.7. Frequency of the second moment in the vertical and horizontal direction for the three degrees of heterogeneity selected.
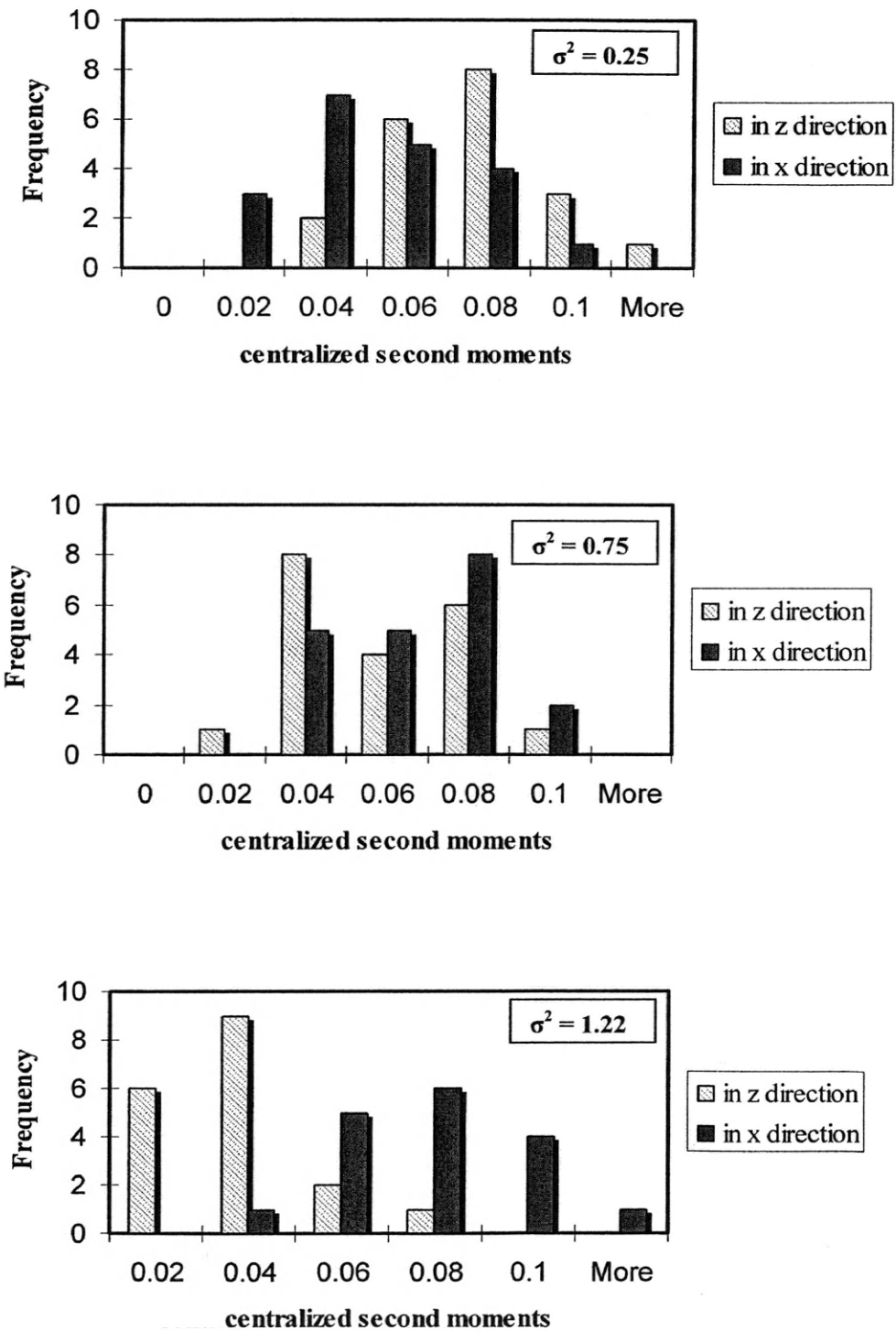
To evaluate tracer performance as a function of the permeability field, three different clusters were selected with the same value of the spatial moments. The purpose of this selection is to isolate the effect of DNAPL entrapment architecture and evaluate exclusively the effect of the variance of permeability in the results.

Figure 7.8 represents the value of second moment for all the realizations, from which three clusters were selected for the same values of spatial moments in both vertical and horizontal direction.

Figure 7.8. Clusters selected based on similar values of the second moments.
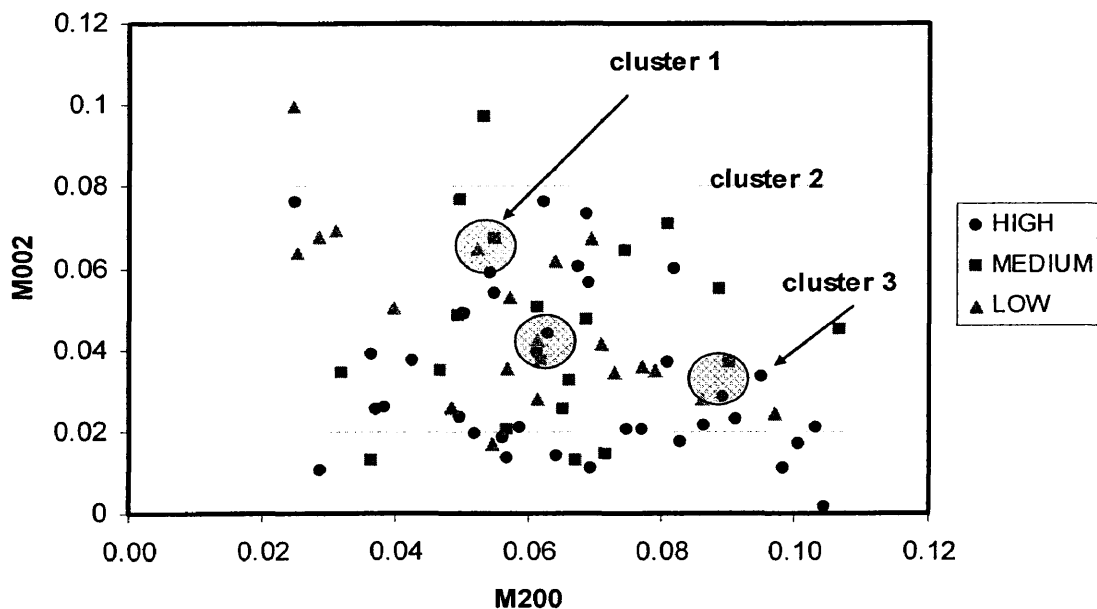
Numerical modeling of tracer tests was conducted using the same application models. Tracer signals were obtained at the same monitoring wells. It can be observed in Figure 7.9 that for each of the clusters, the lower heterogeneity case provides a better estimation of the mass. This feature suggests that the performance of the test is also influenced by the degree of heterogeneity that creates a higher degree of mixing or hydrodynamic dispersion of the tracer signals downstream. There is a direct relationship between the heterogeneity of the aquifer and the estimation error of the tracers given the same spatial distribution of the DNAPL saturation. This procedure could be used as a methodology to predict estimation errors based on the degree of heterogeneity of an aquifer.

Figure 7.9. Mass estimation percentage for each of the clusters.

154
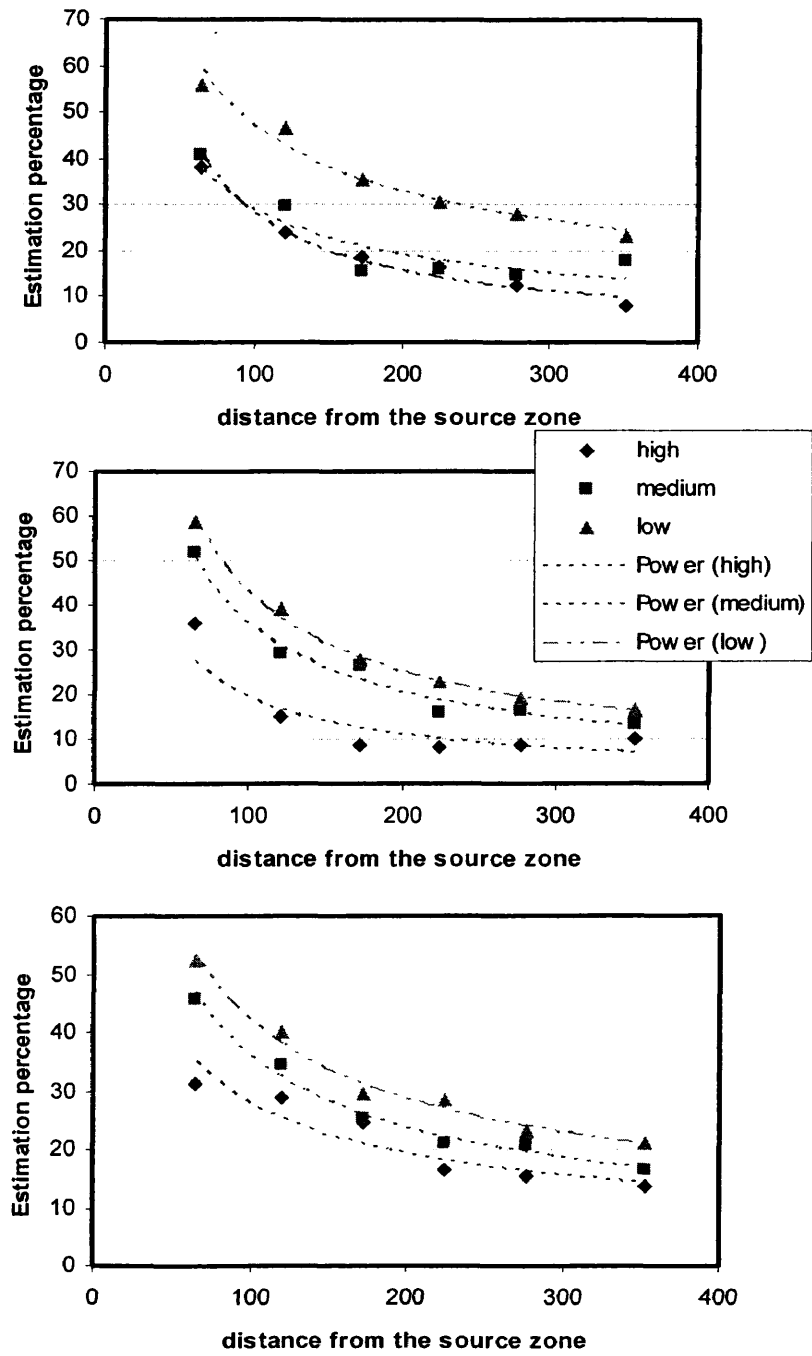
7.4 Three-dimensional Case Simulation Study

In this dissertation, tracer flow and transport have been investigated so far in two dimensional laboratory experiments and numerical simulations. Results of these studies have demonstrated the importance of DNAPL architecture, well location, rate-limited behavior and sweep efficiency. Nonetheless, the use of two-dimensional analysis has constrained the delivery of the tracers to line-drive patterns. The purpose of this three-dimensional study is to evaluate three different injection-extraction patterns for PITT design considerations. The performance of PITT for a realistic distribution of DNAPL in a heterogeneous field was compared for line drive and five spot patterns.

The same statistics used for the highly heterogeneous two-dimensional study were applied to the three dimensional model domain. However, in this case, the permeability distribution was not discretized into five categories and the log-normal distribution of K was applied to the model domain (with values ranging from 0.75 m min^{-1} to 0.0032 m min^{-1}). Figure 7.10 represents the permeability field of the model domain.

The numerical model had 500,000 grid-blocks distributed in 100 rows, 100 columns and 50 layers. The overall size of the three dimensional aquifer is 15 m x 15 m x 5 m.

Figure 7.10. Hydraulic conductivity distribution in the model domain and source zone area.
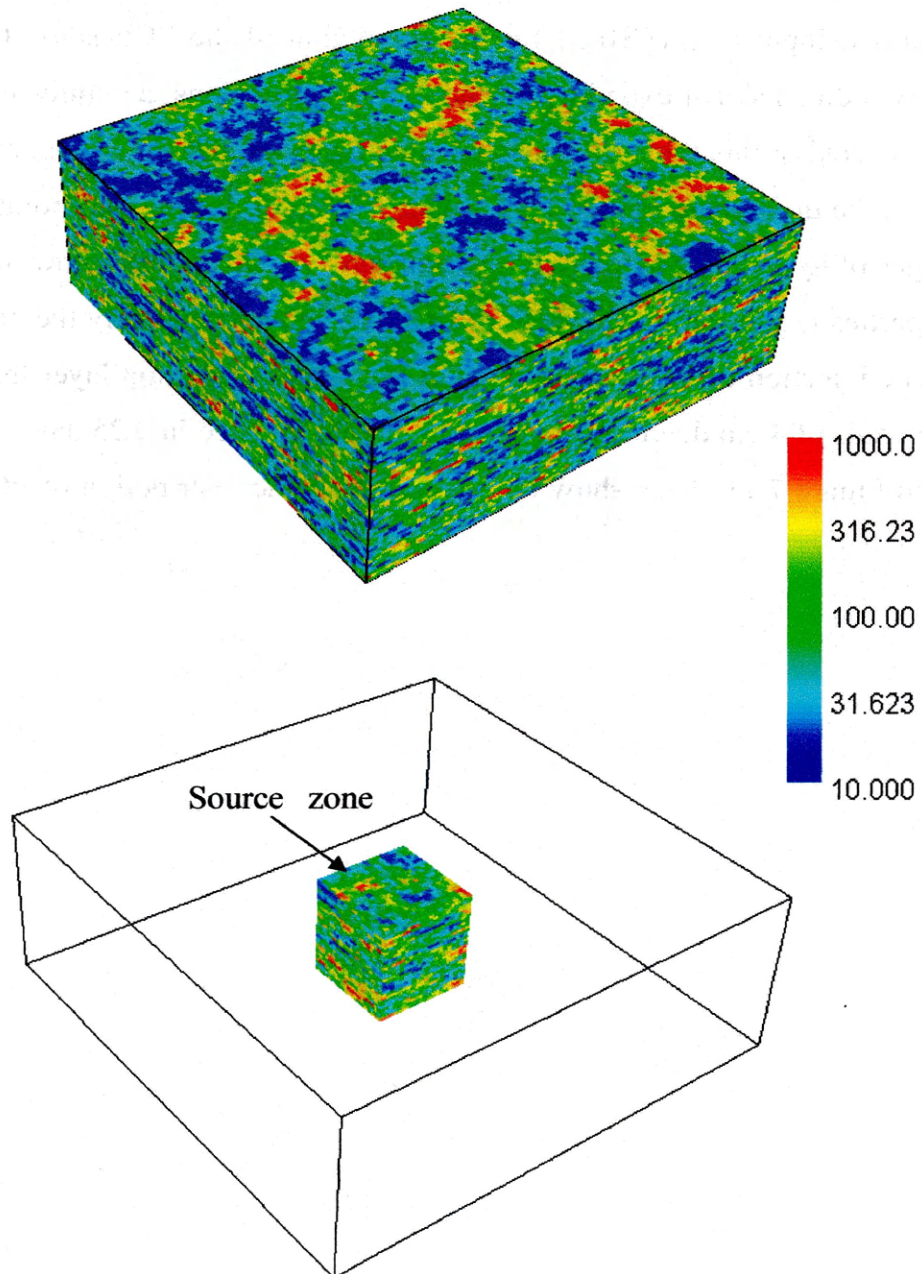
7.4.1 Source Zone Creation

The source zone was located in the center of the domain (3 m x 3m x 3m) and it was extracted and input in UTCHEM for the simulation of the PCE spill. To up-scale results from two dimensional experiments and model simulations, an equivalent volume of PCE was injected in this three-dimensional study. Brooks and Corey parameters were incorporated in the multiphase model. Five values of λ and Pd were incorporated for five different ranges of hydraulic conductivity. In this way we can compare how the capillary pressure properties influence the DNAPL architecture and consequently the performance of the test. The injection of PCE was applied at the center of the top layer through with the use of 32 wells of 4 cm depth. A total of 536 L were injected in 0.25 days. Results are represented in Figure 7.11. They show the variability of the distribution of PCE through the cell.

Figure 7.11. Three dimensional view of the final PCE distribution in the source zone.

158
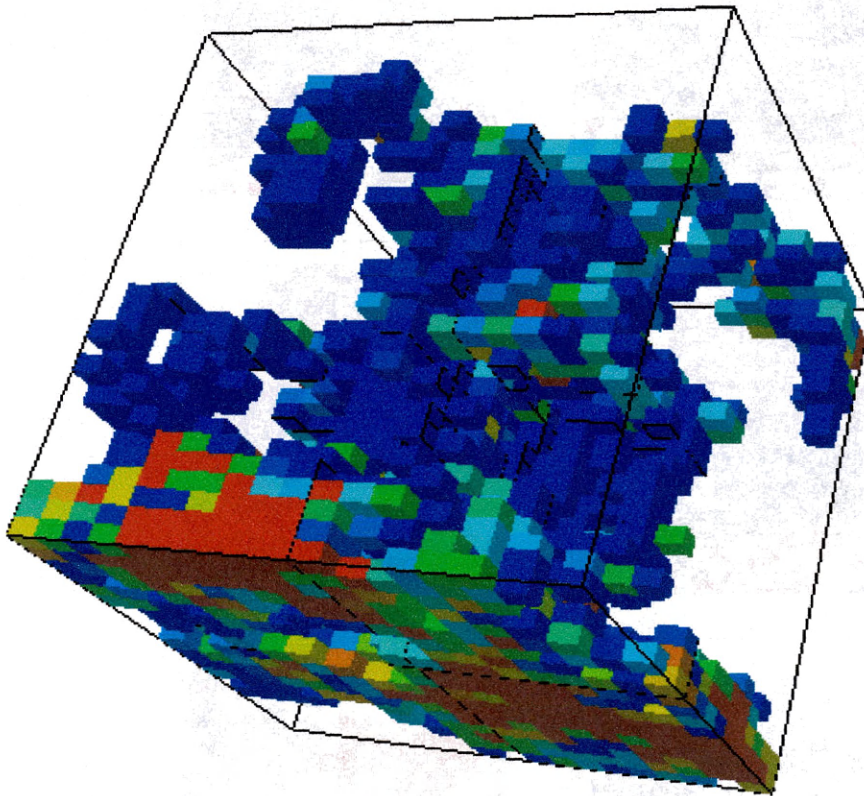
Figure 7.12. View of the source zone box from +x, -x, +y, -y, +z and –z directions
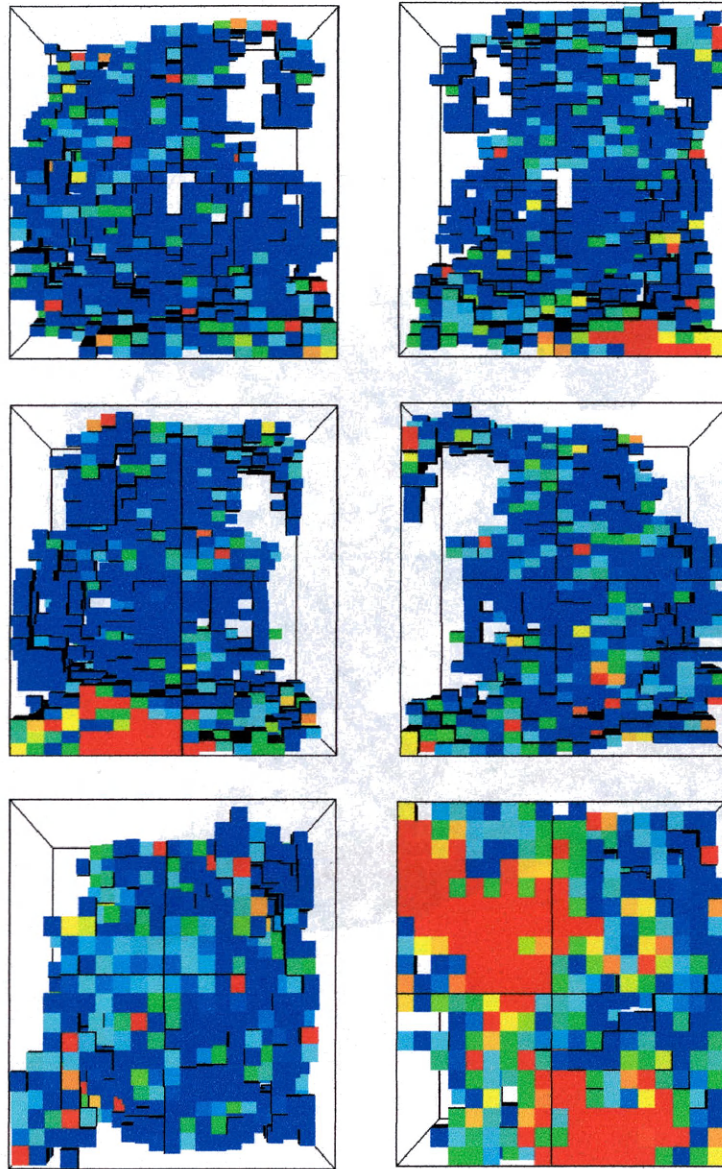
7.4.2 Tracer Transport Modeling

The PCE saturation distribution in the source zone was introduced in the full permeability field and three different injection-extraction patterns were tested for each of the DNAPL distributions.

All the boundaries were considered constant head boundaries and the wells created a forced gradient through the domain as is normally conducted in the field for PITT. The three well patterns used in this investigation were a line-drive pattern, a five spot pattern (convergent) and inverted five-spot pattern (divergent). Figure 7.13 shows the well location for each of the configurations. E symbolizes an extraction well and I symbolizes an injection well. All the wells penetrated the model domain from layer 11 to 40.

Tracers were injected for 0.5 days and concentrations were monitored in the extraction wells for a total of 11 days. In this set of simulations monitoring wells were not used and just the concentration at the extraction wells was used to determine the efficacy of the flow pattern.

Figure 7.13. Well patterns: line drive (left), five-spot divergent (right) and five-spot convergent (bottom).
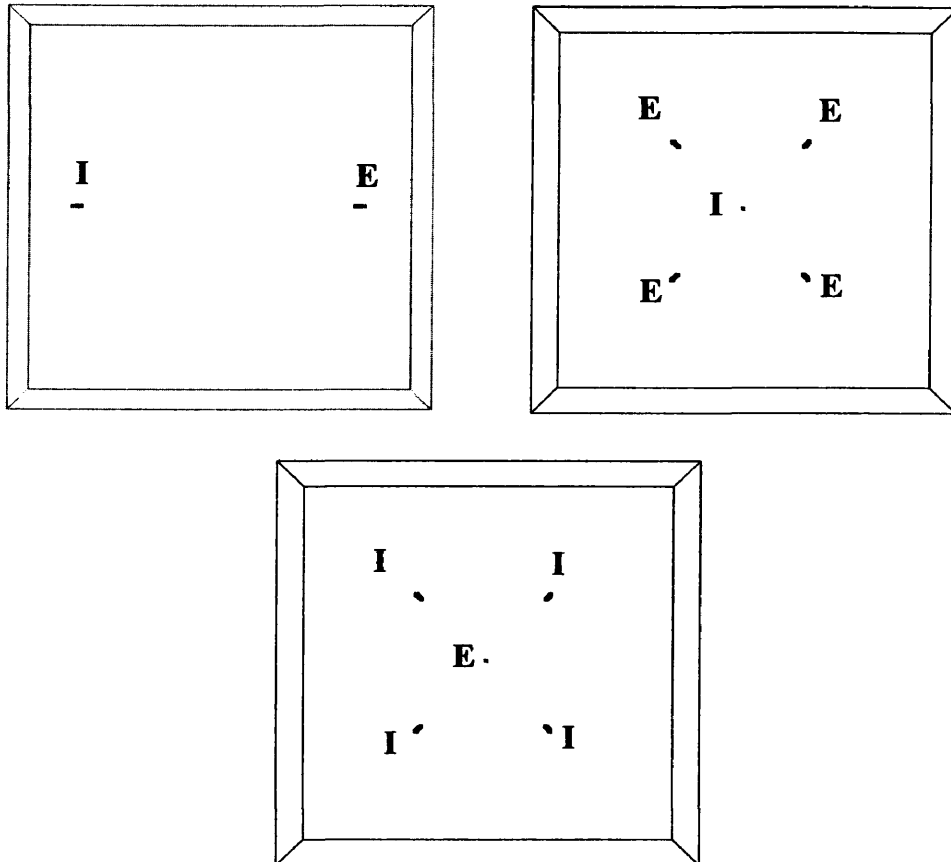
7.4.3 Estimation of PITT Performance

The responses obtained at each of the cells of the wells were averaged using the following expression:

$$C_T = \frac{C_i Q_i}{Q_T} \tag{7.5}$$

Where C_i is the concentration at each of the cells associated with that well, Q_i is the flow rate for each of the cells, and Q_t is the total flow rate of the extraction well. In this way, a breakthrough curve for each of the tracers was obtained at the extraction wells and method of moments was applied to these breakthrough curves.

The performance of PITT was evaluated following procedures similar to the ones conducted in section 7.3.4. However, in this case, there is a flow associated with the tracer response which allows for the calculation of the mass of PCE estimated by the tracers at the extraction wells with the use of the following equation:

$$V_N = S_N V_{swept} = \frac{Q(t_p - t_c)}{K_{NW}} \tag{7.6}$$

where Q is the flow rate associated with the extraction well, t_p is the mean travel time of the partitioning tracer and t_c is the mean travel time of the conservative tracer.

162

7.4.4 Results

Results of these simulations demonstrated the influence of tracer delivery patterns in tracer performance. For the line drive patterns the tracer estimated only 57% of the PCE mass present (see Figure 7.14). On the other hand, five spot patterns provided a much better estimation (83%) based on a more efficient tracer sweep pattern. James et al. (2000) provided similar results; in their study the five spot patterns provided "slightly" better results than line drive patterns. This study demonstrates that the difference between both patterns could be drastic when a more realistic distribution of DNAPL is incorporated in the simulations.

Figure 7.14. Tracer mass estimation
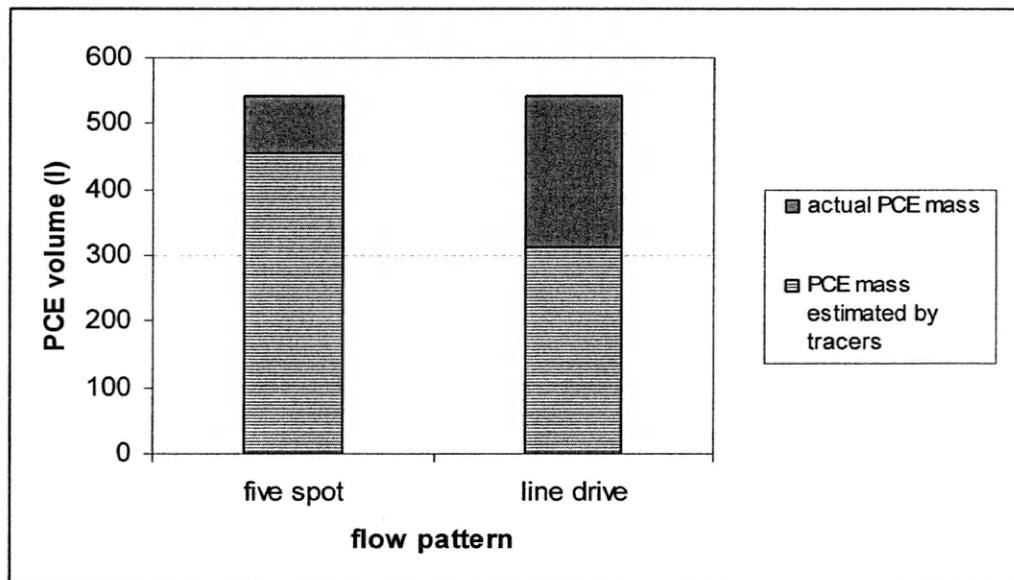
Convergent and divergent tracer tests provide the same mass estimation results, but divergent tracer test contain more information since the results are divided into as many signals as extraction wells are utilized. Since the flow lines sweep four different areas of the aquifer, the signals at the extraction wells provide information about the location of the mass. Analysis developed in previous chapter could be use to detect pool zones based on the degree of tailing of the partitioning tracer breakthrough curves. Figure 7.15 shows the pathlines of the five-spot configuration and the mass obtained at each of the wells.

Figure 7.15. Pathlines for the divergent five-spot pattern and volume estimated at each of the wells.
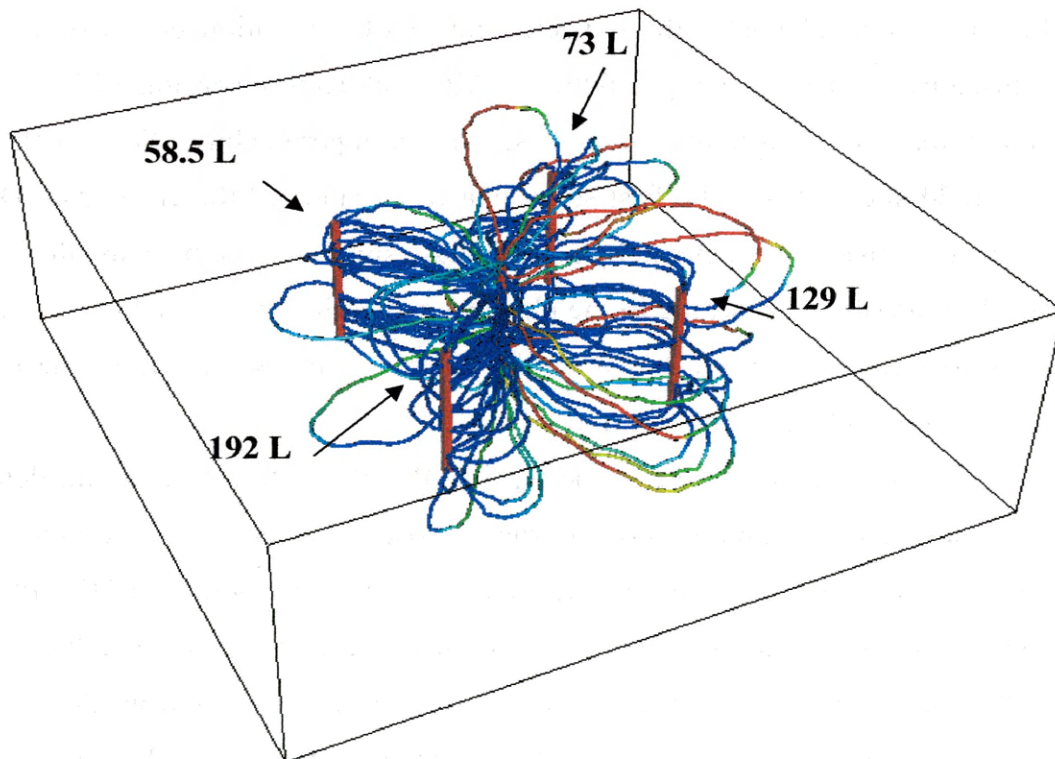
It is important to point out that the underestimation by tracers in these simulations is caused only by the hydrodynamic inaccessibility since equilibrium conditions were assumed. Therefore these results represent "best case scenarios" of underestimation error as results of the two-dimensional studies showed that rate-limited conditions could double up the error caused by hydrodynamic inaccessibility. Also, because of the numerical character of the study, this data were not subjected to other shortcomings of the field data like detection limits or experimental error in the sampling.

7.5 Conclusions

In this numerical study, the expected range of estimation errors of the PITT method caused by the heterogeneity and the DNAPL architecture was quantified.

A systematic procedure was applied using random permeability fields with similar statistics as field sites. This is the first study that has quantified the error from DNAPL architecture based on spills generated by a multiphase simulator. In this way, the DNAPL was allowed to distribute according to the physical properties of the medium. A range of estimation errors were calculated based on the heterogeneity, spreading of the DNAPL mass, well location and well configuration.

For the same degree of heterogeneity, the DNAPL architecture would determine also the efficacy of the technique. For the same geostatistics and same volume of PCE spilled, errors varied from 25% to 70% depending on the distribution of DNAPL in the source zone (more pools than residuals or viceversa). These results show a disagreement with the 6% errors reported by Jayanti (2003). The difference arises from the use of the multiphase simulator to create the DNAPL distribution that created pool areas that constrained tracer interaction between phases as discussed in Chapter 5.

The location of the well is an influential factor on error prediction generating errors up to 35% if is located to far from the source zone. The relationship between the error and the distance from the source zone could be used in field studies as a correction function.

The variance of the permeability has a direct impact on the performance of the test as shown in Figure 7.9. Sites with a σ^2_{lnk} of 0.25 showed estimation errors around 40%, on the other hand sites with a σ^2_{lnk} of 1.22 showed errors up to 70%. This is another limitation that has to be considered to determine whether the PITT is going to be an appropriate characterization technique for a particular site or not.

Results from the three dimensional analysis demonstrated the influence of the selected delivery pattern in the tracer sweep efficiency. Preliminary simulations should always be conducted prior to the PITT to optimize tracer delivery for a set of different DNAPL configurations or release scenarios.

Although this procedure has quantified error intervals for different design scenarios, it is important to realize that this error would be just a part of the overall estimation error expected in the field. The uncertainty in the flow and transport parameters to evaluate proper delivery and the experimental error caused by tracer detection limit and other variables (Dwarakanath et al, 1999) were not considered in this investigation and should be contemplated when evaluating the performance of the PITT.

This investigation demonstrates the importance of preliminary simulation studies prior to the tracer test to quantify the sensitivity of the parameters involved and design options in the final output of the test. Different release scenarios of NAPL should be part of the modeling analysis to determine the range of tracer performance expected for different architectures.

Chapter 8

CONCLUSIONS

8.1 Summary

The task of evaluating the location and amount of NAPLs in the subsurface has presented significant challenges in the past few decades. Innovative research was been conducted in recent years to investigate new approaches beyond the traditional discrete methods to determine DNAPL architecture. The Partition Interwell Tracer Test has been proposed as a method to non-intrusively characterize DNAPL source zones. The technique has been ineffective under conditions of natural heterogeneity. The objective of this research was to analyze fundamental processes of partitioning tracer behavior and extend findings to improve current application of the technique. Therefore, this dissertation focuses not only on the identification of the shortcomings of the tracer technique and the revision of current assumptions, but most importantly on the improvement of application design, data interpretation and analysis.

The knowledge gained from this investigation will help in the development of tracer techniques for field studies since it establishes the applicability of tracers in heterogeneous media. The findings of this investigation are reported in three chapters of this dissertation (Chapters 5, 6 and 7). Each chapter was written to address different aspects of the same problem and to generate independent contributions that will be developed in the form of journal articles. The results are summarized here:

Chapter 5 describes a two dimensional study of tracer transport through a single pool. A set of experiments were conducted and tracer responses were evaluated for a series of well characterized PCE pools. Inverse modeling and method of moments were used for data analysis. Estimation errors caused by rate limited behavior and hydrodynamic inaccessibility were quantified.

- The influence of the DNAPL saturation distribution on the performance of the test was demonstrated. Based on the DNAPL saturation profile, the error estimation of the PITT could vary from 20% to 57% of the total mass.

- Traditional application of the technique using extraction wells to estimate NAPL volume is ineffective if pools are present.

- Multilevel samplers provided information about the DNAPL vertical architecture and the presence of rate limited conditions.

- Method of moment analysis underestimated the DNAPL saturation. On the other hand, inverse modeling analysis provided better saturation estimates and an integrated interpretation of the system.

- The local equilibrium assumption was tested with inverse modeling methods. Results showed that this assumption does not apply in conditions of high DNAPL saturation and could lead to major estimation errors.

- The use of effective partition coefficients obtained in batch experiments relaxes the condition of equilibrium and enhances tracer performance if they are selectively applied to the location where rate limited behavior is detected.

- Rate limited conditions can be qualitatively detected by evaluating tracer breakthrough curves.

- The use of effective partition coefficient (Kp_e) increased tracer estimation performance by 20% in the two dimensional cell.

Chapter 6 validates findings from the previous experiment to more complicated entrapment architectures.

- Results demonstrated the inefficacy of method of moments and the importance of well location and sampling density in the vertical direction to capture DNAPL vertical architecture. As the distance from the source zone increases, the information about the vertical architecture dissipates.

- Multilevel samplers provided information about the DNAPL vertical architecture and the presence of rate limited conditions in conditions of complex architecture.

- The qualitative observation of the breakthrough curves can be used as an indicator of the presence of pools.

- A method originally developed by Valocchi, 1985 was adapted to quantitatively measure the deviation from equilibrium of the observed breakthrough curves obtained at multilevel samplers. The method uses the fractional change in the second moment (ε_2) to determine the deviation from equilibrium.

- Inverse modeling analysis provided valuable information about the validity of equilibrium partition coefficients in situations where tracer partitioning is controlled by non equilibrium behavior. Inverse modeling also showed the importance of collecting different type of observation data like heads, flows or dissolved concentration during PITT to facilitate regression analysis.

- Results showed the constraints of the PITT to estimate remediation performance in heterogeneous media, if the selected remediation technique does not successfully remove pool areas. Combining PITT results before and after remediation, the technique overestimated remediation performance by 40% in the two dimensional tank.

Chapter 7 describes an investigation of the performance of PITT under different design parameters in two and three-dimensional numerical simulations studies. The objective was to isolate different aspects that affect tracer performance: vertical distribution of the DNAPL, variance of the stochastic permeability field, and location of the multilevel samplers.

To investigate the incorporation of the third dimension in the analysis, a 3D study was also conducted to generalize findings regarding injection/extraction patterns.

■ The second spatial moment of the DNAPL mass determines the efficacy of the PITT if sampling is conducted close to the source zone. For the same geostatistics and same volume of PCE spilled, errors varied from 25% to 70% depending on the distribution of DNAPL in the source zone (more pools than residuals or vice versa).

■ The location of the wells is an influential factor on error prediction generating errors up to 35%. The relationship between the error and the distance from the source zone could be used in field studies as a correction function.

■ The degree of heterogeneity (defined by the variance of the permeability field) affects the performance of the test for similar DNAPL architectures and should be considered in preliminary design.

■ In the three dimensional case study, line drive patterns (dipole tracer tests) provided tracer responses with lower sweep efficiency than convergent and divergent flow patterns. For the same PCE source zone, line drive flow patterns estimated only 57% of the PCE mass present and five spot patterns provided an 83% estimation of the true PCE mass. Even though this is not an unexpected result, it demonstrates that the difference between both patterns could be drastic when a more realistic distribution of DNAPL is incorporated in the simulations.

■ Special considerations have to be undertaken in the design of PITT in conditions of heterogeneity. Preliminary simulation studies need to be conducted to evaluate the performance of the technique for different scenarios.

o Different DNAPL release scenarios should be part of the preliminary modeling analysis with the use of multiphase codes.

o Different flow patterns (convergent, divergent, line drive) should be considered to measure tracer sweep efficiency.

o The location of the multilevel samplers needs to be optimized to capture as much information of the source zone architecture as possible.

The results obtained this investigation and the protocols developed would be beneficial for hydrologists, engineers and scientist involved in the location and characterization of DNAPL source zones.

8.2 Recommendations for Future Research

The use of Kp_e could be investigated further to obtain theoretical expressions to predict the range of Kp_e for different scenarios (tracer, NAPL, permeability, etc).

It would be valuable to validate the use of multilevel samplers in the three dimensional domain. In this way, the density of sampling in the x, y and z directions necessary to obtain a complete three dimensional definition of the source zone could be evaluated. Inverse modeling capabilities to determine source zone architecture could be established also in the 3D.

In this investigation, surfactant flushing was used as the remediation technique to determine the efficacy of PITT to measure remediation performance. Since the SEAR technology did not successfully remove high saturation zones, tracer tests were categorized as "unsuccessful" to determine the remediation performance. However, this might not be a fair conclusion since the results directly depend on the efficacy of a particular remediation technique to remove high saturation areas. Further research

concerning other SEAR designs or remediation techniques that remove high saturation zones should be conducted with PITT.

The use of inverse modeling to determine DNAPL architecture by tracers could be refined to allow the relocation of the saturation zones in the optimization process. In this work, the saturation zones were set prior to the simulations. It would be advantageous in field applications to allow the optimization process to determine not only the saturation but also the location of these areas.

REFERENCES

Allison S.B. Analysis of field tracers for reservoir description. *M.S. Thesis, University of Texas at Austin, 1988.*

Allison S.B.; Pope G.A.; Sepehrnoori K.; Analysis of field tracers for reservoir description. *Journal of petroleum science and engineering, 5, 173-186, 1991.*

Ambwani, D.S.; Fort T. In Surface and Colloid Science. *Plenum; Vol 11; Chapter 3, New York, 1979.*

Anderson , M.R.; Johnson R.L.; Pankow J.M. Dissolution of dense chlorinated solvents into groundwater. 3. Modeling contaminant plumes from fingers and pools of solvent. *Environmental Science and Technology. 26, 901-908, 1992.*

Annable, M.D., P.S.C. Rao, K. Hatfield, W.D. Graham, A.L. Wood, and C.G. Enfield (1998), Partitioning tracers for measuring residual NAPL: Field-scale test result, J. of Env. Eng., 124, 901-908.

Aris,R., On the dispersion of linear kinematic waves. *Proc. R.. Soc. London, Ser. A, 245, 268-277, 1958.*

Barth G.R. Ph. D Dissertation. University of Colorado at Boulder, 1999.

Barth, G.R., Illangasekare T.H., Hill M.C., Rajaram H., A new tracer-density criterion for heterogeneous porous media. *Water Res. Res., 37, 21-31, 2001.*

Brewster, M.L., Annan, A.P., Greenhouse, J.P., Kueper, B.H., Olhoeft, G.R., Redman, J.D. and Sander, K.A. 1995: Observed migration of a Controlled DNAPL Release by Geophysical Methods. *Ground Water, Vol. 33, 977-987, 1995.*

Brooks M.C.; Annable M.D.; Rao P.S.C.; Hatfield K.; Jawitz J.W.; Wise W.R.; Wood A.L.; Enfield C.G. Controlled release, blind tests of DNAPL characterization using partitioning tracers. *Journal of contaminant hydrology. 59, 187-210, 2002.*

174

Brusseau M.L.; Nelson N.T.: Oostrom M.; Zhang Z.; Johnson G.R.; Wietsma T.W. Influence of heterogeneity and sampling method on aqueous concentrations associated with NAPL dissolution. *Environmental Science and Technology*, *34* *3657-3664, 2000.*

Clifton, P.M., and S.P. Newman, Effects of kriging and inverse modeling on conditional simulation of the Avra Valley aquifer in southern Arizona, Water Resour. Res., 18(4), 1215-1234, 1995.

Dai D., F. T. Barranco Jr., T.H. Illangasekare. Partitioning and interfacial tracers for differentiating NAPL entrapment configuration: Column-Scale investigation. *Environ. Sci. Technol.*, *35, 4894-4899, 2001.*

Davis M.M., J.D Istok, L. Semprini. Push-pull partitioning tracer tests using radon-222 to quantify non-aqueous phase liquid contamination. *Journal of Contaminant Hydrology 58, 129-146, 2002.*

Deeds N.E.; McKinney D.C.; Pope G.A Laboratory characterization of non-aqueous phase liquids interaction in support of vadose zone partitioning interwell tracer tests. *Journal of Contaminant Hydrology 41, 193-204, 2000.*

Delshad M.; Pope G.A and Sepehrnoori K. A compositional simulator for modeling surfactant enhanced aquifer remediation. *Journal of Contaminant Hydrology*, *23(1-2). 303-327, 1996.*

Demond, A.H., Capillarity in two-phase liquid flow of organic contaminants in groundwater, Ph.D Thesis, Stanford University, Standford, California.

Divine, C.E., J.E. McCray, L.M. Wolf Martin, W.J. Blanford, D.J. Blitzer, M.L. Brusseau, and T.B. Boving (2004), Partitioning tracer test as a remediation metric: Case study at Naval Amphibious Base Little Creek, Virginia Beach, Virginia, Remediation, Spring issue, 7-31.

Divine, C.E, Sanford W., McCray, J.E. Helium and neon tracers to measure residual DNAPL: Laboratory investigation, *Vadose Zone Journal, 2003, in press.*

Doherty,J., PEST: Model-independent parameter estimation. Tech. rept. Watermark Numerical Computing, Corinda, Australia., 1994.

Dwarakanath V.; Deeds N.; Pope G.A.; Analysis of partitioning interwell tracer tests. *Environmental Science and Technology, 33, 3829-3836, 1999.*

Farrel, D.A.; Woodbury, A.D.; Sudicky E.A.; Rivett M.O. Stochastic and deterministic analysis of dispersion in unsteady flow at the Borden tracer test site, Ontario. *Journal of Contaminant Hydrology, 15, 159-185, 1994.*

Fahim M.A.; Wakao N. Parameter estimation from tracer response measurements. *Chemical Eng. Journal, 25, 1-8, 1982*

Feenstra, S. and J.A. Cherry (1998), Subsurface contamination by dense non-aqueous phase liquids (DNAPLs) chemicals, Proceedings of International Groundwater Symposium, Halifax, Nova Scotia.

Fernandez Garcia, D. Scale-dependence of non-reactive and sorptive transport parameters estimated from radial and uniform flow tracer tests in heterogeneous formations. Experimental and numerical investigations. *Ph.D. Dissertation, Colorado School of Mines, 2003.*

Garabedian, S.P.; LeBlanc, D.R.; Gelhar L.W.; Celia M.A. Large-scale natural gradient tracer test in sand and gravel, Cape Code MA, 2. Analysis of spatial moments for a nonreactive tracer. *Water Resources and Research, 27(5), 911-924, 1991.*

Gelhar, L.W., and C.L. Axness, Three dimensional stochastic analysis of macrodispersion in aquifers, Water Resour. Res., 19(1), 161-180, 1983.

Geller, J.T., and J.R. Hunt, Mass transfer from nonaqueous phase organic liquids in water saturated porous medium, Water Resour. Res., 29, 883-846, 1993.

Gerhard, J.I. and B.H. Kueper (2003), Capillary pressure characteristics necessary for simulating DNAPL infiltration, redistribution and immobilization in saturated porous media, Water Resour. Res., 39(8), 1212.

Glover K. Task 1 of NSF Report. "Fundamental Evaluation of tracer techniques of characterization of NAPL retention volumes in heterogeneous aquifers (EAR-0107095)", *2003.*

Gutjahr, A.L., Fast Fourier transforms for random field generation, Project Report for Los Alamos Grant to New Mexico Tech, New Mexico Institute of Mining and Technology, Socorro, New Mexico, 1989.

Harbaugh, A.W., E.R. Banta, M.C. Hill, and M.G. McDonald (2000), Modflow-2000, The U.S. Geological Survey Modular Groundwater model - User guide to the modularization concepts and the groundwater flow process. Open file report, 00-92. U.S. Geological Survey, Reston, VA.

Harvey C.F.; Gorelick S.M. Temporal moment-generating equations: Modeling transport and mass transfer in heterogenous aquifers. *Water Resources and Research, 31, 8, 1895-1911, 1995*

Held J.H.; Illangasekare T.H. Fingering of dense nonaqueous phase liquids in porous media, 2, Analysis and classification. *Water Resources and Research, 31, 5, 1223-1231, 1995.*

Hill E.H.III, L.L. Kupper, Miller C.T, Evaluation of path lengths estimators for characterizing multiphase systems using polyenergetic X-ray absorption, *Soil Science, 167 (11), 703, 2002.*

Hill, E.H. III and T.H. Illangasekare (2004), *Chapter 16 in Hydrogeophysics, eds. Y. Rubin, and S. Hubbard*, Kluwer, Nederlands.

Hunkerler D.; Hoehn E.; Hohener P.; Zeyer J.; ^{222}Rn as a partitioning tracer to detect Diesel fuel contamination in aquifers: laboratory study and field observations. *Environmental Science & Technology, 31, 3180-3187, 1997.*

Illangasekare T.H., J.L. Ramsey, K.H. Jensen, M. Butt, Experimental study of movement and distribution of dense organic contaminants in heterogeneous aquifers. *J. Contaminant Hydrology, 20, 1-25, 1995a*

Illangasekare T.H., Member, ASCE, Ambruster E.J.III., Yates D. Non aqueous phase fluids in heterogeneous aquifers-Experimental Study. *Journal of Environmental Engineering, August 1995b.*

Imhoff, P.T., S.N. Gelyzer, J.F. MCBride, L.A. Vancho, I. Okuda, C.T. Miller, Cosolvent-enhanced remediation of residual dense nonaqueous phase liquids: Experimental investigation. *Environ. Sci. Technol, 29, 1966, 1995*

Imhoff, P. T.; Pirestani, K.; Jafarpour, Y.; Spivey, K. M. Tracer Interaction Effects during Partitioning Tracer Tests for NAPL Detection *Environ. Sci. Technol, 37, 1441-1447, 2003.*

Imhoff, P.T, Pirestani, K, Influence of mass transfer resistance on detection of nonaqueous phase liquids with partitioning tracer test, Advances in Water Resources, doi; 10.1016/j.advwaters.2004.02.010, in press.

Istok, J.D., Humphrey M.D., Schroth, M.R., Hyman, M.R., O'Reilly, K.T. Single well, "push-pull" test for in situ determination of microbial activities. *Ground Water* *35, 619-631, 1997.*

Jalbert, M, Dane J.H, Bahaminayakamwe. Influence of porous medium and NAPL distribution heterogeneities on partitioning interwell tracer tests: a laboratory investigation. *Journal of Hydrology, 272 (2003) 79-94*

Jawitz J.W.; Annable M.D.; Rao P.S.C.; Field implementation of a Winsor Type I surfactant/Alcohol mixture for in situ solubilization of a complex LNAPL as a single phase microemulsion. *Environmental Science and Technology, 32, 523-530, 1998.*

Jayanti, S. (2003), Modeling tracers and contaminant flux in heterogeneous aquifers, Ph.D. thesis dissertation, University of Texas at Austin, Austin, TX.

Jin M.; Delshad M.; Dwarakanath V.; McKinney D.C; Pope G.; Sepehrnoori K., Tilburg C.E. Partitioning tracer test for detection, estimation, and remediation performace assessment of subsurface nonaqueous phase liquids. *Water Resources and Research, 31, 1201-1211, 1995.*

Jin M.; Butler G.W.; Jackson R.E.; Mariner P.E.; Pickens J.F.; Pope G.A.; Brown C.L.; McKinney D.C. Sensitivity model and design protocol for partitioning tracer tests in alluvial aquifers. *Groundwater, v. 36, no. 6, 1997*

Johnson R.L., Pankow J.F. Dissolution of dense chlorinated solvents into Groundwater. 2. Source functions for pools of solvent. *Environmental Science and Technology, 26, 896-901, 1992.*

Kavanaugh, M.C., P.S.C. Rao, L. Abriola, J. Cherry, G. Destouni, R. Falta, D. Major, J. Mercer, C. Newell, T. Sale, S. Shoemaker, R.L. Siegrist, G. Teutsch, and K. Udell. The DNAPL Cleanup Challenge: Source Removal or Long Term Management. Report of an Expert Panel to the U.S. Environmental Protection Agency, National Risk Management Laboratory and Technology Innovation Office, 2003.

178

Kemblowski, M.W.; Chiang C.Y. Hydrocarbon thickness fluctuations in monitoring wells. *Ground Water, 28(2), 244-252, 1990.*

Kim H., Rao P.S.C; Annable M.D. Consistency of interfacial tracer technique: experimental evaluation. *Journal of contaminant hydrology 40, 79-94, 1999.*

Kram, M.L.; Keller A.A.; Rossabi J.; Everett L.G. DNAPL characterization methods and approaches, Part 1: Performance comparisons. *Groundwater monitoring remediation, Fall 2001.*

Kueper B.H., W. Abbot, G. Fraquhar, Experimental observations of multiphase flow in heterogeneous porous media, *J. Contaminant. Hydrology, 5, 83-95, 1989.*

Kueper B.H., E.O. Frind. Two phase flow in heterogeneous porous media. 1. Model development. *Water Resources and Research, vol. 27(6), 1049-1057, 1991.*

Kueper B.H.; Redman D.; Starr R.C.; Reitsma S.; Mah M. A field experiment to study the behavior of tetracholoroethylene below the water table; Spatial distribution of residual and pooled DNAPL. *Groundwater, Vol. 31, No. 5, 1993*

LeBlanc, D.R., Garabedian, S.P., Hess, K.M., Gelhar, L.W. Quadri, R.D., Stopllenwerk, K.G., Wood, W.W., 1991. Large scale natural gradient tracer test in sand and gravel, Cape Cod, Massachussets, 1. Experimental Design and Observed Tracer movement. *Water Res. Res., 27(5), 895-910.*

Mackay, D.M; Cherry J.A. Groundwater contamination: Pump and treat remediation, *Environmental Science and Technology, Vol. 23, No. 6, 1989.*

Mackay, D; Freyburg D.L.; Roberts P.V.; Cherry J.A. A natural gradient experiment on solute transport in a sand aquifer, 1, Approach and overview of plume movement. *Water Resources and Research, 30(2), 369-383, 1994.*

Mariner P.E.; Jin M.; Studer J.E, Pope G.A The first vadose zone partitioning interwell tracer test for nonaqueous phase liquids and water residual. *Environmental Science & Technology, 33, 2825-2828, 1999.*

Matheron, G., The intrinsic random functions and their application, Adv. Appl. Prob., 5, 438-468, 1973.

McWhorter, D.B., B.H. Kueper, Mechanics and mathematics of the movement of dense non-aqueous phase liquids (DNAPLs) in porous media. In: Pankow, J.F. and J.A. Cherry. Dense chlorinated solvents and other DNAPLS in groundwater: history, behavior and remediation. *Waterloo Press, Portland, OR, 1996.*

Meinardus H.W.; Dwarakanath V.; Ewing J.; Hirasaki G.J.; Jackson R.E.; Jin M.; Ginn J.S.; Londergan J.T.; Miller C.T.; G.A. Pope. Performance assessment of NAPL remediation in heterogeneous alluvium. *Journal of Contaminant Hydrology 54, 173-193, 2002.*

Mercer, J.W.; and Coher R.M. A review of immiscible fluids in the subsurface: properties, models, characterization and remediation. *Journal of contaminant hydrology, 6, 107-163, 1990.*

Michalski, A.; M.N. Metlitz and I.L. Whitman, A field study of enhanced recovery of DNAPL pooled below the water table, Ground Water Monitoring and Remediation, Winter, 90-100, 1990.

Miller, R.D., Normal moveout stretch mute on shallow-reflection data, *Geophysics, 57, 1502-1507, 1992.*

Moreno-Barbero, E., T.H. Illangasekare, and D. Dai (2002), Evaluation of the partition interwell tracer technique for possible characterization of DNAPL pools, Eos Trans. AGU, 83(47), Fall Meet. Suppl., Abstract H22A-0863.

Nelson N.T.; Oostrom M.; Wietsma T.W.; Brusseau M.L. Partitioning tracer method of for the in situ measurement of DANPL saturation: Influence of heterogeneity and sampling method. *Environmental Science and Technology, 33, 4046-4053, 1999.*

Noordman W.H; Geert;Wietzes P.; Volkering F.; Janssen D.B. Assessment of the Use of Partitioning and Interfacial Tracers to determine the content and mass removal rates of nonaqueous phase liquids. *Environmental Science and Technology, 34, 4301-4306, 2000.*

Okuda, I., J.F. McBride, S.N.Gleyzer, C.T. Miller. An investigation of physicochemical transport processes affecting the removal of residual DNAPL by nonionic surfactant solutions. *Environ. Sci. Technol., 30, 1852, 1996.*

180

Olhoeft, G.R., Geophysical detection of hydrocarbon and organic chemical contamination, *Proceedings of the Symposium on the Application of Geophysics to Engineering and Environmental Problems, April 26-29, Oakbrook, Illinois*, edited by R.S. Bell, pp. 587-595, 1992a.

Oolman, T.; S.T. Godard, G.A. Pope, M. Jin and K. Kirchner, DNAPL flow behavior in a contaminated aquifer: evaluation of field data, Ground Water Monitoring and Remediation, Fall: 125-137, 1995.

Oostrom, M., C. Hofstee, R.C. Walker, and J.H. Dane., Movement and remediation of tricholoroethylene in a saturated heterogeneous porous medium. 1. Spill behavior and initial dissolution, *J. Contaminant Hydrology, 37, 159-178, 1999.*

Paillet, F.L., Using borehole geophysics and cross-borehole flow testing to define hydraulic connections between fracture zones in bedrock aquifers, *Journal of Applied Geophysics, 30, 261-279, 1993.*

Phillips J.P. and Fitterman D.V. Environmental Geophysics. U.S. National Report to IUGG, 1991-1994 Rev. Geophys. Vol. 33 Suppl., © *American Geophysical Union, 1995.*

Poeter, E.P. and Hill M.C. Inverse models: a necessary step in ground-water modeling. *Groundwater 35(2) 250-260, 1997.*

Poeter, E.P. and Hill, M.C. Documentation of UCODE, a computer code for universal inverse modeling. *Golden, CO, U.S. Geological Survey, International Ground Water Modeling Center, 1998.*

Rao P.S, Annable M.D, Sillan R.K.; Dai.D; Hatfield K.; Graham W.D Field-scale evaluation of in situ cosolvent flushing for enhanced aquifer remediation. *Water resources research, 33, 2673-2686, 1997.*

Rao S.P.R.; Annable M.D; Kim H. NAPL source zone characterization and remediation technology performance assessment: recent developments and applications of tracer techniques. *Journal of Contaminant Hydrology 45, 63-78, 2000.*

Rehfeldt, K.R., J.M. Boggs, and L.W Gelhar, 1992. Field study of dispersion in a heterogeneous aquifer. 3. Geostatistical analysis of hydraulic conductivity, *Water Res. Res., 28(12), 3309-3324.*

Robin, MJ.L., A.L. Gutjahr, E.A. Sudicky, and J.L. Wilson, Cross-correlated random field generation with the direct Fourier transformation method, Water Resour. Res., 29, 2385-2397, 1993.

Roy, J.W., J.E. Smith, and R.W. Gillham (2002), Natural remobilization of multicomponent DNAPL pools due to dissolution, J. Contam. Hyd., 59, 163-186.

Saba, T. Upscaling of Mass transfer from entrapped NAPL sunders natural and enhanced conditions, Ph.D Dissertation, University of Colorado at Boulder, 1999.

Saba, T. and T.H. Illangasekare, Effect of groundwater flow dimensionality on mass transfer from entrapped nonaqueous phase liquid contaminants, Water Resour. Res., 36(4), 971, 2000.

Saenton, S. Prediction of mass flux from DNAPL source zone with complex entrapment architecture, model development, experimental validation and up-scaling. *Ph.D. Dissertation, Colorado School of Mines, CO, 2003.*

Sale, T.C. and D.B. McWorther (2001), Steady state mass transfer from single-component dense nonaqueous phase liquids in uniform fields, Water Resour. Res., 37(2), 393.

Schwille, F., Dense Chlorinated Solvents in Porous and Fractured Media Model Experiments, *translated by J.F. Pankow, 146 pp., A.F. Lewis Boca Raton, Fla., 1988.*

Steeples, D.W., and R.D. Miller, Basic principles and concepts of practical shallow seismic reflection profiling, *Mining Engineering, 45, 1297-1302, 1993.*

Stewart, D.C., W.L. Anderson, T.P. Grover, and V.F. Labson, Shallow subsurface mapping by electromagnetic sounding in the 300 kHz to 30 MHz range: model studies and prototype system assessment, *Geophysics, 1201-1210, 1994.*

Sudicky, E.A. A natural gradient experiment of solute transport in a sand aquifer: spatial variability of hydraulic conductivity and its role in the dispersion process. *Water Resources and Research, 22 (1), 2069-2082, 1986.*

Tang, J.S.; Harker, B. Interwell tracer test to determine residual oil saturation in a gas-saturatied reservoir, Part 1: Theory and Design. *J. C. Pet. Technol., 30(3), 76-85, 1991.*

Thorbjarnarson, K.W.; Mackay D.M. A forced-gradient experiment on solute transport in the Borden aquifer 2. Transport and dispersion of the conservative tracer. *Water Resources and Research, 30(2), 385-399, 1994.*

Valocchi, A.J. Validity of the local equilibrium assumption for modeling sorbing solute transport through homogeneus soils. *Water Resources and Research, Vol. 21, No. 6, 808-820, 1985.*

Vulava M.V.; Perry E.B.; Romanek C.S.; Seaman J.C. Dissolved gases as partitioning tracers for determination of hydrogeological parameters. *Environmental Science and Technology, 36, 254-262, 2002.*

Weil, G.J., Graf, R.J. and Leann, M.F. 1994: Investigations of Hazardous Waste Sites Using Thermal IR and Ground Penetrating Radar. *Photogrammetric Engineering & Remote Sensing, Vol. 60, No. 8, pp. 999-1005, 1994.*

Willson C.S.; Pau O.; Pedit J.A; Miller C.T. Mass transfer limitation effects on partitioning tracer tests. *Journal of Contaminant Hydrology 45, 79-77, 2000.*

Wilson, R.D.; Mackay, D.M, The use of sulphur hexafluoride as a conservative tracer in saturated sandy media. *Ground Water, 31(5), 719-725, 1993.*

Wise W.R; Dai D.; Fitzpatrick E.A.; Evans L.W; Rao P.S; Annable M.D. Non-aqueous phase liquid characterization via partitioning tracer tests: a modified Langmuir relation to describe partitioning nonlinearities. *Journal of Contaminant hydrology 36, 1999.*

Young C.M.; Jackson R.E.; Jin M.; Londergan J.T.; Mariner P.E.; Pope G.A.; Anderson F.J.; Houlk T. Characterization of a TCE DNAPL zone in alluvium by partitioning tracers. *Ground Water Monitoring Remediation, Vol. 19, No. 1, Winter 1999.*

Zhang, D. Stochastic Methods for Flow in porous media, Academic Press, 2002.

Zheng, C. and P.P. Wang (1999), MT3DMS: A modular three multispecies transport model for simulation of advection, dispersion, and chemical reaction of contaminants in groundwater systems, Documentation and user's guide. Contract report SERDP-99-1. US Army Engineer Research and Development Center.

APPENDIX

This appendix contains all the tracer data generated in all the experiments of this dissertation.

184

A.1 Tracer data obtained in the two dimensional cell experiment

A.1.1. PCE saturation profile 1.

Tracer concentrations at the outlet.

Co	254.143	565.024	455.309	752.862
time	**Bromide**	**DMP**	**6M2H**	**Hex**
(min)	**(mg/l)**	**(mg/l)**	**(mg/l)**	**(mg/l)**
0	0.000	0.000	0.000	0.000
120	0.601	2.887	2.231	1.953
150	1.799	5.145	3.561	5.761
180	4.862	12.653	9.319	17.193
210	23.216	33.723	22.800	51.791
240	74.447	126.280	83.562	192.920
270	177.038	322.351	234.240	477.770
300	201.344	401.660	325.133	590.303
330	148.279	310.095	260.170	436.030
360	59.753	163.779	166.221	232.229
390	18.976	59.500	59.741	76.845
420	9.561	32.890	31.606	38.567
450	5.549	23.373	22.183	25.176
480	3.524	15.961	13.995	15.062
510	2.391	13.302	12.407	12.104
540	1.735	10.174	9.351	8.268
570	1.247	9.002	9.112	7.255
600	1.106	7.579	8.138	5.937
630	0.879	6.212	6.998	4.562
660	0.652	5.280	5.731	3.447
690	0.617	4.879	5.697	3.165
750	0.443	3.754	4.815	2.083
810	0.160	3.349	4.234	1.826
840	0.111	3.039	3.666	1.727
900	0.057	2.723	4.063	1.169
1000	0.017	2.019	3.082	0.950
1100	0.005	1.496	2.338	0.772
1200	0.002	1.109	1.774	0.628
1300	0.000	0.822	1.345	0.510
1400	0.000	0.610	1.021	0.415
1500	0.000	0.452	0.774	0.337

A.1.2. PCE saturation profile 2.

Tracer concentrations at the outlet.

Co	184.439	574.887	551.626	796.687
time	**Bromide**	**DMP**	**6M2H**	**Hex**
(min)	**(mg/l)**	**(mg/l)**	**(mg/l)**	**(mg/l)**
0	0.592	4.477	3.645	1.307
60	0.500	7.707	7.237	4.968
120	2.884	15.936	14.407	17.685
150	5.459	19.978	17.478	25.602
180	18.015	32.562	24.145	58.469
210	35.985	63.108	38.321	127.745
240	50.437	110.300	65.057	196.137
270	69.358	196.869	133.452	305.858
300	88.310	303.852	240.790	419.098
330	91.424	333.055	301.522	445.275
360	68.280	268.985	267.679	357.105
390	29.571	142.151	168.359	186.001
420	12.049	65.562	84.083	78.829
450	5.865	35.649	49.141	39.350
480	2.414	23.438	33.241	23.964
510	2.253	17.908	25.946	17.419
540	1.711	14.279	21.020	13.360
570	1.649	11.732	16.959	10.237
600	1.294	9.877	14.124	8.243
630	0.344	8.905	12.607	6.867
660	0.795	7.862	10.989	6.012
690	0.357	6.162	10.243	4.739
720	0.251	5.607	8.922	3.960
780	0.124	5.088	6.768	2.765
810	0.087	4.858	5.894	2.310
900	0.030	3.426	3.894	1.348
1000	0.009	2.370	2.457	0.741
1100	0.003	1.640	1.550	0.407
1200	0.001	1.134	0.978	0.224
1300	0.000	0.785	0.617	0.123
1400	0.000	0.543	0.389	0.068
1500	0.000	0.376	0.246	0.037

Tracer concentrations at sampling ports

Co	193.417	578.447	563.208	804.251

PORT B

time	Bromide	DMP	6M2H	Hex
(min)	(mg/l)	(mg/l)	(mg/l)	(mg/l)
0	0.452	10.092	15.946	5.312
60	0.014	9.565	17.091	3.028
90	0.008	6.671	14.282	1.466
120	5.041	6.891	15.717	6.648
150	105.970	78.551	40.918	234.416
180	180.287	214.304	91.366	517.070
210	192.673	282.658	122.686	599.207
240	114.991	295.975	135.244	554.136
270	31.241	245.658	138.753	332.012
300	4.313	165.347	138.856	127.625
330	0.901	107.343	131.668	54.307
375	0.359	61.151	107.686	25.051
405	0.204	43.870	87.581	16.915
435	0.066	35.413	74.919	13.073
465	0.098	29.117	62.238	10.197
495	0.053	25.120	52.235	8.406
525	0.059	22.617	47.456	7.293
555	0.187	20.494	41.337	6.374
585	0.073	18.291	35.854	5.649
615		16.483	31.338	4.783
645	0.006	15.019	29.341	4.241
675	0.029	14.187	27.792	3.950
705	0.010	14.121	26.721	4.031
735	n.a.	12.706	22.119	3.718

PORT C

time	Bromide	DMP	6M2H	Hex
0	0.044	18.015	19.886	11.024
60		14.881	19.946	7.402
90	1.332	16.194	20.242	8.147
120	26.680	17.649	20.799	22.351
150	79.500	32.052	20.142	100.966
180	159.750	82.935	51.584	222.288
210	171.446	121.354	79.197	306.628
240	110.876	121.937	77.852	300.609
270	53.877	110.036	71.174	245.211
300	16.260	111.517	72.010	247.118
330	4.574	83.471	49.632	168.987
375	2.969	69.876	42.481	105.920
405	2.668	65.137	41.548	91.896
435	1.579	60.702	43.000	75.697
465	1.015	56.490	42.418	64.115
495	0.838	52.783	41.776	58.062
525	0.698	48.458	40.283	50.499
555	0.599	47.605	40.143	48.920
585	0.478	45.066	40.977	43.983
615	0.262	40.536	38.860	37.739
645	0.255	39.064	38.682	35.798
675	0.216	34.994	35.234	31.433
705	0.213	34.756	36.407	31.192
735	0.079	31.669	34.333	27.959

A.1.3. PCE saturation profile 3.

Tracer concentrations at the outlet.

Co	144.000	542.526	551.626	769.086
time	Bromide	DMP	6M2H	Hex
(min)	(mg/l)	(mg/l)	(mg/l)	(mg/l)
0	0.162	5.311	2.973	0.000
30	0.261	5.565	8.150	0.744
60	0.286	6.103	9.255	1.306
90	2.043	12.126	15.151	8.597
120	3.628	19.882	22.133	18.158
150	6.292	27.619	27.304	31.049
180	17.632	36.340	32.127	53.287
210	42.331	70.642	42.248	139.068
240	55.177	111.772	58.932	206.261
270	50.313	143.240	77.803	242.076
300	39.866	176.145	109.275	228.613
330	57.819	233.167	173.432	284.452
360	64.337	259.690	230.206	316.750
390	50.998	208.627	204.790	252.939
420	24.858	125.339	148.977	148.778
450	8.959	56.451	84.095	64.782
510	2.234	17.820	35.960	14.825
540	1.590	13.395	28.161	11.805
570	1.489	10.240	21.545	8.908
600	0.626	8.301	20.602	6.631
630	0.494	7.193	15.098	5.614
660	0.692	6.213	12.325	4.053
690	0.975	5.561	13.880	3.774
720	0.390	5.064	11.847	3.391
780	0.420	4.592	10.876	2.836
810	0.207	4.168	8.801	2.250
840	0.319	3.792	8.116	1.950
870	0.157	3.178	7.329	1.959
900	0.142	3.361	6.260	1.627
1000	0.070	2.550	4.432	0.646
1100	0.034	1.934	3.138	0.407
1200	0.017	1.467	2.221	0.257
1300	0.008	1.113	1.573	0.162
1400	0.004	0.844	1.113	0.102
1500	0.002	0.641	0.788	0.065

Tracer concentrations at sampling ports

Co	143.330	523.534	183.969	735.387

PORT A

time	Bromide	DMP	6M2H	Hex
(min)	(mg/l)	(mg/l)	(mg/l)	(mg/l)
30	0.000	5.792	9.457	1.123
75	0.056	4.325	9.530	0.496
120	17.698	17.356	13.536	41.334
165	121.571	176.413	72.447	406.791
210	131.422	290.135	120.491	559.088
255	56.234	275.426	148.341	366.568
300	10.217	160.932	143.482	97.531
345	1.219	44.611	104.964	8.181
390	0.094	22.608	88.204	1.565
435	0.059	8.478	67.448	0.000
480	0.037	3.435	51.442	0.000
525	0.016	1.662	35.249	0.000
570	0.060	1.011	26.135	0.000
615	0.012	0.667	18.202	0.000
660	0.024	0.507	13.167	0.000
705	0.007	0.377	7.508	0.000

PORT B

time	Bromide	DMP	6M2H	Hex
30	0.050	7.359	11.646	0.723
75	0.462	4.884	12.442	0.605
120	85.815	69.053	39.737	194.439
165	138.826	232.358	103.114	515.302
210	93.019	314.016	138.750	521.736
255	19.264	226.647	155.063	200.113
300	1.641	92.052	124.571	21.291
345	0.676	39.252	104.285	5.475
390	0.042	16.381	85.955	2.441
435	0.163	7.509	58.984	1.461
480	0.015	5.110	42.777	1.240
525	0.011	3.798	32.190	0.937
615	0.006	2.551	17.232	0.617
660	0.039	2.383	12.844	0.507
705	0.027	1.903	10.825	0.385

PORT C

time	Bromide	DMP	6M2H	Hex
30	0.090	7.560	15.661	0.964
75	4.184	10.273	19.464	5.833
120	118.739	105.873	52.708	318.314
165	163.298	225.140	94.264	523.504
210	41.585	195.655	91.569	311.691
255	5.449	140.458	101.559	136.493
300	0.460	82.606	91.275	50.857
345	0.122	50.632	73.473	29.951
390	0.929	36.312	63.176	22.107
435	0.013	30.404	52.234	17.792
480	0.027	25.099	43.272	13.424
525	0.007	22.886	36.307	11.259
615	0.014	18.708	29.707	7.792
660	0.004	15.154	24.365	5.513
705	0.031	13.811	20.662	4.310

A.1.4. PCE saturation profile 4.

Tracer concentrations at the outlet.

| Co | 400.000 | 616.437 | 819.656 |

time	Bromide	DMP	Hex
(min)	(mg/l)	(mg/l)	(mg/l)
30	1.296	1.159	0.000
60	1.727	3.338	2.444
90	6.571	11.183	13.236
120	11.623	18.637	28.311
150	17.285	27.567	42.453
180	63.386	50.319	96.903
210	141.915	102.808	202.364
240	174.946	155.048	291.150
270	148.207	182.695	310.597
300	85.100	185.092	245.190
330	82.820	192.642	203.290
360	107.371	223.506	238.146
390	117.457	226.965	253.756
420	96.097	191.836	223.846
450	55.755	118.810	131.154
480	25.035	66.303	67.351
510	14.284	36.065	32.514
540	7.817	21.303	17.067
570	4.360	14.105	10.724
600	3.957	9.930	6.855
630	3.488	8.720	5.311
660	2.480	5.640	3.737
690	1.280	4.519	3.090
720	1.762	3.594	2.393
780	1.456	3.987	1.848
810	1.343	2.392	1.503
900	1.064	1.500	0.840
1000	0.789	0.863	0.296
1100	0.585	0.497	0.167
1200	0.434	0.286	0.094
1300	0.321	0.165	0.053
1400	0.238	0.095	0.030
1500	0.177	0.054	0.017

Tracer concentrations at sampling ports

Co	443.071	637.034	458.687	884.834

PORT A

time	Bromide	DMP	6M2H	Hex
(min)	(mg/l)	(mg/l)	(mg/l)	(mg/l)
30	0.046	0.000	0.000	0.000
75	0.228	0.000	0.000	0.000
120	34.048	16.354	5.596	19.395
165	324.776	227.120	81.074	474.459
210	355.761	376.785	140.788	641.646
255	123.715	253.587	129.620	285.732
300	25.106	151.874	132.004	72.149
345	4.472	51.197	95.619	6.015
390	2.654	19.327	68.448	1.415
435	0.798	5.574	37.507	0.000
480	0.798	2.180	29.042	0.000
540	0.390	0.935	17.123	0.000
585	0.503	0.453	10.017	0.000
630	0.367	0.294	6.433	0.000
675	0.188		4.290	0.000
720	0.102	0.159	2.226	0.000

PORT B

30	0.098	0.000	0.000	0.000
75		0.000	0.000	0.000
120	185.338	53.641	17.849	71.216
165	388.466	167.153	58.921	454.884
210	78.858	215.043	78.370	294.385
255	46.564	252.347	135.509	211.617
300	3.198	97.378	111.390	14.635
345	0.723	34.866	68.310	2.208
390	0.217	14.006	58.412	0.741
435	0.131	4.775	42.587	0.000
480		1.654	24.275	0.000
540	1.995	0.696	18.415	0.000
585	0.054	0.389	12.691	0.000
630		0.248	8.088	0.000
675	0.048	0.179	5.051	0.000
720	0.050	0.148	3.191	0.000

PORT C

time	Bromide	DMP	6M2H	Hex
(min)	(mg/l)	(mg/l)	(mg/l)	(mg/l)
30	0.599	0.000	0.456	0.000
75	26.047	10.652	3.358	0.000
120	427.142	224.088	69.705	525.202
165	443.942	325.903	98.668	642.427
210	89.904	291.806	142.304	235.844
255	4.089	119.602	116.842	
300	1.317	55.567	101.016	4.123
345	0.286	19.556	71.815	1.007
390	0.303	7.561	44.050	0.000
435	0.025	3.511	34.463	0.000
480	0.039	1.803	21.312	0.000
540	0.087	1.067	14.567	0.000
585	0.132	0.655	7.972	0.000
630	0.051	0.389	6.101	0.000
675	0.041	0.323	3.764	0.000
720	0.031	0.257	3.131	0.000

A.2. Tracer data in two dimensional tank experiments.

A.2.1 PITT 1

Co	977.537	715.299	1318.706	405.759				
PORT A7					**PORT A12**			

time	Bromide	DMP	6M2H	Hex	Bromide	DMP	6M2H	Hex
(min)	(mg/l)	(mg/l)	(mg/l)	(mg/l)	(mg/l)	(mg/l)	(mg/l)	(mg/l)
180	0.000	0.000	1.872	0.000	0.040	0.000	7.450	0.000
300	0.175	0.000	2.046	0.000	102.704	47.102	18.685	54.604
360	40.456	21.384	12.074	14.486	195.111	87.877	28.059	136.652
420	103.450	48.954	17.802	63.459	225.626	101.656	35.748	161.831
540	145.051	66.580	25.458	104.829	219.501	105.113	40.250	164.318
660	112.216	80.885	28.196	96.717	214.234	105.285	41.837	165.564
780	3.385	80.065	36.739	138.014	37.634	119.415	50.487	206.599
900	135.304	87.524	38.957	128.714	5.054	19.831	14.764	7.957
1020	0.104	17.978	12.640	10.670	0.217	1.441	3.362	0.000
1140		1.576	2.118	0.000	0.019	0.000	0.000	0.000
1260		0.356	5.993	0.000	15.880	0.000	1.461	0.000
1380		0.000	4.560	0.000	0.571	7.062	7.583	0.000
1500		0.000	4.620	0.000	0.508	0.000	0.000	0.000
1620		0.000	6.405	0.000	n.a.	0.000	6.989	0.000
1740		0.000	4.252	0.000	0.192	0.000	5.704	0.000
1860		0.000	4.587	0.000	0.029	0.000	7.028	0.000
PORT A16					**PORT A17**			
180	0.082	0.000	0.000	5.410	0.014	0.000	4.055	0.000
300	95.807	6.686	31.177	10.844	25.971	3.793	8.562	6.449
360	157.208	17.091	73.915	9.603	69.946	9.177	7.089	15.485
420	165.025	25.243	87.759	9.304	104.000	12.351	14.453	16.481
540	170.308	35.736	93.306	8.387	131.632	14.516	8.396	32.166
660	159.768	34.347	46.331	13.122	146.676	11.860	8.268	15.261
840	152.528	33.216	123.123	7.996	149.873	17.059	9.544	33.816
900	87.623	32.639	95.282	5.817	110.275	19.208	9.962	52.619
1020	13.560	32.048	72.760	8.570	52.773	12.083	5.075	32.818
1260	0.785	24.244	33.178	7.440	7.511	10.570	4.005	19.630
1500	0.024	16.945	19.949	6.923	1.797	10.238	7.794	15.006
1620		12.951	10.858	9.588	0.391	9.242	9.551	14.210
1740		11.103	7.644	8.970	0.074	8.579	7.426	17.836
1860		10.022	5.446	6.344		7.364	4.537	11.030
1980	0.030	9.019	4.730	11.386		7.034	3.967	10.247
2100	0.043	7.624	3.058	8.948		6.115	4.318	10.103
2220	0.167	7.753	2.921	5.881		5.663	6.242	7.431
2340		7.060	1.906	8.462		5.788	9.433	8.442
2460		6.391	1.694	8.809		5.271	6.962	6.162
2580	0.031	5.974	1.224	5.636		5.028	9.778	6.617
2700		5.332	0.000	4.810		4.386	6.106	3.349
2940	0.048	4.551	0.768	8.757		4.438	9.901	4.590
3120	0.054	3.790	0.475	4.890		3.980	3.536	2.476
3180		3.525	0.431	4.489		3.503	3.702	2.162
3300	0.053	2.962	0.356	7.743		3.391	7.471	2.099
3420		2.747	0.293	3.642		3.026	7.078	1.685

PORT A21 **PORT A26**

time	Bromide	DMP	6M2H	Hex	Bromide	DMP	6M2H	Hex
(min)	(mg/l)	(mg/l)	(mg/l)	(mg/l)	(mg/l)	(mg/l)	(mg/l)	(mg/l)
180	0.056	0.000	3.046	0.000	n.a.	129.524	36.264	232.005
300	49.249	15.613	7.586	0.000	n.a.	133.264	44.660	212.206
360	184.868	59.847	21.646	83.456	n.a.	99.877	27.736	59.338
420	268.804	89.240	24.196	155.229	n.a.	62.175	28.553	12.418
540	295.613	117.524	37.384	188.923	n.a.	11.328	13.514	4.257
660	294.849	108.104	35.081	169.695	n.a.	18.567	14.046	9.034
840	291.300	116.100	43.219	187.711	n.a.	0.831	4.211	0.000
900	262.873	88.922	31.782	110.559	n.a.	0.000	5.893	0.000
1020	83.417	34.015	15.433	27.696	n.a.	0.000	5.763	0.000
1140	8.080	3.827	6.897	0.000	n.a.	0.000	5.765	0.000
1260	3.727	0.693	0.000	0.000	n.a.	0.000	3.197	0.000
1380	0.047	0.000	0.000	0.000	n.a.	0.000	1.917	0.000
1500		0.000	3.565	0.000	n.a.	0.000	5.799	0.000
1620		0.000	1.402	0.000	n.a.	0.000	6.430	0.000
1740		0.000	7.518	0.000	n.a.	0.000	2.942	0.000
1860		0.000	0.000	0.000	n.a.	1.101	5.452	0.000

PORT A31

time	Bromide	DMP	6M2H	Hex
900	n.a.	0.000	0.000	0.000
1020	n.a.	0.368	9.345	3.820
1140	n.a.	1.776	0.000	16.497
1260	n.a.	6.356	4.426	49.989
1380	n.a.	15.017	2.574	76.543
1500	n.a.	28.288	9.836	129.110
1620	n.a.	38.907	9.315	154.206
1740	n.a.	40.074	7.383	153.970
1860	n.a.	45.161	9.837	128.697
1980	n.a.	50.429	8.794	90.214
2100	n.a.	40.388	8.930	23.450
2220	n.a.	34.399	11.181	19.333
2340	n.a.	28.634	10.536	3.337
2460	n.a.	25.060	10.945	3.023
2580	n.a.	0.000	3.019	0.000
2700	n.a.	15.409	9.781	0.000

193

PORT B7

time (min)	Bromide (mg/l)	DMP (mg/l)	6M2H (mg/l)	Hex (mg/l)
180		0.000	4.794	0.000
300		0.000	0.000	0.000
360	2.203	0.000	8.121	0.000
420	6.154	1.368	0.000	0.000
540	58.157	22.942	7.519	19.055
660	96.058	38.987	11.066	14.111
780	114.142	58.346	19.315	75.522
900	122.475	53.185	24.568	91.759
1020	118.965	59.747	25.874	90.623
1140	84.564	42.270	12.549	27.239
1260	40.837	19.059	12.628	6.028
1380	11.893	4.300	7.411	0.000
1500		0.000	2.545	0.000
1620	2.212	0.000	0.000	0.000
1740		0.000	3.272	0.000
1860	2.157	0.000	0.000	0.000
1980	2.242	0.000	3.932	0.000
2100		0.000	0.000	0.000
2220		0.000	0.000	0.000
2340		0.000	3.222	0.000
2460		0.000	0.000	0.000
2580		0.000	4.017	0.000
2700		0.000	0.000	0.000
2840		0.000	7.769	0.000
2940		0.000	3.675	0.000
3060		0.000	3.238	0.000
3180		0.000	0.000	0.000
3300		0.000	7.941	0.000
3540		0.000	3.833	0.000

PORT B12

time (min)	Bromide (mg/l)	DMP (mg/l)	6M2H (mg/l)	Hex (mg/l)
180	2.157	0.000	0.000	0.000
300	2.702	0.000	1.981	0.000
360	49.843	19.293	9.866	7.755
420	127.703	53.838	13.688	65.499
540	166.751	84.042	26.644	105.807
660	178.480	81.132	25.644	101.063
780	175.751	95.833	34.101	132.226
900	169.808	100.583	40.976	123.929
1020	35.237	16.982	4.909	0.000
1140	11.398	2.716	6.642	0.000
1260	2.891	1.193	6.731	0.000
1380	4.032	0.639	2.086	0.000
1500	3.291	0.448	0.000	0.000
1620	2.723	0.000	3.568	0.000
1740	5.857	0.000	3.478	0.000
1860	2.223	0.000	0.000	0.000
1980	3.982	0.000	3.276	0.000
2100		0.000	2.875	0.000
2220		0.000	8.244	0.000
2340		0.000	3.015	0.000
2460		0.000	0.000	0.000
2580		0.000	0.000	0.000
2700		0.000	5.956	0.000
2840		0.000	5.704	0.000
2940		0.000	2.813	0.000
3060		0.000	4.581	0.000
3180		0.000	6.778	0.000
3300		0.000	0.000	0.000
3540		0.000	0.000	0.000

PORT B14

time (min)	Bromide (mg/l)	DMP (mg/l)	6M2H (mg/l)	Hex (mg/l)
180	2.098	0.000	5.305	0.000
300	2.246	3.341	0.000	0.000
360	19.846	16.020	8.422	16.152
420	99.557	36.509	10.637	71.059
540	167.527	51.714	11.537	96.331
660	177.641	61.552	17.410	142.917
780	165.126	67.564	20.729	155.190
900	186.715	52.882	14.169	89.994
1020	90.915	35.198	9.237	28.520
1140	9.095	24.139	8.564	0.000
1260	2.308	17.297	6.437	0.000
1380	2.249	11.963	4.506	0.000
1500		8.852	5.274	0.000
1620		6.354	4.547	0.000
1740	2.101	4.839	6.492	0.000
1860	9.085	3.373	5.070	0.000
1980	8.633	2.552	5.790	0.000
2100		1.996	7.466	0.000
2220	7.845	1.425	4.259	0.000
2340		1.061	4.791	0.000
2460		0.876	7.122	0.000
2580		0.648	5.175	0.000
2700		0.000	7.262	0.000
2840		0.000	5.555	0.000
2940		0.000	4.456	0.000
3060		0.000	3.976	0.000
3180		0.000	0.000	0.000

PORT B17

time (min)	Bromide (mg/l)	DMP (mg/l)	6M2H (mg/l)	Hex (mg/l)
180	3.328	0.000	7.416	0.000
300		0.000	0.000	0.000
360		0.000	2.793	0.000
420	2.106	0.000	4.078	0.000
540	20.441	1.649	2.732	0.000
660	85.390	12.281	9.466	9.549
780	152.287	27.191	12.857	63.870
900	185.901	35.096	9.452	89.802
1020	178.132	38.104	15.758	71.497
1140	172.960	44.442	12.752	75.638
1260	79.064	38.146	16.158	65.674
1380	24.023	21.969	10.408	15.464
1500	4.724	14.170	9.438	7.759
1620		10.747	5.612	2.423
1740	5.311	9.022	6.996	2.502
1860		7.710	6.155	2.233
1980	12.073	7.101	6.698	4.301
2100		5.602	6.249	0.000
2220	5.005	5.256	7.151	4.492
2340	6.441	5.286	8.226	0.000
2460	4.516	4.015	5.940	0.000
2580	2.869	4.019	7.319	0.000
2700		3.684	5.572	0.000
2840		3.032	3.946	0.000
2940		2.646	5.681	0.000
3060		2.822	6.391	0.000
3180		2.840	6.409	0.000

194

PORT B21

time	Bromide	DMP	6M2H	Hex
(min)	(mg/l)	(mg/l)	(mg/l)	(mg/l)
180		0.000	5.933	0.000
300		0.000	3.497	0.000
360	7.548	0.000	0.000	0.000
420	2.119	0.000	0.000	0.000
540	128.465	8.943	4.799	8.949
660	200.518	16.134	8.643	48.493
780	226.310	28.446	8.274	81.082
900	244.344	36.413	8.126	109.835
1020	236.258	41.011	6.492	144.402
1140		42.876	8.158	120.282
1260		39.110	7.491	87.412
1380		34.816	6.745	28.047
1500		29.383	7.134	17.232
1620		24.566	11.756	0.000
1740		20.982	8.998	9.466
1860		16.316	3.886	6.364
1980		12.944	6.693	1.374
2100		4.894	7.024	0.000
2220		9.801	8.396	3.227
2340		8.873	6.359	1.481
2460		6.971	4.867	0.000
2580		5.907	8.552	0.000
2700		5.430	5.839	0.000
2840		4.998	11.155	0.000
2940		4.318	3.842	0.000
3060		3.451	5.832	0.000
3180		2.915	4.343	0.000
3300		2.439	9.428	0.000
3540		2.043	8.397	0.000

PORT B26 / **PORT B31**

time	B26 Bromide	B26 DMP	B26 6M2H	B26 Hex	B31 Bromide	B31 DMP	B31 6M2H	B31 Hex
900	176.971	94.802	22.297	96.836	7.657	1.187	8.908	1.719
1020	180.737	96.492	19.541	28.983	14.956	3.260	4.443	4.715
1140	194.207	110.307	33.863	143.889	30.487	4.454	3.938	7.032
1260	176.895	107.060	35.147	127.666	56.064	6.061	5.266	14.271
1380	86.969	61.879	23.572	58.686	84.071	9.606	8.625	20.989
1500	27.054	14.284	4.828	3.905	135.643	13.500	4.118	46.442
1620	11.401	4.103	3.673	0.000	145.069	19.287	5.997	59.470
1740	5.100	1.557	7.148	0.000	157.673	30.002	9.036	113.967
1860	2.226	0.948	0.000	0.000	147.025	34.566	6.769	118.143
1980	2.736	0.535	3.238	1.168	132.299	37.490	4.423	66.219
2100	2.691	0.000	0.000	0.000	90.610	44.154	8.416	110.279
2220	2.340	0.000	4.239	0.000	44.440	45.489	9.586	79.612
2340	2.646	0.000	1.336	0.000	28.046	41.471	7.960	53.632
2460		0.000	6.618	0.000	17.467	34.263	17.744	30.459
2580		0.000	3.271	0.000	6.900	27.119	11.707	0.000
2700		0.000	1.837	0.000	4.844	19.380	8.863	0.000
2840	2.339	0.000	4.613	0.000	3.192	14.387	13.248	0.000
2940	3.481	0.000	0.000	0.000	4.914	11.229	12.830	0.000
3060	2.105	0.000	5.860	0.000	2.108	8.814	12.245	0.000
3180	5.208	0.000	0.000	0.000	2.301	7.458	8.324	0.000

PORT C7 / **PORT C12**

time (min)	Bromide (mg/l)	DMP (mg/l)	6M2H (mg/l)	Hex (mg/l)	Bromide (mg/l)	DMP (mg/l)	6M2H (mg/l)	Hex (mg/l)
360		0.000	0.000	0.000	2.214	0.000	0.000	0.000
420	2.114	0.000	0.000	0.000	6.270	1.358	8.447	0.000
540		0.000	15.514	0.000	125.014	48.014	13.741	43.285
660	2.299	0.000	8.941	0.000	161.680	62.305	18.151	62.793
780	4.946	0.742	4.234	0.000	102.378	48.555	18.417	55.193
900	30.670	9.295	14.021	0.000	175.025	75.912	28.031	68.708
1020	74.231	27.362	14.294	0.000	179.262	79.742	31.220	52.498
1140	118.544	50.081	0.000	0.000	58.592	23.178	8.823	0.000
1260	132.836	50.674	19.807	45.446	23.484	9.374	7.042	0.000
1380	134.596	56.614	17.298	10.452	18.117	4.767	0.000	0.000
1500	129.412	48.566	14.616	0.594	13.288	3.833	7.651	0.000
1620	66.713	31.974	16.996	20.884	11.071	2.810	0.000	0.000
1740	24.616	10.046	16.478	2.867	7.081	1.482	0.000	0.000
1860	7.633	2.083	4.532	0.000	3.831	0.000	16.289	0.000
1980	2.355	0.000	11.025	0.000	2.420	0.000	5.826	0.000
2100	2.300	0.000	0.000	0.000	2.350	0.000	7.769	0.000
2220	2.146	0.000	0.000	0.000		0.000	0.000	0.000
2340	2.139	0.000	5.820	0.000	2.435	0.000	6.234	0.000
2460	2.102	0.000	15.964	0.000	2.178	0.000	0.000	0.000
2580	4.313	0.000	11.763	0.000	2.166	0.000	4.642	0.000
2700	n.a.	0.000	0.000	0.000	2.155	0.000	12.192	0.000
2840	2.154	0.000	0.000	0.000		0.000	0.000	0.000
2940	2.103	0.000	0.000	0.000		0.000	9.689	0.000
3060	2.148	0.000	8.368	0.000	2.136	0.000	3.749	0.000

PORT C26 / **PORT C31**

time (min)	Bromide (mg/l)	DMP (mg/l)	6M2H (mg/l)	Hex (mg/l)	Bromide (mg/l)	DMP (mg/l)	6M2H (mg/l)	Hex (mg/l)
900	16.263				198.382			
1020	95.148				233.836			
1140		1.500	0.000	0.000		0.498	0.000	0.000
1260	209.363	23.301	9.871	5.412	189.273	76.897	21.887	65.339
1380	218.185	29.555	7.894	69.053	111.807	60.942	16.616	8.617
1500	218.887	25.902	8.735	129.122	56.624	46.447	15.815	2.017
1620	174.135	32.891	6.934	110.839	29.264	31.087	13.595	3.787
1740	100.516	33.625	9.285	100.315	15.857	19.964	5.763	5.529
1860	50.445	33.768	8.515	83.476	8.513	13.197	4.787	0.000
1980	24.613	31.728	14.158	45.346	15.136	10.812	8.938	0.000
2100	13.546	25.080	4.471	10.702	5.574	5.393	5.855	0.280
2220	32.921	30.191	9.479	41.714	3.908	3.568	3.405	0.000
2340	4.446	21.720	8.835	0.000	3.374	5.287	6.325	0.000
2460	3.436	14.636	7.966	0.000	3.155	2.264	2.878	0.000
2580	3.055	11.919	5.894	0.000	5.079	0.000	2.671	0.000
2700	4.669	9.580	6.410	0.000	3.043	2.211	5.021	0.000
2840	4.493	1.685	4.904	0.000	2.941	2.248	2.222	0.000
2940	2.890	10.128	11.912	0.000	2.912	2.454	0.000	0.000
3060		8.992	11.544	2.347	2.922	1.964	8.164	0.000
3180		8.680	11.189	0.000	2.906	1.056	0.000	0.000
3300		7.592	15.259	0.000	3.073	0.816	11.181	0.000
3420		6.187	7.041	0.000		0.000	0.000	0.000
3540		5.444	14.216	0.000	2.878	0.378	10.874	0.000
3660		5.672	16.166	0.000	2.937	0.193	7.451	0.000
3780		3.719	8.515	0.000		1.073	9.620	0.000
4020		3.948	8.870	0.000		0.000	7.146	0.000
4140		3.342	11.326	0.000		0.000	0.000	0.000
4260		0.587	13.511	0.000		0.000	9.638	0.000
4380		2.910	0.000	0.000		0.000	10.110	0.000
4500		1.380	0.000	0.000		0.251	8.695	0.000
4860		2.162	0.000	0.000		0.000	5.890	0.000

196

time (min)	Bromide (mg/l)	DMP (mg/l)	6M2H (mg/l)	Hex (mg/l)	Bromide (mg/l)	DMP (mg/l)	6M2H (mg/l)	Hex (mg/l)
360	5.620	0.000	7.274	0.000		0.000	6.205	0.000
420		0.000	4.097	0.000		0.000	0.000	0.000
540	3.014	0.000	0.000	0.000	4.697	0.538	0.000	0.000
660	5.397	0.000	3.827	0.000	22.787	1.066	4.697	0.000
780	3.312	0.000	7.483	0.000	86.327	10.508	7.562	27.778
900	3.763	0.000	0.000	0.000	128.934	18.180	0.000	17.383
1020	5.080	0.000	1.784	0.000	145.957	27.355	10.961	82.065
1140	7.370	0.000	9.063	0.000	138.826	35.888	9.796	17.712
1260	57.071	7.652	2.351	10.096	136.499	36.205	0.000	17.635
1380	133.245	31.658	7.143	11.432	80.391	37.151	5.922	74.167
1500	166.035	45.952	9.898	12.950	22.004	28.508	0.000	4.697
1620	189.782	49.444	17.071	53.253	4.613	24.124	8.880	10.509
1740	184.677	55.528	17.618	41.020	3.116	18.010	7.719	4.311
1860	164.405	56.612	23.865	8.777	3.106	12.316	4.158	0.000
1980	73.208	37.753	17.574	32.459	2.960	9.797	6.520	0.000
2100	30.419	20.896	9.136	1.795		6.883	6.304	0.000
2220	8.207	6.160	7.464	0.000	5.634	7.047	4.045	0.000
2340	4.219	7.416	0.000	0.000	2.877	5.200	0.000	0.000
2460	3.191	4.357	6.262	0.000	3.854	4.632	5.711	0.000
2580		6.223	6.434	0.000	4.354	4.009	10.488	0.000
2700	2.993	4.697	8.147	0.000	7.147	3.307	0.000	0.000
2840	3.086	4.041	4.962	0.000	2.910	3.500	9.806	0.000
2940		4.033	5.875	0.000	6.146	2.971	3.854	0.000
3060	2.867	2.740	7.066	0.000	2.952	2.471	9.905	0.000
3180		2.685	0.000	0.000				
3300		1.986	0.000	0.000				
3420		2.591	17.646	0.000				
3540		1.975	0.000	0.000				
3660		3.651	19.844	0.000				
3780		2.100	0.000	0.000				
4020		1.495	15.430	0.000				
4140		1.312	16.607	0.000				
4260		1.076	4.946	0.000				
4380		1.322	12.892	0.000				
4500		1.188	13.086	0.000				
4620		1.315	0.000	0.000				

PORT D7 **PORT D12**

time	DMP	6M2H	Hex	Bromide	DMP	6M2H	Hex
(min)	(mg/l)	(mg/l)	(mg/l)	(mg/l)	(mg/l)	(mg/l)	(mg/l)
360	0.000	5.830	0.000	n.a.	0.000	5.948	0.000
480	0.000	7.253	0.000	n.a.	0.000	8.474	0.000
600	0.000	7.875	0.000	39.054	20.659	8.171	0.000
720	7.841	10.260	0.000	95.990	38.405	4.093	0.000
840	17.312	9.622	0.000	115.771	55.313	0.000	0.000
960	22.388	7.682	0.000	134.911	62.643	14.021	3.025
1080	27.299	0.000	0.000	107.519	71.463	18.509	7.659
1200	30.430	15.330	32.640	44.399	59.037	20.435	6.788
1320	22.930	11.509	3.342	18.351	22.161	5.050	0.000
1440	17.665	5.156	0.000	10.439	15.029	5.858	0.000
1560	15.205	9.893	4.558	22.681	10.624	7.160	0.000
1680	14.284	9.130	0.000	2.971	8.954	5.564	0.000
1800	13.394	8.055	0.000	54.745	6.665	4.298	0.000
1920	11.704	9.087	3.905	52.550	2.682	4.110	0.000
2040	6.292	11.765	0.000	44.954	0.314	3.614	0.000
2160	5.332	0.000	0.000	0.412	0.000	7.073	0.000
2280	3.127	6.658	0.000	47.351	0.000	6.446	0.000
2400	1.398	8.607	0.000		0.000	5.138	0.000
2520	0.369	6.357	0.000		0.000	0.000	0.000
2640	0.000	9.977	0.000		0.000	4.957	0.000
2745	0.000	5.728	0.000		0.000	5.083	0.000
2880	0.000	0.000	0.000		0.000	5.559	0.000
3000	0.000	9.385	0.000		0.000	0.000	0.000
3120	0.000	0.000	0.000		0.000	6.785	0.000
3240	0.000	6.744	0.000		0.000	7.036	0.000
3300	0.000	9.572	0.000		0.000	4.060	0.000
3420	0.000	9.009	0.000		0.000	0.000	0.000
3540	0.000	6.199	0.000		0.000	3.605	0.000
3660	0.000	0.000	0.000		0.000	4.078	0.000
3780	0.000	0.000	0.000		0.000	6.653	0.000
3900	0.000	7.508	0.000		0.000	5.438	0.000
4020	0.000	3.787	0.000		0.000	5.423	0.000
4140	0.000	7.744	0.000		0.000	7.127	0.000

	PORT D17				PORT D21		
time	Bromide	DMP	6M2H	Hex	DMP	6M2H	Hex
(min)	(mg/l)	(mg/l)	(mg/l)	(mg/l)	(mg/l)	(mg/l)	(mg/l)
360		0.000	6.258	0.000	0.000	4.539	0.000
480		0.000	7.157	0.000	0.000	6.496	0.000
600		0.000	3.956	0.000	0.000	5.453	0.357
720		0.000	5.872	0.000	0.000	5.206	0.000
840		0.000	0.000	0.000	0.000	2.315	0.000
960	12.096	0.325	6.467	0.000	0.000	2.520	0.000
1080	15.452	2.219	5.392	0.000	0.000	2.462	0.000
1200	67.404	9.024	6.625	6.557	0.000	0.000	0.000
1320	108.014	15.785	6.976	8.384	16.938	2.642	0.000
1440	154.828	2.596	8.617	0.000	34.217	7.447	8.583
1560	133.244	28.761	4.779	15.491	38.455	9.394	0.000
1680	117.829	32.121	7.451	24.848	47.455	11.799	40.143
1800	92.989	32.506	9.502	25.243	48.709	7.833	20.909
1920	34.959	28.522	8.316	17.395	38.907	11.878	26.272
2040	21.571	22.572	7.433	0.000	29.482	5.185	0.000
2160	56.376	17.968	8.603	1.313	23.692	5.186	0.000
2280	38.744	13.375	5.428	0.000	21.953	5.238	0.000
2400	32.093	8.711	5.466	0.000	17.460	2.712	0.000
2520		9.736	5.514	0.000	16.600	5.087	0.000
2640		8.108	3.095	0.000	13.515	4.229	0.000
2745		6.315	5.419	0.000	7.551	6.305	0.000
2880		4.765	4.199	0.000	7.826	6.126	0.000
3000		4.239	6.052	0.000	5.689	6.207	0.000
3120		3.324	0.000	0.000	4.934	4.334	0.000
3240		3.677	3.117	0.000	4.506	3.956	0.000
3300		3.591	5.603	0.000	2.735	4.050	0.000
3420		2.111	5.634	0.000	2.704	4.740	0.000
3540		2.115	5.037	0.000	0.000	0.000	0.000
3660		1.901	4.091	0.000	1.960	3.962	0.000
3780		2.280	6.646	0.000	2.276	4.837	0.000
3900		1.494	4.703	0.000	1.836	2.158	0.000
4020		1.802	3.967	0.000	1.605	5.861	0.000
4140		1.925	5.649	0.000	1.469	4.372	0.000

PORT D28

time	DMP	6M2H	Hex
(min)	(mg/l)	(mg/l)	(mg/l)
360	0.000	4.764	0.000
480	0.000	3.127	0.000
600	0.000	3.966	0.000
720	0.000	1.666	0.000
840	0.000	2.475	0.000
960	1.904	3.337	0.000
1080	12.104	3.405	0.000
1200	32.674	5.336	12.637
1320	0.000	0.000	0.000
1440	56.052	9.230	54.654
1560	61.156	9.663	35.737
1680	55.466	5.997	55.558
1800	41.991	8.337	16.364
1920	32.194	10.066	0.000
2040	26.117	5.067	8.573
2160	22.213	3.447	0.000
2280	19.372	3.918	0.000
2400	8.744	3.935	0.000
2520	19.178	4.561	0.000
2640	16.605	6.020	10.417
2745	10.706	5.086	0.000
2880	0.000	3.114	0.000
3000	7.320	3.898	0.000
3120	3.986	3.638	0.000
3240	3.661	2.807	0.000
3300	2.049	5.811	0.000
3420	0.580	0.000	0.000
3540	0.000	2.869	0.000
3660	1.617	5.515	0.000
3780	0.807	4.395	0.000
3900	0.795	3.626	0.000
4020	0.331	5.206	0.000
4140	0.473	5.146	0.000

200

PORT E7				PORT E12		
time	DMP	6M2H	Hex	Bromide	DMP	6M2H
(min)	(mg/l)	(mg/l)	(mg/l)	(mg/l)	(mg/l)	(mg/l)
480	0.255	17.928	0.000	3.657	0.000	12.972
600	4.502	17.691	0.000		0.000	0.000
720	10.745	15.214	0.000	4.951	1.429	10.900
840	21.898	14.582	0.000	49.377	32.758	8.897
960	25.478	11.197	0.000	87.018	41.696	12.647
1080	0.000	0.000	0.000	105.689	53.855	12.798
1200	27.199	15.358	0.862	109.013	58.838	14.949
1320	21.124	13.549	7.235	119.100	55.535	8.072
1440	14.432	11.003	5.007	82.482	41.884	12.449
1560	11.021	0.000	0.000	60.152	22.087	0.000
1680	9.295	9.684	0.000	9.478	14.477	5.805
1800	9.469	12.306	1.151	5.956	12.317	7.637
1920	7.054	0.000	0.000	25.870	12.881	0.000
2040	3.407	7.414	0.000	18.908	6.648	7.454
2160	2.457	0.000	0.000	70.934	2.307	6.976
2280	1.520	12.637	0.000	2.334	0.651	0.000
2400	0.511	0.000	0.000	8.970	0.000	0.000
2520	0.000	0.000	0.000	57.954	0.000	4.319
2640	0.000	0.000	0.000		0.000	6.118
2745	0.000	0.000	0.000		0.000	5.096
2880	0.000	9.375	0.000		0.000	0.000
3000	0.000	0.000	0.000		0.000	7.756
3120	0.000	9.500	0.000		0.000	0.000
3240	0.000	0.000	0.000		0.000	8.785
3360	0.000	0.000	0.000		0.000	0.000
3420	0.000	8.499	0.000		0.000	5.768
3600	0.000	5.742	0.000		0.000	6.976
3720	0.000	0.000	0.000		0.000	8.606
3960	0.000	9.016	0.000		0.000	7.600
4080	0.000	4.851	0.000		0.000	6.006
4200	0.000	0.000	0.000		0.000	0.000

PORT E17 **PORT E21**

time	Bromide	DMP	6M2H	Hex	Bromide	DMP	6M2H	Hex
(min)	(mg/l)	(mg/l)	(mg/l)	(mg/l)	(mg/l)	(mg/l)	(mg/l)	(mg/l)
480		0.000	13.833	0.000		0.000	5.672	0.000
600		0.000	0.000	0.000		0.000	3.926	0.000
720		0.000	0.000	0.000		0.000	6.486	0.000
840	1.015	0.637	9.962	0.000		0.000	0.000	0.000
960	83.739	1.713	0.000	0.000		0.000	5.450	0.000
1080	98.717	0.000	0.000	0.000		0.000	0.000	0.000
1200	31.622	5.776	14.456	0.000		0.000	5.151	0.000
1320	18.763	9.151	9.148	0.000	6.471	0.372	0.000	0.000
1440	53.296	13.760	11.032	9.959	67.647	10.600	4.015	0.000
1560	93.801	15.905	7.078	3.453	127.353	32.943	7.698	0.000
1680	109.965	21.484	4.251	0.000	188.704	58.067	13.829	0.000
1800	92.793	25.902	5.585	31.856	196.992	71.791	16.374	0.639
1920	77.583	30.370	7.625	36.525	176.857	79.093	21.267	3.701
2040	76.378	32.748	8.019	34.771	102.604	76.730	19.236	3.503
2160	37.204	27.204	10.539	0.000	40.657	54.563	13.075	2.385
2280	20.960	27.789	8.223	16.321	80.916	32.950	10.783	1.363
2400	5.920	21.814	10.124	15.461	9.193	15.456	5.899	0.000
2520	115.114	17.573	7.971	0.000	46.996	9.610	5.499	0.000
2640	80.997	12.702	5.848	3.843	45.632	4.205	3.883	0.000
2745	5.377	9.624	0.000	0.000	48.003	2.360	4.414	0.000
2880	70.875	8.807	7.105	0.000	0.279	2.078	3.030	0.000
3000	50.948	6.633	4.331	0.000	66.978	0.703	3.235	0.000
3120	75.035	6.033	5.103	0.000	0.501	0.435	6.296	0.000
3240	0.805	4.597	8.907	0.000		0.157	4.074	0.000
3360	79.472	4.945	7.712	0.000		0.348	4.247	0.000
3420	82.130	3.224	5.925	0.000		0.206	0.000	0.000
3600	0.300	4.072	7.398	0.000		0.203	5.880	0.000
3720		3.713	5.272	0.000		0.000	4.262	0.000
3960		0.000	0.000	0.000		0.000	3.324	0.000
4080		1.791	7.241	0.000		0.000	3.714	0.000
4200		1.592	6.404	0.000		0.000	5.481	0.000
4320		1.885	5.719	0.000		0.000	4.512	0.000
4440		1.934	6.836	0.000		0.000	4.570	0.000
4560		1.665	6.500	0.000		0.000	3.094	0.000
4740		1.480	8.442	0.000		0.000	3.187	0.000
4680		1.435	4.783	0.000		0.000	4.405	0.000
4740		0.000	0.000	0.000		0.000	4.451	0.000

PORT E28

time	Bromide	DMP	6M2H	Hex
(min)	(mg/l)	(mg/l)	(mg/l)	(mg/l)
480		0.000	2.822	0.000
600		0.000	3.183	0.000
720	3.760	0.000	4.246	0.000
840	2.491	0.000	3.242	0.000
960	5.662	0.000	4.926	0.000
1080	17.598	0.000	2.612	0.000
1200	45.902	5.950	5.631	0.000
1320	88.211	19.647	5.553	0.000
1440	125.222	35.095	4.213	0.000
1560	139.598	41.937	6.443	21.255
1680	129.106	49.433	10.124	25.266
1800		50.730	12.611	10.538
1920	113.684	40.026	11.325	0.982
2040	120.523	2.015	5.117	0.000
2160	81.238	23.438	10.788	0.000
2280	59.889	30.723	11.314	1.426
2400	48.737	14.104	0.000	0.000
2520	32.773	21.971	4.583	0.000
2640	20.975	21.340	4.813	0.000
2745	14.108	16.829	6.712	0.000
2880	5.854	15.902	7.700	0.000
3000	2.752	3.162	5.066	0.000
3120	4.322	3.107	0.000	0.000
3240	6.975	4.801	12.058	0.000
3360	2.545	5.279	0.000	0.000
3420	5.954	2.967	6.636	0.000
3600	1.781	0.902	0.000	0.000
3720	6.301	0.628	6.010	0.000
3960	1.714	0.000	0.000	0.000
4080	5.033	0.441	7.173	0.000
4200		0.000	7.247	0.000
4320		1.034	8.128	0.000
4440		0.000	8.730	0.000
4560		0.000	3.304	0.000
4740		0.000	5.578	0.000
4680		0.000	0.000	0.000

PORT F7 **PORT F12**

time	Bromide	DMP	6M2H	Bromide	DMP	6M2H
(min)	(mg/l)	(mg/l)	(mg/l)	(mg/l)	(mg/l)	(mg/l)
480	5.245			8.934	0.000	12.972
600	24.114			11.764	0.000	0.000
720	41.404			n.a.	1.429	10.900
840	59.361			8.101	32.758	8.897
960	66.467	0.000	5.773	7.581	41.696	12.647
1080	64.811	26.795	0.000	8.258	53.855	12.798
1200	60.573	20.627	9.745	2.519	58.838	14.949
1320	37.853	13.512	7.403	4.929	55.535	8.072
1440	21.716	6.668	0.000		41.884	12.449
1560	13.553	5.885	0.000	41.395	22.087	0.000
1680	11.131	5.535	3.581	131.384	14.477	5.805
1800	5.968	2.853	6.213	142.662	12.317	7.637
1920	5.441	2.995	4.305	118.008	12.881	0.000
2040	2.601	1.153	8.051	86.170	6.648	7.454
2160	3.120	0.367	5.994	34.879	2.307	6.976
2280		0.274	6.769	8.271	0.651	0.000
2400		0.000	4.650	9.260	0.000	0.000
2640		0.000	6.229		0.000	4.319
2880		0.000	0.000		0.000	6.118
3000		0.000	0.000		0.000	5.096
3120		0.000	4.386		0.000	0.000
3240		0.000	4.104		0.000	7.756
3360		0.000	0.000		0.000	0.000
3480		0.000	0.000		0.000	8.785
3600		0.000	4.181		0.000	0.000
3720		0.000	3.752		0.000	5.768
3960		0.000	3.421		0.000	6.976
4080		0.000	6.556		0.000	8.606
4200		0.000	5.544		0.000	7.600

PORT F17   **PORT F21**

time	Bromide	DMP	6M2H	time	DMP	6M2H
(min)	(mg/l)	(mg/l)	(mg/l)	(min)	(mg/l)	(mg/l)
480		0.000	8.037	480	0.000	4.940
600		0.000	6.511	600	0.000	3.762
720	7.284	0.000	6.474	720	0.000	3.173
840	4.965	0.000	6.774	840	0.000	5.277
960	3.889	0.384	0.000	960	0.000	5.550
1080	6.939	1.130	3.641	1080	0.000	3.620
1200	25.852	1.330	0.000	1200	4.177	0.000
1320	32.248	6.540	6.392	1320	0.000	5.705
1440	41.994	7.260	8.087	1440	0.504	4.824
1560	68.783	11.568	9.049	1560	7.024	4.941
1680	55.777	14.736	6.049	1680	17.815	0.000
1800	84.240	20.397	7.785	1800	40.490	5.747
1920	101.134	8.394	5.107	1920	39.176	4.396
2040	101.026	24.828	7.756	2040	37.882	3.967
2160	95.904	26.153	8.660	2160	30.713	5.765
2280	59.115	22.223	6.634	2280	21.186	3.641
2520	56.716	28.945	10.766	2520	20.103	3.932
2640	39.602	24.339	6.960	2640	19.987	3.807
2760	27.663	20.320	7.372	2760	16.386	0.000
2880	20.841	15.160	5.005	2880	7.202	3.921
3000	14.586	12.871	6.694	3000	14.154	2.998
3120	12.058	11.055	4.533	3120	12.366	2.441
3240	9.503	9.430	7.119	3240	10.311	2.860
3360	7.374	8.483	3.694	3360	9.037	2.772
3480	3.142	1.621	0.000	3480	7.533	3.062
3600	1.613	5.910	0.000	3600	6.069	4.256
3720	2.768	4.007	8.532	3720	5.710	5.077
3960	5.041	3.189	7.098	3960	3.819	3.122
4080	6.494	3.372	5.041	4080	3.569	2.478
4200	8.872	2.137	6.035	4200	0.000	0.000
4320		2.436	3.542	4320		
4440		2.210	3.365	4440		
4560		2.502	3.978	4560		
4740		1.631	3.497	4740		
4860		1.805	2.875	4860		

A.2.2 PITT 2

Co	600.020	423.265		
PORT A7			**PORT A14**	

time	Bromide	DMP	Bromide	DMP
(min)	(mg/l)	(mg/l)	(mg/l)	(mg/l)
180	n.a.	0.000	0.000	0.000
360	2.828	0.000	50.256	24.445
480	134.901	108.117	111.444	78.026
600	156.303	95.623	128.006	88.017
720	165.444	112.489	130.788	91.948
840	173.130	127.939	112.465	86.444
960	70.062	46.004	4.736	21.557
1080	19.678	5.450	0.635	1.184
1200	2.393	1.013	0.105	0.000
1320	0.697	0.000	n.a.	0.000
1440	0.544	0.000	n.a.	0.000
1560	0.191	0.000	n.a.	0.000
1680	0.191	0.000		0.000
1800		0.000		0.000
1920		0.000		0.000
2040		0.000		0.000
PORT A17			**PORT A21**	
180	0.000	0.000	4.317	0.000
360	10.760	0.000	n.a.	0.000
480	150.058	46.427	64.476	28.390
600	193.284	80.678	110.261	53.323
720	208.407	104.294	147.422	72.483
840	189.119	113.395	155.763	80.754
960	60.560	124.019	158.899	86.434
1080	6.725	52.104	64.843	43.014
1200	0.328	12.380	15.673	17.740
1320	0.074	5.247	3.345	0.701
1440		1.754	3.354	3.143
1560		1.321	4.524	0.000
1680		0.771	6.269	0.000
1800		0.398	0.051	0.000
1920		0.204	5.420	0.000
2040		0.000	7.835	0.000
2160		0.000	n.a.	0.000
2280		0.000	n.a.	0.000
2400		0.000	6.012	0.000
2520		0.000	n.a.	0.000
2760		0.000	8.293	0.000
3000		0.000	7.663	0.000
3180		0.000	8.476	0.000
3360		0.000	6.271	0.000
3900		0.000	n.a.	0.000

206

	PORT A26		PORT A31	
time	Bromide	DMP	Bromide	DMP
(min)	(mg/l)	(mg/l)	(mg/l)	(mg/l)
180	7.116	0.000		0.000
360	n.a.	0.000		0.000
480	n.a.	0.000		0.000
600	0.753	0.000		0.000
720	60.162	25.032		0.000
840	123.294	63.137	3.404	0.000
960	157.300	68.097	0.537	0.000
1080	174.679	89.537	0.591	0.000
1200	126.038	83.287	17.089	0.000
1320	80.682	0.000	84.506	0.730
1440	19.412	0.463	141.086	3.845
1560	6.493	2.630	167.640	13.259
1680	3.060	0.285	172.180	17.887
1800	1.488	0.341	125.886	27.513
1920	0.427	0.000	49.353	34.386
2040	7.255	0.000	7.284	8.102
2160	0.769	0.000	5.339	33.094
2280	8.262	0.000	0.706	11.708
2400	6.659	0.000	1.317	26.143
2520	6.314	0.000	6.910	7.881
2760	5.984	0.000	9.311	0.227
3000	0.752	0.000	6.070	5.596
3180	7.116	0.000	8.540	6.709
3360	5.860	0.000	n.a.	1.145
3900	0.682	0.000	7.569	0.787

PORT A35		
180		0.000
360		0.000
480	43.937	0.491
600	163.505	17.585
720	226.395	45.349
840	245.322	39.900
1080	148.844	96.151
1200	29.821	62.775
1320	1.576	15.954
1440	5.445	0.413
1560	0.648	6.139
1680	0.937	1.851
1800	3.173	1.719
1920	0.086	0.000
2040	1.462	0.000
2160	5.245	0.000
2280		0.000
2400		0.000
2520		0.000
2760		0.000
3000		0.000
3180		0.000
3360		0.000
3900		0.000

PORT B12			PORT B14	
time	Bromide	DMP	Bromide	DMP
(min)	(mg/l)	(mg/l)	(mg/l)	(mg/l)
180	4.648	0.000	4.651	0.000
360	n.a.	0.000	n.a.	0.000
480	25.001	15.231	12.113	0.507
600	94.582	53.864	95.479	28.742
720	132.598	75.513	143.309	62.403
840	142.900	69.384	142.076	87.375
960	143.777	81.267	144.964	92.257
1080	44.502	13.724	62.835	85.952
1200	1.861	0.308	10.952	37.436
1320	0.232	0.000	1.207	9.222
1440	n.a.	0.000	0.262	3.609
1560	10.359	0.000	6.008	0.000
1680	5.353	0.000	6.873	0.000
1800	n.a.	0.000	n.a.	0.310
1920	4.977	0.000	7.416	0.000
2040	8.299	0.000	5.762	0.000
2160	n.a.	0.000	8.112	0.000
2280	n.a.	0.000	7.736	0.000
2400		0.000	n.a.	0.000
2520		0.000		
2640		0.000		
2760		0.000		
3000		0.000		
3180		0.000		
3360		0.000		
3540		0.000		
3900		0.000		

208

PORT B17			PORT B21	
time	Bromide	DMP	Bromide	DMP
(min)	(mg/l)	(mg/l)	(mg/l)	(mg/l)
180	6.927	0.000	6.572	0.000
360	4.097	0.000	n.a.	0.000
480	n.a.	0.000	4.747	0.000
600	0.040	0.000	0.143	0.000
720	4.152	0.000	24.717	0.000
840	6.517	0.893	114.107	1.891
960	30.484	3.960	142.165	4.457
1080	99.119	27.520	149.659	11.143
1200	167.374	76.515	128.135	24.218
1320	170.386	93.276	35.439	19.156
1440	146.829	94.885	6.812	33.024
1560	69.313	96.183	8.888	31.276
1680	14.575	57.537	5.096	30.390
1800	0.181	22.834	1.321	24.691
1920	6.962	5.680	4.305	20.770
2040	3.631	6.622		5.304
2160	6.029	2.188		8.103
2280	0.490	0.563	4.201	6.525
2400	7.141	0.750	3.588	5.495
2520	n.a.	0.209	9.644	4.753
2640	8.206	0.000		7.225
2760	6.612	0.000		7.239
3000	7.122	0.000		5.800
3180	n.a.	0.000		4.071
3360	n.a.	0.000		1.170
3540	7.609	0.000		2.352
3900	8.359	0.000		1.387

209

PORT B26			PORT B31	
time	Bromide	DMP	Bromide	DMP
(min)	(mg/l)	(mg/l)	(mg/l)	(mg/l)
180	7.785	0.000	4.578	0.000
360	n.a.	0.000	4.714	0.000
480	4.341	0.000	3.896	0.000
600	n.a.	0.000	n.a.	0.000
720	n.a.	0.000	0.166	0.000
840	0.268	0.000	1.315	0.000
960	5.381	0.000	0.872	0.000
1080	39.527	5.455	5.095	0.000
1200	92.556	33.885	4.050	1.953
1320	123.794	54.337	11.967	5.134
1440	138.353	65.633	19.643	7.792
1560	94.314	67.639	43.477	13.811
1680	36.148	36.163	62.575	16.399
1800	13.808	25.726	86.834	16.746
1920	9.668	0.000	102.647	22.432
2040	0.065	0.000	96.763	26.706
2160	0.947	0.000	80.425	28.514
2280	2.989	0.000	51.792	41.425
2400		0.000	35.470	36.621
2520		0.000	19.724	38.970
2640		0.000	7.460	10.730
2760		0.000	2.451	21.073
3000		0.000	1.703	13.036
3180		0.000	6.118	4.726
3360		0.000	0.234	0.000
3540		0.000	10.473	2.570
3900		0.000	n.a.	2.111

PORT C12			PORT C17	
time	Bromide	DMP	Bromide	DMP
(min)	(mg/l)	(mg/l)	(mg/l)	(mg/l)
300	2.069	0.000	n.a.	0.000
420	6.158	0.000	5.141	0.000
480	5.810	0.000	n.a.	0.000
600	5.791	1.704	n.a.	0.000
720	61.286	22.544	4.137	0.000
840	104.498	64.761	3.695	0.000
960	119.274	72.747	44.934	9.434
1080	116.817	78.309	104.890	43.686
1200	71.682	52.799	144.267	77.445
1320	14.828	7.878	146.138	88.664
1440	2.443	0.804	109.249	91.380
1560	7.899	0.000	29.921	53.392
1680	9.866	0.000	13.870	17.161
1800	10.017	0.000	1.412	0.252
1920	0.071	0.000	10.720	0.000
2040	4.328	0.000	5.813	0.000
2160	n.a.	0.000	7.672	0.000
2280	n.a.	0.000	4.129	0.000
2400	n.a.	0.000		0.000

PORT C21			PORT C26	
time	Bromide	DMP	Bromide	DMP
(min)	(mg/l)	(mg/l)	(mg/l)	(mg/l)
300	3.185	0.000	3.671	0.000
420	4.766	0.000	0.063	0.000
480	6.187	0.000	6.173	0.000
600	4.300	0.000	n.a.	0.000
720	0.169	0.000	4.438	0.000
840	n.a.	0.000	0.190	0.000
960	4.455	0.000	4.057	0.000
1080	0.056	0.000	0.386	0.000
1200	4.876	0.000	2.888	0.000
1320	4.488	0.000	0.116	0.000
1440	0.175	0.000	29.191	0.000
1560	6.406	0.000	85.206	0.514
1680	7.913	0.000	128.776	12.606
1800	3.138	0.000	121.241	19.333
1920	48.131	5.494	69.479	30.406
2040	110.040	24.796	28.400	24.413
2160	156.036	57.019	12.586	22.105
2280	162.263	74.337	3.249	13.221
2400	145.249	91.462	17.568	38.464
2460	72.572	85.606	0.504	12.420
2640	16.313	59.397	1.578	31.789
2760	13.018	26.508	0.332	4.761
2880	8.700	12.920	5.229	11.893
3000	0.117	4.925	2.596	7.398
3180	4.530	1.653	4.204	1.076
3360	1.583	0.329	n.a.	1.363
3540	0.543	0.157	1.364	2.757
3660	0.115	0.000	0.308	0.395
3780	6.896	0.000	0.173	2.993
3900	1.237	0.000	0.234	2.029

212

PORT C31			PORT C35	
time	Bromide	DMP	Bromide	DMP
(min)	(mg/l)	(mg/l)	(mg/l)	(mg/l)
300	n.a.	0.000	4.395	0.000
420	n.a.	0.000	n.a.	0.000
480	n.a.	0.000	n.a.	0.000
600	3.943	0.000	n.a.	0.000
720	0.359	0.000	3.265	0.000
840	13.562	0.525	3.647	0.000
960	72.952	17.657	0.864	0.000
1080	135.702	46.767	4.942	0.000
1200	136.712	22.740	37.658	8.901
1320	155.569	88.506	62.380	2.415
1440		84.011	77.060	24.803
1560	43.472	60.602	91.637	33.470
1680	25.670	36.838	70.110	28.388
1800	15.587	23.948	41.113	22.798
1920	3.762	3.131	31.061	29.696
2040	2.045	1.426	2.298	0.454
2160	0.281		0.080	0.000
2280	1.514	0.645	20.645	7.435
2400	1.332	0.943	18.405	7.364
2460	0.503	0.000	19.500	6.625
2640	0.712	0.000	14.378	16.650
2760	0.509	0.000	12.005	12.140
2880	0.231	0.000	8.023	9.474
3000	0.077	0.000	9.549	13.840
3180	1.429	0.000	3.263	2.799
3360		0.000	0.253	0.000
3540	7.425	0.000	0.900	0.000
3660		0.000	0.150	0.000
3780	7.495	0.000	0.486	0.000
3900	10.838	0.000		0.000

PORT D12			PORT D17	
time	Bromide	DMP	Bromide	DMP
(min)	(mg/l)	(mg/l)	(mg/l)	(mg/l)
300	0.340	0.000	0.592	0.000
420	1.009	0.000	n.a.	0.000
480	n.a.	0.000	4.726	0.000
660	0.140	0.000	n.a.	0.000
780	6.170	1.560	n.a.	0.000
900	52.694	8.641	0.045	0.000
1020	102.912	58.241	0.616	0.000
1140	117.650	77.971	3.607	0.578
1260	116.731	75.952	6.873	1.089
1380	87.918	64.276	23.531	7.330
1500	17.524	13.363	53.305	25.491
1620	2.560	1.115	1.284	33.867
1740	9.307	0.000	0.624	44.045
1860	0.897	0.000	0.383	59.446
1980	0.457	0.000	0.256	44.927
2100	5.793	0.000	0.242	0.000
2220	0.336	0.000	n.a.	9.157
2340	0.025	0.000	0.777	10.329
2460	5.021	0.000	0.127	0.000
2580	0.019	0.000	3.194	0.000
2700	7.662	0.000	7.871	0.000
2820	6.646	0.000	8.209	0.000
2940	0.407	0.000		0.000
3060	0.478	0.000		0.000
3120	6.749	0.000		0.000
3300	6.086	0.000		0.000
3480	7.112	0.000		0.000
3600	5.780	0.000		0.000
3720	0.691	0.000		0.000
4320	7.224	0.000		0.000

214

PORT D21			PORT D28	
time	Bromide	DMP	Bromide	DMP
(min)	(mg/l)	(mg/l)	(mg/l)	(mg/l)
300		0.000	n.a.	0.000
420		0.000	n.a.	0.000
480		0.000	n.a.	0.000
660	0.242	0.000	n.a.	0.000
780	2.177	0.000	0.027	0.000
900		0.000	9.289	0.000
1020		0.000	1.924	0.000
1140	2.839	0.000	6.695	0.388
1260	0.426	0.000	15.274	0.206
1380	3.514	0.000	28.961	15.352
1500	8.070	0.000	35.967	21.317
1620	2.964	0.250	54.294	23.723
1740	9.222	1.808	59.401	30.323
1860	40.110	4.243	54.484	34.761
1980	72.721	8.125	54.681	21.633
2100	91.750	7.896	42.168	9.469
2220	77.466	17.398	41.849	17.513
2340	57.443	17.254	34.991	1.689
2460	44.637	19.866	26.529	4.961
2580	14.061	23.704	21.605	21.116
2700	5.181	23.407	14.394	1.865
2820	14.722	13.930	8.870	18.415
2940	1.121	19.726	4.861	7.775
3060	13.354	17.356	1.992	1.315
3120	0.647	14.157	0.334	4.644
3300	6.410	8.841	0.327	0.000
3480	5.998	7.996	0.039	0.000
3600	5.306	5.889	n.a.	
3720	n.a.		0.030	0.000
4320	7.179	3.095		

	PORT E12		PORT E17	
time	Bromide	DMP	Bromide	DMP
(min)	(mg/l)	(mg/l)	(mg/l)	(mg/l)
540	0.348	0.000	n.a.	0.000
660	0.062	0.000	1.412	0.000
780	2.228	0.000	0.083	0.000
900	0.040	0.000	n.a.	0.000
1020	1.562	0.153	0.305	0.000
1140	14.786	0.869	5.383	1.066
1260	46.249	19.056	15.607	4.802
1380	78.322	10.340	27.587	12.153
1500	107.384		33.753	
1620	31.750	21.283	54.836	14.920
1740	96.824	32.329	61.131	35.783
1860	57.014	37.882	54.157	39.335
1980	29.537	9.786	61.457	40.054
2100	16.333	7.560	60.352	
2220	20.047	6.118	44.942	
2340	3.303	0.474	40.176	29.171
2460	0.769	0.000	31.734	25.607
2580	0.609	0.000	21.412	18.503
2700	0.203	0.000	16.706	14.853
2820	0.159	0.000	12.870	
2940	0.062	0.000	7.085	6.454
3060	1.517	0.000	5.546	5.465
3120	0.018	0.000	1.894	3.565
3240	n.a.	0.000	1.020	1.954
3300	n.a.	0.000	2.263	0.977
3480	0.118	0.000	0.263	0.366
3600	0.092	0.000	0.127	0.000
3720	n.a.	0.000	2.079	0.000
3840	n.a.	0.000	2.665	0.000
4020	n.a.	0.000	2.964	0.000

216

| PORT E21 | | | PORT E28 | |
| time | Bromide | DMP | Bromide | DMP |
(min)	(mg/l)	(mg/l)	(mg/l)	(mg/l)
540	1.304	0.000	n.a.	0.000
660	1.677	0.000	3.570	0.000
780	1.014	0.000	0.851	0.000
900	1.088	0.000	5.526	0.000
1020	0.026	0.000	1.221	0.000
1140	0.175	0.000	n.a.	0.000
1260	0.150	0.000	3.413	0.276
1380	0.409	0.000	2.127	2.455
1500	0.223	0.000	6.706	0.000
1620	0.998	0.000	4.266	0.000
1740	0.105	0.000	18.060	18.205
1860	7.350	0.000	35.354	5.142
1980	34.993	2.424	43.315	9.676
2100	144.337	0.000	56.602	23.156
2220	120.663	15.721	59.835	17.062
2340	152.164	50.576	62.170	19.534
2460	146.654	51.849	61.641	21.140
2580	67.993	52.929	45.806	19.269
2700	40.222	39.250	35.792	15.388
2820	12.040	6.493	32.505	1.916
2940	4.463	13.406	24.359	5.578
3060	0.609	9.629	20.493	6.484
3120	2.358	7.197	12.743	8.435
3240	1.313	0.000	8.772	0.256
3300	0.177	4.370	3.772	0.000
3480	0.928	2.280	1.745	0.000
3600	0.319	0.000	0.347	0.927
3720	4.404	0.000	0.275	0.470
3840	n.a.	0.303	0.337	0.000
4020		0.000	0.301	0.000

PORT F7			PORT F12	
time	Bromide	DMP	Bromide	DMP
(min)	(mg/l)	(mg/l)	(mg/l)	(mg/l)
540	0.348	0.824		0.000
660	0.062	0.000		0.000
780	2.228	17.639	n.a.	0.000
900	0.040	29.663	n.a.	0.000
1020	1.562	17.636	n.a.	0.000
1140	14.786	1.227	n.a.	0.000
1260	46.249	0.000	n.a.	0.000
1380	78.322	9.507	0.380	0.000
1500	107.384	4.444	5.330	0.373
1620	31.750	2.013	29.944	24.699
1740	96.824	5.548	31.505	23.122
1860	57.014	0.000	39.763	27.418
1980	29.537	0.000	61.865	8.205
2100	16.333	0.000	78.881	0.831
2220	20.047	0.000	72.851	10.707
2340	3.303	0.000	58.396	0.651
2460	0.769	0.000	48.548	0.304
2580	0.609	0.000	20.343	22.546
2700	0.203	0.000	5.585	2.621
2820	0.159	0.000	5.053	0.000
2940	0.062	0.323	2.039	0.379
3060	1.517	0.000	0.455	0.326
3120	0.018	0.000	0.578	0.000
3240	n.a.	0.000	0.396	0.000
3300	n.a.	0.000	n.a.	0.000
3480	0.118	0.000	n.a.	0.000
3600	0.092	0.000	0.109	0.000
3720	n.a.	0.000	n.a.	0.000
3840	n.a.	0.000	n.a.	0.000
4020	n.a.	0.000	0.648	0.000

PORT F17

time	Bromide	DMP
(min)	(mg/l)	(mg/l)
540	0.049	0.000
660	n.a.	0.000
780	n.a.	0.000
900	n.a.	0.000
1020	n.a.	0.000
1140	1.415	0.200
1260	8.106	3.761
1380	12.977	5.926
1500	25.880	15.919
1620	35.197	16.650
1740	28.837	31.030
1860	32.169	34.586
1980	30.805	24.259
2100	30.184	10.360
2220	25.896	27.377
2340	25.659	23.680
2460	12.057	22.934
2580	18.375	18.521
2700	17.872	18.366
2820	18.823	14.992
2940	14.061	13.867
3060	12.161	12.793
3120	9.238	11.266
3240	5.014	8.473
3300	2.713	5.703
3480	1.726	2.046
3600	1.143	0.979
3720	0.584	0.829
3840	0.504	0.454
4020	n.a.	0.228